

BROOKHAVEN NATIONAL LABORATORY

JULY 1998	RHIC DETECTOR NOTE	RHIC/DET Note No. 27
	PHENIX Technical Note	PHENIX/Tech. Note No. 354

Explosion Analysis for the RHIC PHENIX Detector

Gaby Ciccarelli
Department of Advanced Technology
Brookhaven National Laboratory
Upton, NY 11973-5000

Executive Summary

PHENIX is one of the major detectors used in the Relativistic Heavy Ion Collider (RHIC) at Brookhaven National Laboratory. The PHENIX detector consists of several systems, each with its own role in detecting subatomic particles. Combustible gases such as ethane, isobutane, and methane are used in several of the detector systems. Due to the scale of the PHENIX detector, the inventory of such combustible gases are relatively large compared to other detectors found at BNL. As a result, concerns over potential explosion hazards involving these combustible gases are being addressed as part of the PHENIX Safety Review. The purpose of this report is to document an independent evaluation of the potential explosion hazards, and to provide input to the PHENIX Group to establish a Design Basis Accident (DBA) for which safety systems will be implemented. Two DBAs were considered in the analysis. In both cases, it is assumed that all the safety systems fail to detect the release of combustible gas, and as a result, no action is taken to shut down power to instrumentation which could serve as ignition sources.

In the first DBA the full PHENIX inventory of combustibles is released into the Interaction Region (IR), mixed with the existing IR air and then ignited. During flame propagation in the IR, gas is vented from the IR into the Assembly Hall and the North and South Mezzanines. Gas venting mitigates against substantial pressurization of the IR. The results of the analysis indicate that the effects of this DBA would be completely confined to the IR, and that the block shield wall is a stable and effective safety barrier between the fire and the outside world. The analysis also demonstrates that if a combustible cloud of the correct size and concentration is formed in the IR, and the ignition is timed perfectly, the wall could topple as a result of the ensuing explosion. No scenarios by which such a cloud can form in reality has been identified.

The second DBA analysis explores the effects of the ignition of an explosive mixture of isobutane within the confinement of the Muon magnets. This DBA presumes the release of the full inventory of isobutane from the detectors, and assumes containment of the resulting isobutane-air mixture within the magnet "lampshade" shaped outer shell. The analysis shows that the magnets are sufficiently robust to withstand the overpressure produced by an explosion involving the ignition of the mixture, and thus, the effects of the DBA are limited to the Muon system itself.

Analyses are also performed to determine the response of the three different shielding walls to "theoretical" worst-case explosions. These worst-case explosions are considered theoretical since the underlying assumptions made are non-physical and thus can not be considered the consequence of any credible accident

scenario. The results from the analyses should not be used directly to set regulations concerning hazard classifications or occupancy restrictions to any of the areas within Building #1008.

The first analysis deals with an explosion in the IR involving the full combustible gas inventory of PHENIX. Several nonphysical conservative assumptions are made: it is assumed that the combustible gas mixes with just enough air to produce a spherical gas cloud with a mixture composition which yield the highest possible constant volume pressure for an equivalent ethane-air mixture, 2) it is assumed that this *unconfined* gas cloud explodes producing a similar size cloud of combustion product gases at the constant volume pressure. This high-pressure, high-temperature gas cloud then expands producing a shock wave which interacts with the IR block shield wall and the closest Muon ID plate. It is shown that due to the very short duration of the shock wave loading the block wall does not move by an appreciable amount but is sufficient to tip the Muon plate over towards the back wall. This indicates that even under this theoretical worst case scenario the block wall serves its purpose to shield personnel outside the IR from not only neutrons but also missiles which could be generated from an IR explosion. The analysis also shows that the duration of the combustion product gas depressurization from the IR following the shock loading is sufficiently long that the block wall does collapse.

The second analysis looks at the consequences of a theoretical worst case explosion occurs in the north and south mezzanines. For this analysis it is assumed that the full gas inventory is released in the IR and mixes to form a homogeneous 7% ethane in-air spherical cloud. It is then assumed that the burn occurs at constant pressure displacing the maximum amount of ethane-air into the mezzanines. The nonphysical assumption is then made that this displaced gas mixture then displaces the air in the Mezzanine forming a combustible "slug" of gas. This gas slug then explodes, with no change in volume, generating a pressure equal to the mixture constant volume pressure. The high pressure gas cloud then expands out into the tunnel progressively lowering the pressure in the slug starting at the free end. The most severe pressure time history, corresponding to the location in the mezzanines on the other side of the IR wall, is applied to the entire wall without taking credit for any additional venting generated by the motion of the top of the wall. The results indicate that even under these theoretical worst-case explosions, movement of the block shield walls in the north and south mezzanines are limited to less than 15 cm.

Based on the analysis described in this report, the results of the DBA analysis indicate that the wall will not topple over, however, the PHENIX group should exercise caution and limit the occupancy of the AH. The justification for this is that there is some degree of inherent uncertainty in the model concerning scaling of the

combustion phenomenon. There is also some uncertainty linked to the possibility of producing a higher ethane concentration cloud via some nonidentified accident scenario. The possibility of the North Mezzanine block wall collapsing due to any credible accident scenario involving the release and ignition of the PHENIX combustibles in the IR is so remote so as not to require any limitations on the occupancy of the electronics and counting house.

Acknowledgments

The author gratefully acknowledges the assistance of Mike Marx and Bill McGahern for their support and technical input concerning the PHENIX detector and safety systems. Valuable discussions were also held with other PHENIX members including Peter Kroon, Jim Rank, Tom Shea, Wlodek Guryn. The author would also like to thank John Boccio of the Department of Advanced Technology for reviewing the document.

Table of Contents

Executive Summary

Acknowledgments

Table of Contents

1.0	Introduction	1
2.0	PHENIX Detector Location	1
3.0	PHENIX Detector	3
4.0	Basics of Combustion Phenomenon	5
4.1	Deflagration and detonation mode of combustion	6
4.2	Confined and unconfined explosions	7
4.3	Explosion overpressure prediction	8
5.0	Design Basis Accident	9
5.1	Design Basis Accident I: Burn in the IR	10
5.1.1	Volumes and vent area of the building	11
5.1.2	Gas mixture composition	12
5.1.3	Fixed vent area explosion pressure	13
5.1.4	Transient burn/vent model with variable vent area	15
5.1.5	Sensitivity analysis of the burn/vent model	20
5.1.6	Effect of Higher Concentration Cloud	21
5.1.7	Conclusions	21
5.2	Design Basis Accident II: Explosion in the Muon Magnets	22
5.2.1	Muon Tracker Magnet	22
5.2.2	Lampshade explosion pressure	24
5.2.3	Structural response of the Muon Magnet lampshade	26
5.2.4	Conclusions	29
6.0	Theoretical Worst Case Explosion	30
6.1	Explosion in the IR	31
6.1.1	Spherical gas cloud composition and size	33
6.1.2	Shock pressure at the sphere surface	33
6.1.3	Shock pressure and impulse decay with distance	34
6.1.4	Wall averaged shock wave pressure	37
6.1.5	Quasi-static pressure decay	39
6.1.6	Wall response to shock loading and blowdown	41
6.1.7	Muon plate response to shock loading	43
6.1.8	Conclusions	44
6.2	Explosion in the North and South Mezzanines	45
6.2.1	Description of Phenomenon	45

6.2.2	Pressurization of the Mezzanines	46
6.2.3	Wall Response	48
6.2.4	Conclusions	49
7.0	Summary and Recommendations	50
8.0	References	52
FIGURES		54
APPENDICES:		
A	Burn and Vent Model	78
B	Dynamics of a Tilting Wall	82
C	MathCad Worksheets for Burn and Vent Model	86
D	IR Blowdown With Fixed Vent Area and Volume	90
E	IR Blowdown With Variable Vent Area and Volume	92
F	MathCad Worksheets for Depressurization Model	95
G	MathCad Worksheets for Burn/Vent Model in Mezzanines	97

Explosion Analysis for the RHIC PHENIX Detector

Gaby Ciccarelli

1.0 Introduction

PHENIX is one of the major detectors used in the Relativistic Heavy Ion Collider (RHIC) at Brookhaven National Laboratory. The PHENIX detector consists of several systems, each with its own role in detecting subatomic particles. Combustible gases such as ethane, isobutane, and methane are used in several of the detector systems. Due to the scale of the PHENIX detector, the inventory of such combustible gases are relatively large compared to other detectors found at BNL. As a result, concerns over potential explosion hazards involving these combustible gases are being addressed as part of the PHENIX Safety Review. The purpose of this report is to document an independent evaluation of the potential explosion hazards, and to provide input to the PHENIX Group to establish a Design Basis Accident (DBA) for which safety systems will be implemented.

2.0 PHENIX Detector Location

PHENIX is housed in the Major Facility Hall located in Building #1008 at roughly the 8 o'clock position of the RHIC Ring. A layout drawing of Building #1008 is given in Figure 1. The complex is subdivided into the following units:

Interaction Region (IR) - area where the RHIC beams cross and the PHENIX detector is located.

Assembly Hall (AH) - area where the major detector systems are assembled before being positioned in the IR.

Electrical Room - area where the data acquisition and control consoles as well as other electrical equipment are located.

Counting House - area where the data acquisition and control terminals are located.

Engineering Room - area where small-scale technical work is carried out.

N. and S. Mezzanine - transition area from the IR to the RHIC Tunnel where the DX magnets are located.

Also shown in Figure 1 are the locations of several block shield walls which play key roles in the determination of the consequence of an explosion in the IR and Mezzanine areas. The South Mezzanine block wall acts as a radiation shield for the tunnel and also acts as a barrier for the gas mixing trailer located just outside the wall. Since personnel are only present in this area for routine maintenance, it is considered a low occupancy area. The IR is separated from the AH by a block shield wall, of which a large portion consists of a plug door which can be rolled into and out of position. In the initial phase of testing, only half of the PHENIX detector will be used with no combustible gases. During this phase the AH will be used for assembly of the second half of the detector. Once the complete detector is in place in the IR, and operating with combustible gases, occupancy of the AH will be low. There is a third shield block wall which separates the North Mezzanine and the Electrical Room/Counting House. The Electrical Room has relatively low occupancy but the counting house is occupied around the clock with as many as 20 operators at a time.

Aside from the block shield walls, the IR and the Mezzanines are constructed from thick reinforced concrete walls and both the Mezzanines are covered with earth backfill. Assuming an internal explosion, the weakest structures in all three areas are the block shield walls which are free to move. Note, the strength of the concrete walls and the inertia of the earth backfill act as an effective boundary. One of the objectives of the analysis is to determine the impact of an explosion in the IR and the Mezzanines on the movement imparted to these block shield walls and the consequences of this movement.

3.0 PHENIX Detector

Shown in Figure 2 is a schematic of the PHENIX detector subsystems, the various large magnets, and the Muon steel plates. The bulk of the detectors are mounted on two carriages which are positioned on either side of the beam line axis, at the 10 and 2 o'clock positions. The detectors are layered in the radial direction. There are also two large detector systems, to the north and south of the interaction point, used for Muon tracking and identification. The Muon Tracking Chambers are located within two large radial-field magnets. The various PHENIX detectors employ mixtures of gases, some of which contain combustible constituents. Table 1 provides some basic data on some of the detector gases which will be discussed throughout the report.

Table 1: Properties of detector gases used in PHENIX

Gas	Symbol	Molecular Weight	Heat of Combustion (MJ/kg)*	
			MJ/kg	KJ/mol
Air		29	-	-
Nitrogen	N ₂	28	-	-
Argon	Ar	40	-	-
Methane	CH ₄	16	50.00	800
Ethane	C ₂ H ₆	30	47.40	1422
Isobutane	C ₄ H ₁₀	58	45.60	2645
Tetrafluoromethane	CF ₄	88	-	-

* Energy released when burned with oxygen at standard temperature and pressure to form water vapor and carbon dioxide, source Baker et al., 1983

A summary of the type and quantity of combustible gas used under normal operating conditions in each of the detector systems shown in Figure 1 is provided in Table 2.

Table 2: Combustible Gas Volume per Detector

Detector	Gas	Mix (by volume)	Total Detector Volume (m ³)	Total Comb. Volume (m ³)
Drift Chamber (DC)	Ar/C ₂ H ₆	50/50	5.6	2.8
Pad Chambers (PC)	Ar/C ₂ H ₆	50/50	1.12	0.56
Time Expansion Chamber (TEC)	Ar/CH ₄	90/10	11.5	1.15
Ring Imaging Cherenkov Counter (RICH)	C ₂ H ₆	100	80	80
Muon Tracker (MuTr)	CF ₄ /C ₄ H ₁₀	50/50	2.92	1.46
Muon Identifier (MuId)	CO ₂ /C ₄ H ₁₀	91/9	59	3.31
TOTAL				91.28

The detector with the most volume of combustible gas is the RICH detector which has 80 m³ of 100% ethane gas. The RICH detector consists of a welded aluminum frame with two large 0.005 inch thick aluminized

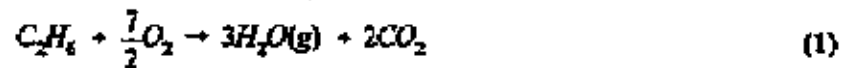
KAPTON windows, perpendicular to the radial direction. As shown in Figure 2, the pad chambers (PCS) are located on either side of these windows with roughly a one inch gap between the RICH window and the PC. Nitrogen gas is continuously flushed through this gap in order to cool the PC electronics. This nitrogen flush also serves to maintain an inert gas buffer between the RICH window and the PC electronics, whose electronics serve as potential ignition source. Because of the large ethane inventory, the RICH detector has received the most attention in terms of explosion hazards. *In the analysis that follows, it is assumed that the entire RICH inventory of ethane is released and mixed with air in the IR. This assumption is very conservative since there is no clear mechanism to achieve this dispersion and mixing within realistic time frames.* The molecular weight of ethane is 30 g/mol which is only slightly less than that of air, and the ethane is at the same temperature as the surrounding air, there is very little buoyancy force which can drive the dispersion of the ethane. Furthermore, although the RICH detector has very thin KAPTON windows, the adjacent PC chambers provide a secondary containment for the ethane should the windows fail. The only opening available for the ethane to leave the chamber is through very narrow slits, roughly 2.5 cm wide, which exists between the RICH and the two PC chambers.

The second largest quantity of combustible gas is used in the Muon Identifier detectors. The isobutane/carbon-dioxide detector gas is housed inside of small plexiglass units which are stacked inside of CO₂ flushed panels. Because of the compartmentalization of the units it is difficult to release all the gas at one time. Furthermore, the 9/91 isobutane/carbon-dioxide detector gas mixture is nonflammable. An isobutane-tetrafluoroethane mixture is used in the Muon Tracking detectors located within the two "lampshade" shaped Muon Magnets. There are three detector stations per magnet, each roughly filling the internal cross-sectional area of the magnet. This is the only detector where the flammable gas and air are enclosed (e.g., lampshade enclosure) such that if the detector containment fails, mixing of the combustible gas and air is imminent. For this reason, a separate analysis is performed to look at the explosion hazard associated with this detector.

The remaining detectors do not contain substantial amounts of combustible gas, and there are no features of their structure or location within PHENIX which warrant any special consideration.

4.0 Basics of Combustion Phenomenon

Combustion is defined as the initiation and progress of an exothermic process involving the chemical reaction of a gas mixture from one state to another. In order for this reaction to occur, constituents of the gas mixture must include an oxidizer (e.g., oxygen) and a fuel (e.g., hydrocarbons). The energy liberated is the result of the net change in the chemical bond energy of the molecules in transition from the unburned state to the burned state. This energy release manifests itself in an increase in the temperature of the gas products relative to the unburned fresh gas mixture. The magnitude of the temperature increase depends on the amount of energy released and the heat capacity of the product gas, which for the combustion of hydrocarbons in air typically consists of a mixture of water vapor, carbon dioxide, nitrogen and residual oxygen and the fuel. A stoichiometric mixture is defined as one in which the products of combustion do not include any residual oxygen or fuel. For example, the following stoichiometric ethane-oxygen mixture consists of 22.2% ethane.



In order for a combustion process to occur, an ignition source must be present and the fuel-air composition must be within a specific range, commonly referred to as the flammability limit. An ignition source can be an electrical spark, as in an internal combustion engine, or a hot surface at a temperature above the so-called "autoignition temperature". Table 3 provides some flame properties for the two fuels of interest in this analysis (note: the properties for n-butane are listed instead of isobutane). The difference between the two molecules is that n-butane has a straight chain structure and isobutane has a branched chain structure, however, they have similar chemical properties.

Table 3: Flame Properties

Fuel	% Fuel in stoichiometric air	Flame Temperature (K)	Minimum Ignition Energy (mJ)	Autoignition Temperature (K)	Flammability Limits (% fuel in air)	
					Lower	Upper
Ethane	5.7	2170	0.25	788	3.0	12.4
n-butane	3.1	2170	0.26	678	1.8	8.4

In general, the minimum ignition energies for hydrocarbons are very low, and in many cases static electricity is sufficient to ignite a mixture.

Physical damage caused by combustion can include; structural deformation and failure due to shock pressure loading, and structure charring and melting due to thermal loading. If the initial state of the combustible gas mixture is in the form of an unconfined cloud, the combustion process occurs at roughly constant pressure. Since the process occurs at roughly constant pressure, the product gas mixture is at a lower density than the fresh gas. If the initial combustible gas mixture is confined, the combustion process occurs at constant volume. Since the process occurs at constant density i.e., constant volume and mass, there is an increase in the system pressure. The peak pressure occurs when all the mixture is consumed. The theoretical maximum pressure, under constant volume combustion and adiabatic boundary conditions, is referred to as either the constant volume or adiabatic isochoric complete combustion (AICC) pressure. This maximum pressure is typically 9 times the initial pressure for most stoichiometric hydrocarbon air mixtures. Figure 3 is a plot of the constant volume pressure as a function of fuel composition in air for ethane and isobutane, for an initial temperature and pressure of 298K and 1 atmosphere. The data plotted in Figure 3 was calculated using the chemical equilibrium code STANJAN (Reynolds, 1986), where standard air was taken as 21% oxygen and 79% nitrogen. In general, for fuel-air mixtures, the peak in the constant volume pressure corresponds to a mixture slightly richer than stoichiometric. In general, for off-stoichiometric mixtures, the constant volume pressure decreases, where the drop is typically more severe on the lean side.

4.1 Deflagration and Detonation Mode of Combustion

There are generally two types of combustion modes possible for any combustible mixture. The deflagration mode involves the propagation of a flame at a velocity which is subsonic relative to the gas ahead of the flame. The second is a detonation mode which propagates supersonically and thus the gas ahead has no communication with the detonation wave.

For a deflagration, a flame corresponds to the interface between the burned and unburned gas. The rate at which the gas is burned depends on the thermal and molecular diffusivity of the gas and the chemical kinetic rates of reactions for the mixture. Under laminar conditions the "burning velocity" is very slow, e.g., below 0.5 m/s for a stoichiometric hydrocarbon air mixture. If the flame is ignited in a closed rigid tube, the

velocity at which the flame advances can be up to 8 times this laminar burning velocity since the hot combustion gases expand convecting the flame forward along with the unburned gas. This observed velocity is referred to as the "flame velocity". Under quiescent conditions, the burning velocity depends solely on the mixture properties. However, if the gas is in motion, turbulence will exist at high enough free stream velocities. The burning velocity within this flow depends on the turbulence intensity since combustion can occur via turbulent convection, as opposed to only diffusion processes which govern the laminar case. Therefore, if one takes into account turbulence, a spectrum of burning velocities (or flame velocities) are possible for any given mixture depending on the free stream velocity and the presence of turbulence generating obstacles.

In a detonation wave, the flame (in this context, more commonly referred to as the reaction zone) is coupled to a leading shock wave. The shock wave adiabatically compresses the unburned gas, raising the temperature. This increased temperature initiates an exothermic chemical reaction in the mixture which leads to a further increase in the mixture temperature and a decrease in the pressure from the peak post shock temperature. The energy that is released in the reaction zone sustains the leading shock wave so that the complex is self-sustained. The length of the reaction zone, which also includes a thermally neutral induction zone immediately after the shock wave, dictates the "sensitivity" of the mixture to undergo detonation. For example, the smaller the reaction zone, the smaller the amount of energy required for direct initiation of a detonation wave, and thus the more sensitive the mixture. In general, an initiation source with the required energy content and energy release rate required for direct initiation of a detonation is not present under most accident scenarios. A detonation wave can also be initiated indirectly via an accelerating flame. In long narrow channels with flow obstructions, a flame can accelerate due to turbulence. This flame acceleration process can lead to the development of a strong precursor shock wave resulting in the initiation of a detonation. The requirement of strong lateral confinement and long axial distances are not generally met in most industrial plants, except for pipelines in the chemical industry and deep coal mines. In general, most industrial explosions involve deflagrations and not detonation waves.

4.2 Confined and Unconfined Explosions

If ignition occurs at the center of a confined spherical gas cloud, i.e., enclosed in a rigid chamber, a flame propagates radially outward converting the fresh gas mixture into high temperature combustion products. The expanding combustion product gas acts like a spherical piston pushing the gas ahead of it. If the flame

velocity is slow, the pressure in the entire volume is uniform since compression waves have sufficient time to equalize the pressure. The system pressure increases proportionally to the volume of the fresh gas consumed and the rate of pressure rise depends on the volume of the system and the burning rate. If the flame velocity is fast, i.e., close to the mixture speed of sound, a shock wave forms ahead of the flame. The shock wave reflects off the boundary and reverberates within the confinement. Through the mechanism of shock reflection one can obtain short duration pressure spikes which are above the maximum constant volume pressure defined above. When the shock wave attenuates, for an adiabatic boundary condition, the system pressure equilibrates at the theoretical maximum.

For an unconfined gas cloud, the same principles described for the confined cloud apply with the exception that there is no uniform increase in system pressure. If the flame velocity is very slow, the combustion product gas expansion rate is much shorter than the burning rate, and as a result, the pressure in the cloud remains at atmospheric pressure and the unburned gas ahead of the flame is convected radially outward increasing the radial extent of the gas cloud. For higher flame velocities, the expansion of the hot gas can not keep up with the consumption of fresh gas resulting in pressurization in the burned gas and the formation of a shock wave ahead of the flame. The strength of the shock wave depends on the magnitude of the flame velocity (or burning velocity).

4.3 Explosion Overpressure Prediction

As part of the analysis we will be interested in determining the strength of the blast wave generated by the explosion of a combustible gas cloud. For a given gas cloud size and mixture composition, the strength of the blast wave depends on the rate of combustion. Shown in Figure 4 are the results from numerical calculations (Baker et al., 1983) for the combustion of an unconfined spherical cloud in terms of normalized shock overpressure versus energy scaled distance. The energy density and combustion product ratio of specific heats used in the calculations was chosen to model most stoichiometric hydrocarbon-air explosions. For the cases where a deflagration is ignited at the center of the cloud, bottom four curves, the strength of the shock wave produced in the cloud, and the blast wave outside the cloud, depends on the burning rate M_u (burning rate normalized with the speed of sound in the fresh gas). A typical speed of sound is about 350 m/s, so the range in burning velocity is 11.9 m/s ($M_u = 0.034$) to 76.3 m/s ($M_u = 0.218$). The laminar burning velocity for most hydrocarbon-air mixtures is below 0.5 m/s, so the four curves in Figure 4 correspond to very high burning rates. The curve labeled "S" corresponds to the blast pressure generated by a bursting sphere where

the initial sphere pressure corresponds to the constant volume combustion pressure for the mixture. This is essentially the upper limit for the deflagration curves since it corresponds to an infinite burning rate. The curve labeled "D" corresponds to the calculated blast overpressure for a detonation wave in the cloud. Note the initial scaled sphere radius for the "S" and "D" curves are identical, in the case of the bursting sphere all the gas is burned instantaneously so the cloud radius does not grow and for the supersonic detonation wave the edge of the cloud does not have any communication with the combustion front. The vertical dashed line represents the final radius of the cloud when the energy is added so slowly that there is no pressure rise. The last curve in Figure 4, corresponds to the blast overpressure generated by the detonation of high explosives with the same energy density. For this case one is dealing with a point source so the initial scaled radius is zero and the local pressures are very high compared to all the other solutions. It is important to note that far (i.e., dimensional distance) from the cloud center, the slope of all the curves can be approximated by an inverse scale law (see sloping dashed line), as predicted by acoustic theory.

The above discussion serves the purpose to show that even for a given cloud size and mixture composition one can predict a spectrum of blast wave pressures depending on the assumed burning rates and mode of combustion. In many cases the simplistic, yet least realistic approach is simply to use the TNT equivalency method (Factory Mutual, 1994) to predict far field blast pressures. That is, the blast pressure is predicted using standard high explosive blast wave decay curves for a TNT charge weight equivalent to the stored chemical energy available in the gas cloud. Curve "D" in Figure 4 shows that this approach leads to very high pressures, especially near the source. In most cases, the assumption of a point source explosion, implicit in the TNT equivalence approach, can not be justified. However, this approach is often taken since it can easily be applied to any accident scenario so long as the amount of energy involved is known.

5.0 Design Basis Accident

This section describes the analysis of two scenarios which encompass the worst case credible accidents for PHENIX, and are thus considered the Design Basis Accidents (DBA) which must be mitigated by the full complement of PHENIX safety systems and procedures.

The first DBA consists of burning the ethane equivalent of the entire gas inventory of PHENIX, i.e. 100 m³. The probability of achieving such starting conditions for combustion are extremely remote, requiring multiple

failures of flammable gas detection, detection of oxygen within the detector volumes, safety interlocks of ignition sources, and hall ventilation systems. In addition the times required to achieve such a mixture are sufficiently long that lack of intervention by trained operators is also extremely remote. The results of the analysis indicate that the effects of this DBA would be completely confined to the IR, and that the block shield wall is a stable and effective safety barrier between the fire and the outside world.

The second DBA analysis explores the effects of the ignition of an explosive mixture of isobutane within the confinement of the Muon magnets. This DBA presumes the loss of the full inventory of isobutane, its containment within the magnets, the failure of all systems to detect the loss and to shut down ignition sources. The analysis shows that the magnets are sufficiently robust to withstand the overpressures induced by such an explosion, and thus the effects of the DBA are limited to the Muon system itself.

5.1 Design Basis Accident I: Burns in the IR

In this accident scenario the full PHENIX inventory of combustibles is released into the IR. Since the normal HVAC air exchange rate in the IR is very high, one IR volume per 4 minutes (15000 CFM), and the release rate of the ethane from the RICH is assumed to be slow, the released gas is quickly diluted with the air mixing to form a homogeneous mixture in the IR. Under this assumption, the global IR ethane concentration starts at zero, before the start of the release, and then slowly increases with time. During this release time the global ethane concentration is below 3% in air and therefore global burning is not possible. Only after the full ethane inventory is released does the global ethane concentration reach the flammability limit. However, small sized higher ethane concentration clouds can form in the direct vicinity of the release point both immediately after the start of ethane release (initial "puff") and during steady-state release, and in areas where the IR HVAC air flow is blocked. It is assumed that ignition of these smaller local pockets will not impact the block shield wall but could cause local damage to the detector. For the purpose of the analysis, no credit is taken for the 1500 CFM of IR atmosphere which is exhausted outside Building #1008 by the HVAC. This "well mixed" IR assumption does not apply when:

- 1) The normal HVAC air exchange is not operational such that mixing of the gases occurs solely through gas diffusion which would take days to achieve a homogeneous mixture. If ignition was to occur during the diffusion process ethane concentrations near the release point would be elevated.
- 2) Some hypothetical catastrophic event occurs whereby the ethane is ejected very quickly, e.g., less than one minute, producing a local high ethane concentration cloud mixture and ignition occurs on

the same time-scale.

Ignition of the combustible mixture is assumed to occur producing a pressure load on the block shield wall in the IR. The objective of this analysis is to determine the combustion pressure loading within the IR and the response of the block shield wall to this loading.

In order to determine the stability of the block shield wall to a burn in the IR one must predict the resulting overpressure time-history given: a) the volume of the IR, b) the gas mixture composition, c) the available fixed and variable vent area.

5.1.1 Volumes and Vent Area of the IR Building

For the purpose of this analysis, the internal dimensions of the IR are taken as:

North-South Length = 18.6 m (61 ft)

East-West Length = 15.8 m (52 ft)

Height = 14.3 m (47 ft)

These dimensions yield a 4200 m³ total internal volume for the IR building, of which 850 m³ (value provided by PHENIX personnel) consists of PHENIX detector hardware volume. Therefore, the total free volume of 3350 m³. The total internal surface area of the IR is 1572 m².

The main gas vent path from the IR is through the 9.1 m (30 ft) x 4.9 m (16 ft) openings in the North and South IR building walls, as shown in Figure 5. These openings are grossly obstructed by the North and South Muon ID plates and Magnets. The Muon plates are each 13.1 m (43 ft) wide by 10.7 m (35 ft) high with a 1.6 m (5.33 ft) square central cut out. These plate cut outs are partially blocked by the DX magnets which provide a blockage, of diameter of 1.2 m (4 ft). There are five plates on each side of the IR, where the 0.28 m (11 in) gaps between plates are filled with detectors, mounted within large panels which are hung in place like curtains. As shown in Figure 5, possible vent paths from the IR into the RHIC Tunnel include: A) between the Muon magnet back plate and the first Muon plate, B) between each of the plate gaps, and C) between the last Muon plate and the IR wall. The A and B flow paths merge through the Muon plate central cut outs, so the unobstructed cut out area represents the maximum vent area for these two combined vent paths. The flow

path between the plates is very narrow and long (5.75 m), and severely obstructed by the detector panels. The pressure drop associated with these two factors will limit the flow through this path. There are no detector panels between the last Muon plate and the IR wall, and therefore there is no corresponding pressure drop. The only source of pressure drop is due to viscous flow through the 2 m long channel produced by the overlap between the IR wall and the last Muon plate. The flow path between the end of the Muon magnet and the first Muon plate is clear. On the north side, the gap is very tight (0.28 m) whereas on the south side the gap is 1.82 m, due to the shorter Muon magnet.

An accurate modeling of the vent flow is beyond the scope of this analysis, therefore engineering approximations will be made concerning the "effective" vent area. The sensitivity of this parameter will be determined later. On the north side, the vent area will be taken as the minimum gap area between the last Muon plate and the wall. There are two areas to consider: 1) the area at the outer Muon plate edge which is $0.28 (13.1 + 2 \times 10.7) = 9.62 \text{ m}^2$, and 2) the area at the edge of the Mezzanine wall which is $0.28 (2 \times 9.1 + 2 \times 4.9) = 7.83 \text{ m}^2$. The smaller of the two areas is taken, e.g., 7.83 m^2 . It is assumed that the losses through the vent path C is balanced by the limited venting through A and B. On the South side, the vent area is taken as 7.83 m^2 , corresponding to the vent path C, plus the unobstructed plate cut out area ($2.64 - 1.17 = 1.47 \text{ m}^2$) since the vent flow path A is completely unobstructed. This yields a total fixed IR vent area of 17.1 m^2 . There is also a variable vent area associated with the gap which opens up with any movement of the wall. The gap forms at the top edge of the block wall and the ceiling concrete beam of the IR building. The instantaneous vent area is equal to the distance traveled by the top edge of the block wall multiplied by the 18.6 m (61 ft) wall span.

5.1.2 Gas Mixture Composition

For this analysis we will assume that all of the combustible gas present in the IR participates in the burn. As tabulated in Table 2, the total volume of combustible gas is 91.3 m^3 , of which 80 m^3 is ethane. For the analysis we will base the combustible gas inventory which participates in the explosion on an effective volume of ethane which is equal to the total energy available within the IR. No credit is taken for detector combustible gas mixtures which are effectively inerted by either argon or carbon dioxide. The effective ethane volume is calculated based on a heat of combustion weighted average of the three different combustible gases present in the IR, as follows

$$\begin{aligned}
 V_{C_2H_6} &= V_{C_2H_6} + \left(\frac{E_{CH_4}}{E_{C_2H_6}}\right)V_{CH_4} + \left(\frac{E_{C_2H_2}}{E_{C_2H_6}}\right)V_{C_2H_2} \\
 &= (2.8+0.56+80) + \left(\frac{800}{1422}\right)(1.15) + \left(\frac{2645}{1422}\right)(1.46+5.31) \\
 &= 96.6 \text{ m}^3
 \end{aligned}
 \tag{2}$$

The value of 96.6 m³ is rounded up to 100 m³ to take into account combustible gas in the various detector feed lines. As calculated earlier, the total free internal volume of the IR building is 3350 m³. For an equivalent ethane volume of 100 m³, the nominal ethane concentration is 100/3450 or 2.9%. This is just below the lower flammability limit of 3% ethane for ethane-air mixtures at standard temperature and pressure.

5.1.3 Fixed Vent Area Explosion Pressure

In the chemical industry it is very common to install safety vents on various containments, ranging in size from small reactors to buildings, which house flammable gases. The purpose of these vents is to limit the peak overpressure produced during an accidental explosion to a level which can be supported by the containment structure. Typically the volume of the containment and quantity of flammable gas is known and the vent area required to limit the peak overpressure is sought. The determination of this required vent area is made based on empirical correlations developed from data obtained from experimental vented explosions in vessels of various size. The National Fire Protection Association (NFPA) has published a guide for venting of deflagrations (NFPA 68, 1994) which is based largely on data from the work by the U.S. Bureau of Mines and work in Great Britain and Germany. Other notable contributions to the prediction of vented explosions are by Bradley and Mitcheson (1978). Their work included the comparison of predictions of pressure-time histories for vented explosions using their theoretical model with experimental results from many investigators. In this work they also give an upper limit curve for the scaled maximum explosion overpressure versus a scaled venting parameter. According to Baker et al. (1983) the use of the NFPA 68 guides can lead to gross overestimates of the vent area required for limiting the maximum vented vessel overpressure and recommends the use of the Bradley and Mitcheson correlation.

In this section we will calculate the peak IR overpressure using the Bradley and Mitcheson (1978) correlation,

considering only the fixed vent area. Shown in Figure 7 is the Bradley and Mitcheson curve which denotes the maximum scaled overpressure, ΔP_m , versus the scaled vent parameter, A/S_o , which is given by

$$\frac{\Delta P_m}{S_o} = \frac{\frac{A_v C_d}{A_i}}{\left(\frac{P_x}{P_b} - 1\right) \frac{s_o}{c_o}} \quad (3)$$

where A_v is the vent area, A_i is the vessel internal surface area, C_d is the vent opening discharge coefficient, s_o is the laminar burning velocity and c_o is the speed of sound in the gas ahead of the flame. For overpressures below 1 atmosphere, Bradley and Mitcheson recommend the use of the following expression for the

$$\Delta P_m = 0.7 \left(\frac{S_o}{A} \right)^2 = 0.7 \left(\frac{\left(\frac{P_x}{P_b} - 1\right) \frac{s_o}{c_o}}{\frac{A_v C_d}{A_i}} \right)^2 \quad (4)$$

maximum overpressure. Since a burning velocity can only be defined for a flammable mixture, we consider the mixture to be 3% ethane in air. As calculated by STANJAN, the speed of sound and the density ratio across the flame for a mixture of 3% ethane in air, is 336.4 m/s and 5.221, respectively. A discharge coefficient of 0.6, which is the smallest value possible for a sharp edge orifice, will be used for the calculations. The laminar burning velocity is a parameter which is measured experimentally. Shown in Figure 6 is a plot of laminar burning velocities measured for a range of ethane-air mixtures in various size vessels. The data used in the plot was taken from Kunz (1998), which also included data from Kuchta (1985). Burning velocities at 3% ethane in air were not measured, a simple linear extrapolation of the data yields a burning velocity range of 9-15 cm/s. A value of 15 cm/s will be used in the analysis. Taking these values for the various parameters, equation 4 gives a peak overpressure of

$$\Delta P_m = 0.7 \left(\frac{(5.22-1) \frac{0.15}{336.4}}{\frac{17.1}{1572} (0.6)} \right)^2 = 0.058 \text{ atmospheres} \quad (5)$$

The minimum pressure required to move the wall against friction is simply

$$\Delta P_{\text{vent}} = \frac{\mu M_w g}{A_w} = \mu(\rho_w t)g = 27714 \text{ Pascals (0.273 atmospheres)} \quad (6)$$

where μ is the coefficient of friction (0.7 for concrete on concrete), ρ_w is the wall concrete density (2408 kg/m³, 150 lb/ft³), t is the wall thickness (1.676 m), and g is gravitational acceleration (9.81 m/s²). The minimum pressure required to tilt the wall, assuming the wall acts as a single structure and pivots about the bottom front edge, is

$$\Delta P_{\text{tilt}} = \frac{WM_w g}{hA_w} = \left(\frac{W}{H}\right)(\rho_w t)g = \left(\frac{0.838}{7.31}\right)0.391 = 0.045 \text{ atmospheres} \quad (7)$$

where W is the wall half thickness ($t/2$) and H is the wall half height. From this analysis one can see that the predicted maximum vent pressure is too low to drag the wall forward but is large enough to tilt the wall, if the pressure was applied statically (e.g., indefinitely).

5.1.4 Transient burn/vent model with variable vent area

In an actual burn, the pressure-time history within the containment would be exponential in nature and if the wall tilts forward the top edge separates from the IR building generating more vent area. A burn/vent model is developed here in order to take into account the transient nature of the pressure and the effect of the variable vent area produced by the motion of the wall. The burn/vent model is benchmarked with the fixed vent area deflagration venting correlation of Bradley and Mitcheson.

The one-dimensional model predicts the flame velocity and pressure-time history within an empty spherical vented enclosure. The model is an extension of the one used by Chan et al. (1983) to model flame propagation in a vented rectangular channel. In the current model ignition occurs at the center, and the fresh unburned gas is converted into high-temperature combustion products with a fixed burning rate. The unburned gas ahead of the flame is allowed to escape the volume through a vent opening which can be either fixed or variable area. For the one-dimensional assumption it implies that the flame surface is smooth and

the vent area is uniformly distributed. The gases are treated as being ideal and isentropic processes are assumed throughout. A detailed description of the model is provided in Appendix A.

Prediction of the containment pressure-time history requires the integration of the following two coupled differential equations describing the time rate of change of the pressure and flame sphere radius

$$\frac{dP}{dt} = \frac{1}{\left(\frac{V_o - V_b}{\gamma_o} + \frac{V_b}{\gamma_b}\right)} \left[\left(\frac{P_o}{P_b} - 1\right) s P A_f - P A_f c C_D K \right] \quad (8)$$

$$\frac{dR}{dt} = \frac{1}{\left(\frac{P_o}{P_b}\right) \frac{V_b}{V_o - V_b} + 1} \left[\left(\frac{\gamma_o}{\gamma_b}\right) s + \frac{\left(\frac{\gamma_o}{\gamma_b}\right) V_b}{V_o - V_b} \left(s + \frac{A_v}{A_f} c C_D K \right) \right] \quad (9)$$

If the change in pressure P , and correspondingly the change in temperature, is not great, one can assume that all the gas parameters remain constant over time. The various gas parameters are obtained using the chemical equilibrium code STANJAN. The density of the burned gas is calculated for a constant pressure burn at one atmosphere and 273K. The main approximation in the model is that the burning velocity is constant throughout the burn. Because of this approximation, the burning velocity is treated as a free parameter which is fixed based on bench marking with the Bradley and Mitcheson (1978) deflagration venting correlation. This is done by using the correlation to calculate the peak overpressure for the mixture and the fixed vent area, i.e., assume that the wall does not move for the bench marking calculations. The constant burning velocity used in the model is then adjusted to give the same peak overpressure as predicted by the correlation. Note, the Bradley and Mitcheson correlation is based on a survey of tests done in vessel of various size, the largest being about 40 m³. Therefore, any scale effects on flame instabilities, which can enhance the effective burning rate, beyond this size are not accounted for in the correlation, and thus in the current model.

A model for the rotational motion of the wall, under the pressure loading from the IR, is developed in

Appendix B. The wall is treated as a unit structure which pivots about the front lower edge. The angular acceleration of the wall is predicted by the following expression

$$\frac{d^2\theta}{dt^2} = \frac{PA_1H + PA_2W - M_w g(W - H\theta)}{\frac{4}{3}M_w(H^2 + W^2)} \quad (10)$$

where θ is the tilt angle of the wall. In the numerator, the first two pressure terms are offset by the restoring third gravity term. For angles above the critical angle, $\theta_{crit} = W/H = 0.838/7.3 = 0.115$ radians = 6.56 degrees, the restoring gravity term changes sign resulting in further rotation of the wall leading to collapse. The critical angle corresponds to the situation where the center of mass of the wall is directly above the pivot point. To solve for the wall dynamics, equation 10 is solved simultaneously with the burn/vent model equations, 9 and 10.

Wall Response to the DBA

In order to solve for the wall response we must first determine the effective burning velocity for the 3% mixture by bench marking the burn/vent model with the Bradley and Mitcheson correlation which predicts a peak overpressure of 0.058 atmospheres (see equation 5). The two differential equations 8 and 9 are integrated using the commercially available Mathcad (MathSoft, 1997) software. Since the model is one-dimensional, the volume of the IR is used to define an equivalent containment radius

$$R_e = \left(\frac{3}{4\pi} V_{IR} \right)^{\frac{1}{3}} = \left(\frac{3}{4\pi} (3350) \right)^{\frac{1}{3}} = 9.28 \text{ m} \quad (11)$$

The initial conditions for the calculation are 1 atmosphere pressure and an initial flame radius of 0.01 m (this is required to avoid the singularity which exists for a flame radius of 0). The following list provides the mixture properties, pertinent dimensions and constants used in the calculation.

For 3% ethane in air mixture (obtained from STANJAN):

Unburned gas ratio of specific heats = 1.4

Burned gas ratio of specific heat = 1.28

Unburned gas density = 1.183 kg/m³

Burned gas density = 0.2262 kg/m³

Unburned gas speed of sound = 336.4 m/s

Burned gas speed of sound = 756.9 m/s

Boundary conditions:

IR open volume = 3350 m³

Fixed vent area = 17.1 m²

Wall length = 18.6 m

Wall height = 14.6 m

Wall width = 1.7 m

Wall mass = 1098000 kg

Constants:

Gravitational acceleration = 9.81 m/s²

Vent discharge coefficient = 0.6

The free parameter is the burning velocity, which is varied to give a system pressure of 1.058 atmospheres when the flame has propagated a distance of 9.282 m. The Mathcad worksheet (PHENIX1a) for this calculation is provided in Appendix C. Shown in Figure 8 is the calculated flame radius and system pressure-time history for a burning velocity of 0.22 m/s which yields a pressure of 1.058 atmospheres when all the gas is consumed. This burning velocity is relatively close to the referenced 0.15 m/s laminar burning velocity used in the correlation, providing credibility to the model. The time required to burn the entire inventory of gas is roughly 8 seconds and the flame velocity is almost constant the entire time. The flame velocity relative to a fixed observer, is equal to the product of the ratio of the densities across the flame and the burning velocity, which yields a value of 1.17 m/s. Therefore the time required to traverse a distance of 9.28 m is 7.9 seconds, which also agrees with the model prediction, which is expected since the change in gas properties associated the increase in pressure during the burn is small. Considering the exponential nature of the pressure-time history, calculating the wall motion based on a constant pressure with a magnitude equal to the peak pressure, is not accurate.

Using the bench marked burning velocity of 0.22 m/s the coupled burn/vent model equations and the wall dynamics equation are integrated to determine the motion of the wall resulting from such a burn. For this calculation the variable vent area produced by the motion of the top of the wall is included. This calculation

is broken up into two parts, 1) calculation carried out until the flame consumes all the gas, 2) no further burning, only venting of the burned gas. The Mathcad worksheet (PHENIX1b) for this two part calculation is also provided in Appendix C. As shown in Figure 9, during the first phase, the wall does not move until the system pressure reaches the critical pressure of 1.045 atm as determined by equation 7. The peak pressure at the end of the burn is 1.057 atm which is just slightly under the 1.058 atm calculated for the fixed vent area. During this first phase the final wall tilt angle, θ , is only 0.082 deg. and it achieves an angular velocity, $d\theta/dt$, of 0.487 deg/s. During the second phase, the pressure drops to atmospheric pressure in about 0.1 seconds, see Figure 10. As a result, the wall does not acquire much more kinetic energy, as observed in the angular velocity time history which peaks at a value just over the 0.487 deg/s achieved in the first phase. Once the system pressure drops to atmospheric conditions the wall inertia continues to tilt the wall to a maximum angle of 0.127 deg. which occurs when the wall angular velocity is zero. After that point, the angular velocity becomes negative, which corresponds to gravity pulling the wall back to its initial position of zero degree tilt.

This calculation demonstrates that for the DBA conditions modeled there is virtually no motion of the wall expected. This is because the peak pressure of 1.058 atm is only slightly larger than the 1.045 atm minimum required to set the wall in motion. From Figure 9, the wall only starts to move after 7.7 s into the burn, when the pressure reaches 1.045 atm. The burn is complete by 8.2 s. The combustion product gas vents to atmospheric pressure in about 0.1 s, see Figure 10. Therefore, only during the last 0.5 s, of the full 8.2 s that the IR is pressurized, does the wall acquire kinetic energy.

By the time the critical pressure of 1.045 atm is achieved in the IR, the flame has propagated a distance of 8.751 m; a complete burn requires 9.282 m of propagation, which corresponds to a volume of 2807 m³. Based on this we can estimate the minimum amount of ethane required to be released into the IR for the wall to start moving. The minimum volume of ethane which needs to be released and mixed with air to form a combustible spherical cloud of ethane-air (note: flammability limit is 3% ethane), of radius 8.751 m, is 86.8 m³. Therefore, in order to even set the wall in motion one must release at least 87% of the full gas inventory of PHENIX without ignition and then ignite the mixture. As mentioned in Section 3, no mechanism exists by which such a large amount of gas is released. Equally improbable is that one can release a total of 86.8 m³ of ethane, at the low release rates expected, without ignition during the release.

5.1.5 Sensitivity Analysis of the Burn/Vent Model

The two key parameters of the model are the burning rate and the fixed vent area. In this section the sensitivity of the model solution to these two parameters will be explored. This will be done by calculating the critical values for these two parameters required to topple the wall. The same Mathcad worksheets are used with conditions as listed above, except:

Iterate Burning Velocity

For a fixed vent area of 17.1 m^2 , the burning velocity is incrementally increased until the limiting condition is met where the wall tumbles over. For a burning velocity of 0.32 m/s the peak system pressure is 1.078 atm and the tilt angle and angular velocity at the end of the burn phase is 1.8 deg and 4.35 deg/s . During the second phase the wall achieves a maximum tilt angle of 5.8 deg and then swings back to its initial position.

For a burning velocity of 0.33 m/s , the peak system pressure at the end of the burn phase is 1.080 atm . As shown in Figure 11, the pressure peaks and then drops before all the gas is burned. This is because as the wall starts to tilt, the vent area increases to the point where the mass of fresh mixture vented is greater than the volume consumed by the flame and thus the pressure drops. The final tilt angle and angular velocity at the end of the burn phase is 1.94 deg and 4.7 deg/s , respectively. In the second phase, as shown in Figure 12, again the pressure drops to atmospheric in about 0.1 s . Almost immediately after the burn the wall's angular velocity drops. However, it never drops to zero since the wall surpasses the critical tilt angle of 6.5 . At the point where the critical angle is achieved, the angular velocity increases rapidly as the wall collapses. Note the solution is only good for small tilt angles, so beyond the critical angle the values are inaccurate.

Using a burning velocity 0.33 m/s , the peak pressure achieved with only the fixed 17.1 m^2 vent area is 1.125 atm . Using the Bradley and Mitcheson correlation, equation 4, this peak pressure corresponds to a laminar burning velocity of 0.22 m/s .

Iterate the Fixed Vent Area

For the burning velocity of 0.22 m/s , obtained from bench marking with the correlation, the vent area is incrementally decreased until the limiting condition is met where the wall tumbles over. For a vent area of 12 m^2 the peak system pressure is 1.065 atm and the tilt angle and angular velocity during the burn phase are 2.5

deg. and 3.79 deg/s. During the second phase the wall achieves a maximum tilt angle of 5.6 degrees and then swings back to its initial position. For a vent area of 11.5 m² the peak system pressure is 1.066 atm and the tilt angle and angular velocity during the burn phase are 2.94 deg. and 3.77 deg/s. During the second phase the wall surpasses the critical tilt angle of 6.5 and topples over.

5.1.6 Effect of Higher Concentration Cloud

The basic assumption used for the DBA is that as the combustible gas is leaked it mixes with the IR to form a uniform mixture. The analysis has shown that at the end of the release, ignition of the mixture does not result in the toppling of the wall. Also part of the DBA is that there could be small pockets of combustible gas that form which are not large enough to impact the results of the DBA analysis. This section looks at the hypothetical scenario where the ethane is released sufficiently fast that the normal HVAC recirculation of the IR does not completely mix the air and the ethane. Using the burn/vent model the volume of a mixture which must be burned to topple the wall is calculated. This is done by taking a uniform concentration of ethane in air, larger than 3% ethane, in the entire IR and allow the flame to progress to the point where the acquired kinetic energy of the wall is sufficient to topple the wall if burning ceases. The rapid release of ethane would produce a cloud with varying ethane concentration. In terms of participation in a burn, the lower limit for the cloud concentration is set by the flammability limit (greater than 3% ethane) and the upper limit is the most reactive concentration which is 5.7% ethane. Note, mixtures with concentrations above 5.7% are less reactive than a stoichiometric 5.7% ethane mixture. For a mixture of 3.5% ethane in air, using an effective burning velocity of 0.38 m/s corresponding to a fixed vent overpressure of 0.21 atm, the flame must burn to a radius of at least 8.5 m (recall the effective IR radius is 9.3 m) for the wall to topple. For a stoichiometric ethane-air mixture (5.7% ethane), using an effective burning velocity of 0.53 m/s corresponding to a fixed vent overpressure of 0.0711 atm, the flame must burn to a radius of at least 7.1 m.

5.1.7 Conclusions

A model is developed to predict the pressure-time history within the IR building resulting from the combustion of the full inventory of combustible gases used in the PHENIX detector. The initial condition for the calculation is taken to be a homogeneous mixture including all the IR combustibles and air. It is assumed that such a mixture can develop and that an ignition source is available. The calculations show that the IR has sufficient natural venting that such a burn does not result in the toppling of the block shield wall. A

sensitivity analysis of the two key parameters in the model indicates that the predictions are not highly sensitive to these parameters. Hypothetically, if a cloud of the correct size and concentration is formed and the ignition time is timed perfectly, the burn/vent model predicts that it is possible that the wall could topple. The ignition time is critical since, if it is premature a burn involving a limited amount of gas would result, and if it is delayed, the cloud is overly diluted by mixing with the ambient air. The requirements for this to occur is that the ethane must be released very quickly on a time-scale of tens of seconds. No scenarios by which this can occur in reality has been identified.

5.1 Design Basis Accident II: Explosion in the Muon Magnets

The DBA explosion analysis outlined in Section 5.1 uses the full inventory of combustible gases in the IR. In this section we will focus the analysis on the consequences of an explosion inside of the Muon Tracking Magnets. The detectors located within the magnets contain isobutane which if released could mix with air within the magnet forming a potentially explosive mixture. The objective of this analysis is to determine if such an explosion could fail the outer shell of the magnet catastrophically, producing large missiles which could in turn damage the rest of PHENIX and the block shield wall.

5.2.1 Muon Tracker Magnet

There are two Muon Tracking magnets located on either side of the interaction point. As described in Section 3.0, the outer shell of the Muon Tracking magnet is shaped like a lampshade with an inner core, referred to as a piston. The lampshade has six equal size sides constructed from 8 cm thick steel plate. A cross-sectional view of the lampshade is shown in Figure 13a. The lampshade plates and the piston are fastened to a backplate, not shown in Figure 13a. The "large" lampshade on the north side is 4.3 m long, and the "small" one on the south side is 2.8 m long. For both magnets, the distance between plates at the front end opening of the lampshade is 3.014 m, and the inclination angle of the plates relative to the centerline of the magnet is 37 degrees. For the north magnet, the plate separation distance at the backplate is 9.494 m and for the south magnet the separation is 7.234 m. The lampshade is constructed such that each of the three top plates (10, 12, and 2 o'clock positions) are made up of two plate sections, one which is fixed and the other retractable. The fixed plate is located at the open end of the lampshade. The transition between the two plate sections for the north and south magnets are at an axial distance of 1.4 m and 0.9 m, respectively. The retractable plates are bolted to the fixed plates and to the backplate using 24 mm diameter bolts. The piston is shaped like a

cut off cone, with a 10 degree angle of inclination relative to the magnet centerline. For both magnets the cone diameter at the opening is 0.704 m.

The internal lampshade volume is a quantity which is required to calculate the average detector gas concentrations within the magnet. The lampshade internal volume can be estimated by treating it as a truncated cone. The volume of a cone is given by $1/3\pi R^2L$, where R is the base radius and L is the cone length. The volume of a truncated cone is given by $1/3\pi(R^2L-r^2L)$, where R and L is the base radius and length of the total cone, r is the radius of the opening of the truncated cone and L-l is the length of the truncated cone. For the purpose of calculating average detector gas concentration, a conservative estimate of the lampshade volume is made by taking the cone diameter to be the distance between opposite plate internal surfaces. A similar calculation is performed to calculate the volume occupied by the piston. For the large Muon Magnet, the internal lampshade volume, V_{LM} , and piston volume, V_{LP} , is

$$V_{LM} = \frac{\pi}{3}(4.75^2(6.3)-1.51^2(2.0)) = 144.1 \text{ m}^3$$

$$V_{LP} = \frac{\pi}{3}(1.11^2(6.3)-0.352^2(2.0)) = 7.9 \text{ m}^3$$

yielding a net internal free volume of 136.2 m³. For the small Muon Magnet, the internal lampshade volume, V_{SM} and piston volume, V_{SP} , is

$$V_{SM} = \frac{\pi}{3}(3.62^2(4.8)-1.51^2(2.0)) = 61.1 \text{ m}^3$$

$$V_{SP} = \frac{\pi}{3}(0.846^2(4.8)-0.352^2(2.0)) = 3.3 \text{ m}^3$$

giving a net internal free volume of 57.8 m³.

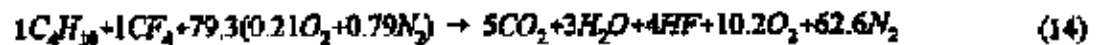
An isobutane-tetrafluoromethane mixture is used in the Muon Tracking detectors which are located within the magnet lampshades. There are three detector stations per magnet, each filling the internal cross-sectional area between the lampshade inner surface and the piston. There is one detector at the lampshade opening (120 liter gas volume), one up against the back plate (710 liter gas volume), and the third one roughly midspan

(630 liter gas volume). The total detector gas volume is thus 1460 liters, or 1.46 m³. If we assume that all the detector gas mixes with air in the magnet lampshade, this yields for the small magnet a mixture of 2.46% by volume detector gas in air, and for the large magnet a mixture of 1.06% detector gas in air.

5.1.2 Lampshade Explosion Pressure

For this DBA analysis it is assumed that all detector gas inventory is released within the magnet lampshade. It is further assumed that all the detector gas mixes homogeneously with the available air and then ignites. The peak pressure produced during combustion within the magnet is assumed to be the constant volume pressure for the mixture. This assumption is very conservative because it implies a complete and isentropic burn, and more importantly, does not consider the venting of the gas during combustion through the magnet opening.

As shown in Table 2, the detectors use a 50/50 mix by volume of isobutane (C₄H₁₀) and tetrafluoromethane (CF₄). Tetrafluoromethane when mixed with air is nonflammable. However, when burned in air with a combustible gas such as isobutane, CF₄ breaks down to form HF exothermically. The STANJAN species data files do not include CF₄ or HF so it is not possible to calculate the constant volume pressure for the mixtures in question. Using STANJAN the constant volume pressure for isobutane in air was calculated for a range of mixtures, see Figure 3. For the small magnet, the detector gas mixture volume is 2.46% of the total lampshade volume, therefore the reaction equation is



For an adiabatic constant volume reaction, the internal energy, $\sum n_i u_i$, of the products and the reactants is equal, where n_i and u_i are the number of moles and molar specific internal energy for compound constituent i . This yields the following

$$5u_{CO_2} + 3u_{H_2O} + 4u_{HF} + 10.2u_{O_2} + 62.6u_{N_2} = u_{C_4H_{10}} + u_{CF_4} + 16.7u_{O_2} + 62.6u_{N_2} \quad (15)$$

In terms of molar specific enthalpy, h , and using the ideal gas equation of state, i.e. $u = h - Pv = h - RT$

$$5h_{CO_2} + 3h_{H_2O} + 4h_{HF} + 10.2h_{O_2} + 62.6h_{N_2} - 84.88T_2 = h_{C_4H_{10}} + h_{CF_4} + 16.7h_{O_2} + 62.6h_{N_2} - 81.38T_1 \quad (16)$$

where R is the Universal gas constant, T_1 and T_2 are the temperatures of the reactants and products, respectively. The enthalpy of a compound at a state other than the standard state of 298K and 1 atm is found by adding the specific enthalpy change, Δh , between the standard state and the state of interest to the compound's enthalpy of formation, h_f , i.e., $h(T,P) = h_f + \Delta h$. Substituting into equation 16 yields

$$5(h_f + \Delta h)_{CO_2} + 3(h_f + \Delta h)_{H_2O} + 4(h_f + \Delta h)_{HF} + 10.2(h_f + \Delta h)_{O_2} + 62.6(h_f + \Delta h)_{N_2} - 84.88T_2 = (h)_{C_4H_{10}} + (h)_{CF_4} + 16.7(h)_{O_2} + 62.6(h)_{N_2} - 81.38T_1 \quad (17)$$

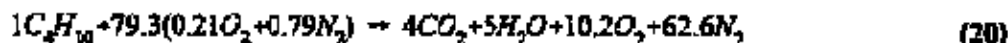
Note, the heat of formation for stable elements such as O_2 and N_2 is zero. Rearranging yields

$$5(h)_{CO_2} + 3(h)_{H_2O} + 4(h)_{HF} - (h)_{C_4H_{10}} - (h)_{CF_4} = -5(\Delta h)_{CO_2} - 3(\Delta h)_{H_2O} - 4(\Delta h)_{HF} - 10.2(\Delta h)_{O_2} - 62.6(\Delta h)_{N_2} + 84.88T_2 - 81.38T_1 \quad (18)$$

where the expression on the left hand side of equation 18 is referred to as the reactant mixture's heat of combustion, ΔH_R . The constant volume combustion temperature is obtained by iterating the product gas temperature until equation 18 is satisfied. Using the equation of state, the product gas temperature can then be used to determine the constant volume pressure. Using the JANAF thermochemical tables (Chase et al., 1985) for the individual heats of formation, the heat of combustion for the reaction given in equation 14 is

$$\Delta H_R = 5(-394) + 3(-242) + 4(273) - (-132) - (-933) = -2723 \text{ KJ per mole } C_4H_{10} \quad (19)$$

If we now ignore the CF_4 in the detector gas, treating it as air, and only consider the isobutane we get the following reaction for the same 2.46% detector gas mixture (1.23% isobutane mixture),



The corresponding heat of combustion for the reactant mixture in equation 20 is

$$\Delta H_R = 4(-394) + 5(-242) - (-132) = -2654 \text{ kJ per mole } C_4H_{10} \quad (21)$$

The heat of combustion for the mixture with both C_4H_{10} and CF_4 (equation 19) is only 2.6% higher than the heat of combustion for the mixture with only C_4H_{10} (equation 20). This is because the energy released from the formation of HF is balanced by the energy required to dissociate the CF_4 , which has a very high heat of formation. Furthermore, the major components of the product gas, e.g., O_2 and N_2 , remain the same. Therefore, the constant volume pressure for the actual mixture, as given in equation 14, will be almost identical to that for the isobutane-air mixture given in equation 20. As a result, the peak pressure expected in the lampshade can be obtained from Figure 3 by treating the CF_4 as air.

For the small Muon Magnet, the isobutane concentration in air is 1.23% (i.e., half the 2.46% detector gas). From Figure 3, this corresponds to a constant volume pressure of 5.5 atm. For the large Muon Magnet, the isobutane concentration in air is 0.53% (i.e., half the 1.06% detector gas). From Figure 3, this corresponds to a constant volume pressure of 3.1 atm.

5.2.3 Structural Response of the Muon Magnet Lampshade

In this section, the response of the 8 mm thick retractable lampshade plates to the calculated constant volume pressure is analyzed. The shape and dimensions of the lampshade plates are shown in Figure 13b, note the dimensions not in brackets are for the large magnet and those in brackets are for the small magnet. Each plate is fastened at both ends using 24 mm diameter steel bolts. For the large magnet, there are 8 bolts running the length of the "long" plate edge, and 5 bolts on the "short" plate edge, see Figure 13b. For the smaller magnet, there are 6 bolts running the length of both edges. The bolted plate edges will be treated as fixed boundary conditions for the purpose of the analysis. The internal combustion pressure applies a uniform load across the entire plate. This load is transferred through the bolts into the magnet back plate and the fixed lampshade plates. In the analysis the stress in the bolts and plates are determined and compared with allowable stresses for the materials used.

Standard solutions for uniformly loaded trapezoidal plates are not available in the literature. Therefore, the

plate is analyzed as a beam of constant cross section with a uniformly increasing load, as shown in Figure 14. Where q is the unit load (Newtons per linear meter) and is given by the product of the pressure and beam width, w ,

$$q = \frac{F}{dx} = Pw \quad (22)$$

As shown in Figure 13, the end of the beam designated as "1" corresponds to the short edge of the lampshade plate, and the long edge is designated by a "2". Since the plate is bolted in place, the beam is treated as being fixed at both ends, which results in a reaction force, R , and reaction bending moment, M , at each end. The following are expressions (Roark and Warren, 1975) for the reaction forces

$$R_1 = \frac{1}{2} q_1 l + \frac{3}{20} (q_2 - q_1) l \quad (23)$$

$$R_2 = \frac{1}{2} (q_1 + q_2) l - R_1 \quad (24)$$

and the reaction bending moments are

$$M_1 = -\frac{1}{12} q_1 l^2 - \frac{1}{30} (q_2 - q_1) l^2 \quad (25)$$

$$M_2 = R_1 l + M_1 - \frac{1}{2} q_1 l^2 - \frac{1}{6} (q_2 - q_1) l^2 \quad (26)$$

The reaction forces and bending moments are different for the two plates since the pressure loading, P , is different and the length of the plate, l , is different. Table 4 summarizes the reaction forces and bending moments calculated using equations 23-26.

Table 4: Summary of the reaction forces and bending moments

Muon Magnet	Length, l (m)	q_1 (N/m)	q_2 (N/m)	R_1 (N)	M_1 (Nm)	R_2 (N)	M_2 (Nm)
Large	3.631	$2.122P_1$	$3.932P_1$	$4.838P_1$	$-3.126P_1$	$6.153P_1$	$-3.524P_1$
Small	2.379	$1.810P_2$	$2.996P_2$	$2.576P_2$	$-1.043P_2$	$3.141P_2$	$-1.156P_2$

where P is in units of Pascals (N/m^2) and the subscripts 1 and 2 correspond to the large and small magnets, respectively. By convention a negative value for the bending moments places the top fibers of the beam in tension.

Bolt Stress

The load per bolt is obtained by using the expressions for R_1 and R_2 in Table 4 to determine the total edge reaction force for each of the plates using the respective magnet constant volume pressures, outlined in Section 5.2.2. The bolt load is obtained by dividing the total reaction force by the number of bolts on the plate edge. For example, for the large magnet the average isobutane concentration is 0.53% which yields a constant volume overpressure of 2.13 atm, or 215.7 KN/m^2 . Using equation 23, or Table 4, this yields a total reaction force along the short edge of the plate (R_1) of 1044 KN. Since there are 5 bolts along this edge, the load per bolt is 209 KN. The results for all the bolts are summarized in Table 5.

Table 5: Summary of the bolt loads

%C ₄ H ₁₀	Overpressure (KN/m ²)	Load per Bolt (KN)			
		Large Muon Magnet		Small Muon Magnet	
		Back (R ₂ /8 bolts)	Front (R ₁ /5 bolts)	Back (R ₂ /6 bolts)	Front (R ₁ /6 bolts)
1.23	455.9			239	196
0.53	215.7	165	209		

The tensile strength of the 24 mm bolts used is 441 KN. This gives a safety factor of roughly 2 for the highest loaded bolt corresponding to the back edge of the small Muon Magnet.

Plate Stress

For the boundary and loading conditions, the maximum bending moment in the entire beam is M_2 .

Therefore, the maximum fiber stress in the plate at any cross-section is given by

$$\sigma_{\max} = \frac{M c}{I} = \frac{3M}{2wc^2} \quad (27)$$

where c is half the plate thickness, w is the long edge plate width, I is the section moment of inertia ($I = w(2c)^3/12$). Since the maximum bending stress occurs at the edges, the maximum stress will also be located at one of the two edges. A summary of the calculated stress for the two plates is given in Table 6.

Table 6: Summary of plate stresses

%C ₂ H ₁₀	Overpressure (KN/m ²)	Plate Edge	Large Muon Magnet		Small Muon Magnet	
			M (KNm)	σ (MPa)	M (KNm)	σ (MPa)
1.23	455.9	Short			475	246
		Long			527	165
0.53	215.7	Short	674	297		
		Long	760	181		

Although the maximum bending on the plate is located on the long edge, the maximum stress is on the short edge because of the smaller moment of inertia. The tensile strength of the steel plate material used for the lampshades is 413 MPa (60 ksi). This gives a safety factor for plate failure of 1.4 for the large magnet and 1.7 for the small magnet.

5.2.4 Conclusions

The analysis has shown that all the bolts and the two retractable lampshade plates would survive an explosion within either Muon Magnet. For the analysis it was assumed that the explosion pressure corresponds to the constant volume pressure for the mixture. As discussed in Section 4, the constant volume pressure represents

the theoretical maximum pressure which can be achieved by a deflagration in a closed volume. For the Muon Magnets this is conservative since the natural venting of the lampshade, which would lower this pressure, was not incorporated into the analysis.

6.0 Theoretical Worst-Case Explosions

In this section, analyses are performed to determine the response of the three different shielding walls to "theoretical" worst-case explosions. These worst-case explosions are considered theoretical since the underlying assumptions made are non-physical and thus can not be considered the consequence of any credible accident scenario. The results from the analyses should not be used directly to set regulations concerning hazard classifications or occupancy restrictions to any of the areas within Building #1008.

The first analysis deals with an explosion in the IR involving the full combustible gas inventory of PHENIX. Several nonphysical conservative assumptions are made: 1) it is assumed that the combustible gas mixes with just enough air to produce a spherical gas cloud with a mixture composition which yield the highest possible constant volume pressure for an equivalent ethane-air mixture, 2) it is assumed that this *unconfined* gas cloud explodes producing a similar size cloud of combustion product gases at the constant volume pressure. This high-pressure, high-temperature gas cloud then expands producing a shock wave which interacts with the IR block shield wall and the closest Muon ID plate. It is shown that due to the very short duration of the shock wave loading the block wall does not move by an appreciable amount but is sufficient to tip the Muon plate over towards the back wall. This indicates that even under this theoretical worst case scenario the block wall serves its purpose to shield personnel outside the IR from not only neutrons but also missiles which could be generated from an IR explosion. The analysis also shows that the duration of the combustion product gas depressurization from the IR following the shock loading is sufficiently long that the block wall does collapse.

The second analysis looks at the consequences of a theoretical worst case explosion occurs in the north and south mezzanines. For this analysis it is assumed that the full gas inventory is released in the IR and mixes to form a homogeneous 7% ethane in-air spherical cloud. It is then assumed that the burn occurs at constant pressure displacing the maximum amount of ethane-air into the mezzanines. The nonphysical assumption is then made that this displaced gas mixture then displaces the air in the Mezzanine forming a combustible

"slug" of gas. This gas slug then explodes, with no change in volume, generating a pressure equal to the mixture constant volume pressure. The high pressure gas cloud then expands out into the tunnel progressively lowering the pressure in the slug starting at the free end. The most severe pressure time history, corresponding to the location in the mezzanines on the other side of the IR wall, is applied to the entire wall without taking credit for any additional venting generated by the motion of the top of the wall. The results indicate that even under these theoretical worst-case explosions, movement of the block shield walls in the north and south mezzanines are limited to less than 15 cm.

6.1 Explosion in the IR

In this analysis it is assumed, as in the DBA case I, the total inventory of combustibles in the IR (equivalency of 100 m³ of ethane) are released and participate in the combustion process. One of the main differences between this analysis and that of the DBA is that for this analysis it is assumed that the ethane mixes with air to form the most reactive mixture possible. In order to achieve a mixture concentration of higher than 2.9% ethane in air, the ethane must mix with less air. A further conservative assumption is that the mixture takes the form of a spherical homogeneous combustible gas cloud. Clearly there is no physical mechanism by which this can occur, normally gas diffusion and convection would prevent this from occurring. It is the ignition and subsequent explosion of this gas cloud which generates the pressure loading on the block shield wall.

The prediction of shock overpressures generated by a gas cloud explosion typically requires detailed numerical simulation of compressible turbulent reactive flows (Hjertager, 1982). A common very simple approach used to calculate the shock overpressure time-history resulting from an outdoor gas cloud explosion is the so-called "TNT equivalent method." This approach is very common since the only input required is the total energy stored in the gas cloud. In this method the total energy available in the gas cloud is calculated based on the mass and heat of combustion of the fuel. Using the heat of combustion of TNT, this cloud energy is converted into an equivalent TNT weight, and using standard blast decay graphs for TNT explosion, the blast overpressure is determined, as a function of distance from the cloud center. This approach is satisfactory for large distances, e.g., energy-scaled distance (defined later) greater than about one, however, at short distances this method over predicts the loads from a gas cloud explosion. This is due to fact that the energy density in a TNT charge is very large compared to a gas cloud explosion, and thus, the pressure close to the source is much higher. In this analysis we use a methodology to predict near field blast overpressures using an approach as simple as the TNT equivalent method but much more reliable.

The second significant difference from the DBA analysis is that in this analysis, it is assumed that the mixture burns at a nonphysically achievable high rate, yielding the maximum possible combustion pressure, i.e. constant volume pressure. For a spherical gas cloud this could only be achieved if, 1) the cloud is rigidly confined to a volume equal to the cloud volume during the burn, or 2) the burning rate is so great that effectively the entire cloud ignites as a whole (see Figure 4). Both these assumptions are nonphysical since the IR building volume is much larger than the assumed spherical cloud volume and there is no means to accelerate the flame to such speeds through the entire cloud. The pressure generated can be calculated from the mixture's composition and the cloud's thermodynamic initial conditions. Once the cloud is completely consumed, at constant volume, the combustion products expand, producing a spherical blast wave which propagates into the surrounding air. The decay of the blast wave, as it moves radially out from the sphere, is governed by several parameters, including the speed of sound of the gas products and the initial energy contained within the pressurized gas. The shock decay produced by such an explosion can be simulated by the pressure field generated by the bursting of a pressurized frangible glass sphere. This so-called "bursting sphere" problem has been studied extensively both experimentally and numerically (Boyer et al., 1958; Stelow et al., 1976).

The shock wave generated by the gas cloud explosion reflects off of the IR building walls and reverberates within the building until nonisotropic effects dampen the strength of the shock wave. Since the IR building has natural vent openings, whereby the combustion product gases can escape, the IR pressure drops very quickly. The objective of the analysis is to determine the movement in the block shield wall resulting from the shock loading and the depressurization of the IR. Also, the response of the closest Muon plate to the shock loading will be investigated.

The following is an outline of the various calculations which are performed in the analysis:

- 1) Determine the gas cloud diameter based on the mixture concentration corresponding to the highest constant volume pressure
- 2) Calculate the strength of the shock wave produced at the sphere's radius,
- 3) Calculate the decay of the shock pressure with distance,
- 4) Determine the shield wall response to the shock wave.
- 5) Determine the IR building pressure time history resulting from the venting of the product gas
- 6) Determine the shield wall response to this depressurization

These steps are described in the following sections.

6.1.1 Spherical Gas Cloud Composition and Size

For this analysis it is assumed that the full 100 m³ of ethane is released into the IR and mixes with air to produce a homogeneous spherical gas cloud. The size of the spherical cloud, or conversely the amount of air in the cloud, is chosen such that the resulting ethane-air mixture composition corresponds to the highest constant volume pressure. As plotted in Figure 3, the maximum constant volume pressure is 9.43 atmospheres which corresponds to a mixture of 7% ethane in air. This is slightly "richer" in ethane than a stoichiometric mixture of 5.7% ethane in air. For a mixture of 7% ethane by volume (or by mole) in air, the 100 m³ of ethane is mixed with 1328 m³ of air. Therefore, the total volume occupied by the ethane-air cloud is 1428 m³. For a spherical cloud this volume corresponds to a radius of 7.0 m.

It is assumed that the cloud burns with no change in volume resulting in a spherical volume of gas composed of combustion products at 9.43 atmospheres. Using STANJAN the gas temperature and speed of sound are 2583 K and 990 m/s, respectively. Assuming an ideal gas this yields a mixture specific heat ratio of 1.21.

6.1.2 Shock Pressure at the Sphere Surface

To calculate the strength of the shock wave which is produced at the start of the expansion of the combustion products, we assume that the high-pressure and temperature gas is contained in a sphere. The sphere instantaneously bursts, producing expansion waves that propagate radially inwards inside the sphere progressively lowering its pressure and producing a shock wave in the surrounding air which propagates radially outwards. Assuming that the shock wave is locally one-dimensional at the sphere's surface, which is a good assumption for a large radius, the following expression (Liepmann and Roshko, 1967) implicitly gives the shock overpressure, P_s , as a function of the initial sphere pressure P_0 , the ratio of the specific heats, and the ratio of the sound speeds, c ,

$$\frac{P_{sph}}{P_0} = \frac{P_s}{P_0} \left(1 - \frac{(\gamma_s - 1)(c/c_s) \bar{P}_s}{\sqrt{2\gamma_0(2\gamma_0 + (\gamma_0 + 1)\bar{P}_s)}} \right)^{-\frac{2\gamma_s}{\gamma_s - 1}} \quad (28)$$

The subscript "o" refers to conditions in the surrounding air and \overline{P} is the dimensionless shock overpressure which is given by $(P/P_o - 1)$. The initial mixture consists mainly of air so $\gamma_o = 1.4$. The speed of sound in air at 298K and 1 atmosphere is taken to be 340 m/s. Inserting these values, along with the values for the sphere gas given in the last section, into equation 28 and iterating for the dimensionless shock overpressure yields a value of 4.2. Therefore, the shock wave produced at the sphere's surface has a shock overpressure of 4.2 atmospheres.

6.1.3 Shock Pressure and Impulse Decay With Distance

The shock wave's strength is maximum at the point where it is generated at the sphere radius. Once the shock wave propagates away from the radius, its strength is attenuated as more volume of gas is pressurized within the shock sphere. Unlike in the problem of a point-source explosion, which lends itself to an analytic solution, the bursting-sphere problem does not have a closed form solution. Numerical studies have been made to determine the shock attenuation as a function of distance for spheres of various initial pressures, temperatures and specific-heat ratios (Boyer et al., 1958; Baker et al., 1983). In these calculations the sphere is treated simply as an interface between the sphere gas and the surrounding gas, i.e. the calculations do not consider the interaction of the gas flow and the sphere glass fragments. These calculations have shown good agreement with experimental results obtained using actual bursting pressurized glass spheres.

Baker et al. (1983) have a graph, reproduced in Figure 15, summarizing the results of their calculations. The graph plots the dimensionless shock overpressure versus the dimensionless-scaled distance, that is defined as

$$\tilde{R} = r \left(\frac{P_o}{E} \right)^{1/3} \quad (19)$$

where r is dimensional distance measured from the center of the sphere, and E is the initial sphere energy. To use the graph, one locates the point that defines the initial shock-wave conditions, which is given by the initial dimensionless shock overpressure and the scaled initial sphere radius. The decay in the shock overpressure is obtained from the graph by following parallel the nearest curve.

The sphere's initial energy is taken to be the total stored chemical energy in the spherical gas cloud. The number of moles of ethane in a 100 m³ volume of gas at 1 atmosphere and 298K is

$$n_{C_2H_6} = \frac{PV}{RT} = \frac{(101300)(100.0)}{(8.314)(298)} = 4077 \text{ moles} \quad (30)$$

where R is the Universal Gas constant (8.314 J/mol K). The molar heat of combustion for ethane is determined in a fashion similar to equation 18, i.e.,

$$\Delta H_R = 2(h_f)_{CO_2} + 3(h_f)_{H_2O} - (h_f)_{C_2H_6} = 2(-394) + 3(-242) - (-85) = -1599 \text{ KJ per mole } C_2H_6 \quad (31)$$

where the heat of formation of ethane is taken from Weast (1980). Therefore the initial sphere energy is $4077 \times 1599 = 6519$ MJ, or 1442 kg of TNT. Taking an initial sphere radius of 7.0 m, and energy of 6519 MJ, equation 29 yields a scaled distance of 0.17. Taking the dimensionless initial shock overpressure of 4.2, as calculated in Section 6.1.2, one can now identify the initial condition point in Figure 15. Table 5 gives some sample points taken from Figure 15 for a line starting at the initial condition and running parallel to the nearest curve. Also shown in Table 7 is the nondimensional impulse which is plotted as a function of the scaled distance in Figure 16 (Baker et al., 1983). The nondimensional impulse is given by

$$\bar{i} = \frac{i c_o}{P_o^{2/3} E^{1/3}} \quad (32)$$

from which the dimensional impulse can be obtained.

Table 7: Decay in the shock overpressure and impulse with distance

Shock Radius (m)	\bar{R}	\bar{P}_s	Dimensionless Shock Impulse	Shock Impulse (Ns/m ²)
7.0	0.17	4.2	.39	4656
7.1	0.18	4.0	.35	4179
7.9	0.20	3.6	.27	3224
9.0	0.22	3.4	.25	2985
9.5	0.24	3.1	.23	2746
11.8	0.29	2.5	.17	2030
12.2	0.30	2.4	.16	1910
14.0	0.35	2.1	.14	1672

The shock loading that a rigid wall will experience depends on the orientation of the shock wave relative to it. If the shock wave propagates parallel to the wall, it will experience the static pressure behind the wave, also referred to as the side-on pressure. If the shock wave is reflected off the wall, it will experience a dynamic pressure, which is associated not only with the shock wave but also with the deflection of the flow behind the shock wave. The maximum shock loading on a wall occurs when the shock wave is reflected normally. In this case, all the flow behind the shock wave is stopped, and the pressure is considerably higher than the side-on pressure. At the acoustic limit, associated with very weak shock waves, the reflected shock overpressure is twice the side-on shock overpressure; for very strong shock waves, the amplification can be eight times as high. The dimensionless, normally reflected shock overpressure, is related to the dimensionless side-on shock overpressure by the following expression (Baker et al., 1983)

$$\bar{P}_R = 2\bar{P}_s + \frac{(\gamma+1) \bar{P}_s^2}{(\gamma-1) \bar{P}_s + 2\gamma} \quad (33)$$

For oblique shock reflections, the ratio of the reflected and incident shock overpressures is also a function of the angle of incidence, which is defined as the angle between the incident shock and the reflecting wall, e.g., for a normal reflections the incident angle is zero. For incident angles greater than 40 degrees a complex shock reflection phenomenon, referred to as Mach reflection, occurs. For incident angles less than 40 degrees

one can use equation 33 to predict the reflected shock overpressure (Baker et al., 1983). Table 8 gives the reflected shock overpressure calculated using equation 33 for the incident shock overpressure given in Table 7 at various distances. Also given in Table 8 is the reflected shock impulse which is taken to be proportional to the ratio of the reflected and incident shock pressure.

Table 8: Decay in the reflected shock overpressure and impulse with distance

Shock Radius (m)	\bar{P}_i	\bar{P}_R	Reflected Shock Impulse (KNs/m ²)
7.0	4.2	17.9	16.9
7.1	4.0	16.7	14.8
7.9	3.6	14.5	10.9
9.0	3.4	13.5	9.8
9.5	3.1	11.9	8.6
11.8	2.5	9.0	5.8
12.2	2.4	8.5	5.3
14.0	2.1	7.1	4.4

The nondimensional incident and reflected shock overpressure from Table 8 is plotted and curve fit as a function of distance in Figure 17. The curve fit for the reflected overpressure is

$$\bar{P} = 4.127 + 11.197e^{-\frac{(R-7.864)}{4.668}} \quad (34)$$

where R is dimensional distance from the sphere center.

6.1.4 Wall Averaged Shock Wave Pressure

The shock wave produced by the explosion of the spherical cloud is also spherical in geometry, e.g., shock sphere. Therefore, the loading on a planar surface, i.e., the Mucan plate and block shield wall, is not uniform. The incident angle and strength of the shock wave that reflects from each point on the surface with a different

distance from the center of the sphere is different. The shock wave is strongest at the closest point on the planar surface to the sphere center. The distance from the sphere center to the closest points on the block wall and the Muon plate are 7.9 m and 7.1 m, respectively. Note, the sphere is not centered vertically with either the block wall or the Muon plate.

Calculating the average pressure on a planar rectangular surface such as the block wall or Muon plate is difficult since the pressure drops off radially from the point of maximum pressure on the plate (i.e., shortest distance to sphere center) and this point of maximum does not correspond to the center of the plate. The approach taken here is to define an equivalent circular area and determine the average pressure using the shock wave decay data from Figure 17 to get a pressure plate-radius profile. The average pressure on the plate is obtained by integrating the pressure over the plate area and dividing by the plate area, i.e.,

$$P_{avg} = \frac{2\pi \int_0^R P(r) r dr}{\pi R^2} \quad (35)$$

where r is the radial distance from the center of the circular plate, R is the radius of the circular plate, and $P(r)$ is the pressure-radius profile on the plate. The function $P(r)$ is obtained by obtaining the reflected shock overpressure at several radii on the circular plate, using the distance from the cloud center to the radius r on the circular plate and equation 34.

Block Wall

The area of the block wall exposed to the blast wave is $14 \times 18.6 = 260.4 \text{ m}^2$ which yields an equivalent circular area with radius 9.1 m which is a distance of 7.9 m from the center of the cloud. Therefore, the distance from the cloud center to the edge of the circular plate is 12.1 m. The reflected shock overpressure as a function of plate radius is given in Figure 18 (note: r is not the distance from the sphere center). The data was curve fit to give

$$P(r) = 15.244 - 0.0313r - 0.1537r^2 + 0.00847r^3 \quad (36)$$

Performing the integration shown in equation 35 yields an average pressure of 11.2 atm. The corresponding average impulse is obtained by interpolation in Tables 8 to give 7.9 KNs/m².

Muon Plate

The area of the Muon plate is 10.7x13.1= 140.2 m² which yields an equivalent circular area with radius 6.7 m which is a distance of 7.1 m from the center of the cloud. Therefore, the distance from the cloud center to the edge of the circular plate is 9.8 m. The reflected shock overpressure as a function of plate radius is also given in Figure 18. The data was curve fit to give

$$P(r) = 17.3206 + 0.0134r - 0.2271r^2 + 0.0145r^3 \quad (37)$$

Performing the integration shown in equation 35 yields an average pressure of 14.0 atm. The corresponding average impulse, obtained by interpolation, is 10.4 KNs/m².

6.1.5 Quasi-static Pressure Decay

As described in the previous sections, the expansion of the high pressure spherical gas cloud produces a shock wave which propagates radially outwards and reflects off the first Muon plates and the block shield wall. The reflected shock wave then propagates across the IR and reflects off the opposite wall. During this transit the shock wave weakens due to nonisentropic effects associated with shock compression. These reverberations continue until the shock wave energy is dissipated into the IR gas. While the shock wave reverberations are occurring the spherical gas cloud expands such that the extent of the cloud increases and the average cloud pressure decreases. As the cloud volume increases it pressurizes the air in the IR which was outside the boundary of the initial gas cloud. Under normal conditions, as the air outside the gas cloud is compressed it starts to vent out of the IR. For this analysis it is assumed, conservatively, that venting does not start until the gas cloud expansion is complete. An estimate of the IR average pressure at that point can be obtained simply by adding the initial stored chemical energy in the ethane into the full gas volume of the IR, which includes all the ethane and air. This is possible because the energy carried away by the shock wave from the gas cloud is returned to the gas as a result of the nonisentropic shock reverberations. One can assume that all the shock energy is returned to the gas on a time scale which is comparable with the expansion

of the cloud to the full volume of the IR. If the energy is released isentropically, the maximum IR pressure is equal to the constant volume pressure for the ethane-air mixture corresponding to the dispersion of the full ethane inventory into the IR, i.e., 2.9% ethane. From Figure 3, a 2.9% ethane in air mixture yields a pressure of 6.2 atm. The IR then depressurizes with the venting of the gas through the natural fixed and variable vent areas outlined in Section 5.1.1.

Fixed IR Vent Area and Volume

The IR pressure decays exponentially starting from an initial pressure of 6.2 atm. The blowdown duration, which is the time required for the IR pressure to drop to atmospheric pressure, is a function of the IR volume, surface area and the speed of sound of the gas being vented. The scaled blowdown duration, τ ,

$$\tau = \frac{r c_o A_v}{V} \quad (38)$$

is plotted as a function of the normalized initial pressure in Figure 19, which is given in Baker et al. (1983) for a fixed vent area. For a scaled initial pressure of 6.2, Figure 19 yields a value of 0.85 for the scaled blowdown duration. Using the volume and fixed vent areas determined in Section 5.1.1, e.g., $V = 3350 \text{ m}^3$ and $A_v = 17.1 \text{ m}^2$, and a speed of sound of 821 as calculated from STANJAN for a constant volume combustion process for a 2.9% ethane in air mixture yields a blowdown duration of 0.203 s.

A model was developed to predict the pressure time history for a vented volume with fixed volume and vent area to compare with Baker's prediction. The model is outlined in detail in Appendix D where the final expression for the pressure time history is given by

$$\frac{P}{P_i} = \left[1 + \frac{A_v c_o t}{V} \left(\frac{\gamma-1}{2} \right) \left(\frac{\gamma+1}{2} \right)^{\frac{\gamma+1}{2(\gamma-1)}} \right]^{\frac{2\gamma}{1-\gamma}} \quad (39)$$

where P_i is the initial volume pressure. One can see that equation 39 has the same parameter grouping used in Baker's expression given in equation 38. For a fixed vent area of 17.1 m^2 and a specific heat ratio of

1.26, as calculated using STANJAN for the product gas condition after a constant volume burn of a 2.9% ethane mixture, equation 39 reduces to

$$\frac{P}{P_i} = \left[1 + \frac{(17.1)(821)P}{3350} (0.13)(1.13)^{-4.35} \right]^{-9.89} = [1 + 0.320t]^{-9.89} \quad (40)$$

Using equation 40, the time for the IR pressure to drop from an initial pressure of 6.2 atm to a pressure of 1 atm is 0.647 s, which is almost 3 times the blowdown time predicted using Baker's method.

Variable IR Vent Area and Volume

In reality, during the IR blowdown the pressure induces motion in the block shield wall which creates a variable vent area between the top edge of the wall and the IR building. Furthermore, as the wall moves, the effective volume of the IR increases. Both these parameters enhances the pressure drop rate in the IR. A second blowdown model, given in Appendix E was developed to include these effects. The model requires the integration of the following equation

$$\frac{dP}{dt} = -\rho^{-\frac{1}{2}} P^{\frac{3}{2}} \left(\frac{A_v}{V} \right)^{\frac{3}{2}} \left(\frac{2}{\gamma+1} \right)^{\frac{\gamma+1}{2(\gamma-1)}} - \frac{P}{V} \frac{dV}{dt} \quad (41)$$

where the last term is attributed directly to the change in volume of the IR as the wall moves forward. The vent area A_v includes the fixed vent area in addition to the variable vent area and the volume V is equal to the initial IR volume plus additional volume created by the motion of the wall. These two variable components of the vent area and the IR volume are obtained from the wall displacement.

6.1.6 Wall Response to Shock Loading and Blowdown

In this section the response of the block wall to the pressure loading associated with the blast wave calculated in Section 6.1.4 and the blowdown calculated in section 6.1.5 will be investigated. These two loadings occur, to a certain extent, simultaneously. In this analysis they will be treated sequentially. Recall from equation 6, the minimum IR overpressure required to translate the wall is 0.273 atm. In this scenario the IR pressure is almost always well above this value so the wall does translate. Note, that since there is also a rotational

torque on the wall, see equation 10, the wall will also rotate. For simplicity only the translational motion is modeled here. The translational motion of the wall, which is treated as a single unit, is calculated using Newtons Law, applied in the direction of motion, to give

$$\frac{d^2(X_w)}{dt^2} = \left(\frac{A_w}{M_w}\right) \Delta P - \mu_w g \quad (42)$$

where the two external forces acting on the wall are the pressure force and friction force which is taken to be proportional to the weight of the wall. The wall coefficient of friction is taken to be 0.7. Integration of equation 42, with a linearly decaying pressure, i.e., $P = P_m - kt$, yields the wall velocity

$$V_w = \left(\frac{A_w}{M_w}\right)\left(P_m t - \frac{kt^2}{2}\right) - \mu_w g t \quad (43)$$

and integration of equation 43 yields the wall displacement

$$X_w = \left(\frac{A_w}{M_w}\right)\left(\frac{P_m t^2}{2} - \frac{kt^3}{6}\right) - \frac{\mu_w g t^2}{2} \quad (44)$$

Wall Motion Due to Blast Loading

The wall motion due to the blast loading can be calculated using equation 42 with a specified pressure-time profile. From Section 6.1.4 the peak average wall pressure is 11.2 atmospheres and the impulse is 7.9 KNs/m². For simplicity we will assume a linear decaying pressure, i.e., $P = P_m - kt$, where P_m is the peak wall averaged shock pressure, and the constant k is given by

$$k = \frac{P_m}{\tau} = P_m \left(\frac{P_m}{I}\right) \quad (45)$$

where τ is the time for the pressure to drop to 1 atmosphere and I is the impulse. Substitution of the peak wall pressure and the impulse into equation 45 yields a value of 81470025 for k and 0.0139 s for τ . Taking

this value of k , equations 43 and 44 yield a wall velocity and displacement of 1.86 m/s and 0.017 m. If there was no pressurization of the IR, the kinetic energy gained by the wall would be expended in doing work against friction. The total displacement of the wall would be 0.252 m.

Wall Motion Due to Blowdown Loading

In order to determine the wall motion, equations 41 and 42 are integrated simultaneously using MathCad, see Appendix F for the MathCad worksheet (PHENIX 2). The physical dimensions used in the calculations are the same as those used in Section 5.1.4. The following list provides the initial gas blowdown condition obtained from STANJAN by calculating the product gas condition for a constant volume combustion of a 2.9% ethane in air mixture:

Initial Pressure = 6.2 atm

Initial speed of sound = 821.4 m/s

Ratio of specific heats = 1.26 (treated as constant)

The initial wall velocity and displacement, taken from the results of the blast loading, are 1.86 m/s and 0.017 m, respectively. Figure 20 gives plots of the predicted time histories of the IR pressure, block wall velocity and displacement. Included in the pressure plot is the Baker prediction (see PB curve) and the prediction based on fixed vent area and IR volume from equation 40 (see PP curve). From the pressure plots it is clear that including the variable vent area and volume has a great effect on the blowdown rate. For the variable case, the pressure drops from its initial value to atmospheric pressure in about 0.264 s. By this time the wall has already moved 3.0 m and acquired a velocity of 15.2 m/s. From this time on, there is no net pressure acting on the wall and it comes to rest due to the retarding frictional force. The final displacement of the wall is roughly 20 m. Realistically, by a combination of the torque on the wall and the limited sill width on which the wall stands, the wall would collapse before achieving such a displacement.

6.1.7 Muon Plate Response to Shock Loading

In this section the response of the nearest Muon plate to the blast loading given in Section 6.1.4 will be discussed. The time required to equilibrate the pressure on either side of the Muon plate is given roughly by the round trip time for a sound wave to propagate from the edge of the plate to the center and back to the edge

of the plate. This transit time is about 0.031 s which is longer than the blast duration. Therefore, the pressure difference across the Moon plate can be taken to be the blast overpressure. The Moon plate is anchored at the bottom and only lightly held in place at the top. For the analysis, it is assumed that the constraint on the top is relieved instantaneously and the plate pivots about the front bottom edge. An expression for the angular acceleration of such a plate, for small angles, is given in Appendix B and equation 10. Simplifying for a slender plate and considering a linearly decaying pressure, yields the following expression for the plate tilt angle

$$\theta = \frac{FA_{mp}}{\frac{1}{3}M_{mp}H^2} \left(\frac{P_{av}t^2}{2} - \frac{kt^3}{6} \right) \quad (46)$$

where H is the plate half height, P_{av} is the peak average blast pressure calculated to be 14 atm in Section 6.1.4, k is defined in equation 45. From Section 6.1.4 the impulse is 10.4 KNs/m², which yields a value of 96696694 for k and τ is 0.0147 s. Taking values of 140.2 m² for the plate area and 109059 kg for the plate mass, equation 46 yields a tilt angle of 0.073 radians (4.2 degrees) at the end of the blast loading. The plate stability tilt angle is only 0.5 degrees, so the plate topples over.

6.1.5 Conclusions

The response of the block shield wall and the closest Moon plate to a theoretical worst case accident is presented. The accident scenario considered is considered theoretical since nonphysical assumptions are made concerning the mixing of the ethane with the air to form a uniform mixture with the most reactive composition. Furthermore, the combustion of this unconfined mixture is assumed progress at an infinite rate. The analysis demonstrates that under these assumptions, the block wall collapses and the Moon plate topples over creating a domino effect whereby all the plates would topple over and end up against the IR wall. Both these outcomes are confined to Building #1008. The analysis also shows that the block wall is influenced more by the longer duration IR blowdown than the blast wave loading and therefore the wall acts as a blast shield as well as a missile shield for the inhabited sections of Building #1008.

6.2 Explosion in the North and South Mezzanines

In this analysis we concentrate on the effect of an explosion on the block shield walls in the North and South Mezzanines. As in the last section, many conservative nonphysical assumptions are made, classifying this accident scenario as a theoretical worst case for the block walls in the Mezzanines. Since the analysis shows that even with these extreme assumptions, the effect on the walls is minimal, one can conclude that under more realistic accident conditions the effect on the walls would be minimal.

6.2.1 Description of Phenomenon

Any accident scenario involving PHENIX must originate within the IR since the combustible gas and ignition sources are an integral part of the detector. Any involvement of the Mezzanines is through the venting of either burned or unburned gas from the IR through the fixed vents, i.e., gap between the last Muon plate and the IR wall. In the case of the theoretical accident scenario of Section 5, only combustion product gas would be vented into the Mezzanine and RHIC tunnels since the combustion of the ethane is assumed instantaneous. Under this scenario the only pressurization of the Mezzanines would be due to the pressure drop associated with the flow of the combustion products through the Mezzanines and down the tunnel, and there would be no secondary explosion in the Mezzanines. Under the DBA described in Section 4, the venting of the IR takes place in two steps; 1) unburned combustible gas is vented due to pressurization of the IR and gas displacement caused by the flame ball, and 2) burned gas is vented due to pressurization of the IR. Unburned gas vented into the Mezzanine could then be ignited by the flame which precedes the venting of the burned gas. If one considers the DBA, unburned gas is vented into the Mezzanines at relatively low flow rates since the pressurization of the IR is very low, see Appendix A equation 7. The flow velocity through each vent area starts at practically zero increasing proportionally to the IR pressure. For example, for the DBA with the IR uniformly mixed with 3% ethane, at its peak, when the flame reaches the walls and the pressure is 1.057 atm, the flow velocity is about 10 m/s. In the worst case, where the burning involves a stoichiometric mixture, the flow velocity at each vent area is about 30 m/s.

As the unburned gas is vented, it mixes with air in the Mezzanines due to turbulence generated by the vent flow. The degree of mixing depends on the vent area flow velocity. For a very low flow velocity the mixing is very small and essentially a "slug" of vented gas forms in the Mezzanines. For a higher flow velocity, the degree of mixing is higher and the vented gas is diluted with air. Since the higher vent area flow velocity is

associated with the venting of a more reactive mixture, i.e., higher ethane concentration, this process is self limiting since these are the mixtures which would result in the most air dilution.

Once the flame reaches the vent area, if the cloud formed in the Mezzanine is within the flammability limits, it is ignited. The reaction rate depends on the composition of the cloud and the level of turbulence within the cloud. This reaction rate determines the peak pressure which is generated in the Mezzanines. The impulse delivered to the Mezzanine block walls depends on the volume of the mixture that burns. For example, if a small cloud of very reactive mixture burns the peak pressure may be high but the impulse will be low. This volume depends on the composition of the combustible mixture in two ways: 1) the higher the ethane concentration, the smaller the cloud size is in the IR (since there is less air mixed with the 100 m³ of ethane), and 2) the higher the ethane concentration, the higher the burning rate, the higher the pressurization in the IR and thus more gas is burned in the IR and less is vented into the Mezzanines.

For the analysis, all the assumptions made are very conservative and often nonphysical. The above discussion of the phenomenon makes it clear that the conservative choice of the mixture composition is not straightforward since there are many competing effects. For this analysis it will be assumed that a nonphysical spherical cloud mixture containing 7% ethane forms in the IR. Recall, this is the ethane-air mixture with the highest constant volume pressure. This cloud then burns at a nonphysically slow rate, i.e., no IR pressurization, so as to maximize the amount of the gas cloud which is displaced into the Mezzanines. This displaced gas cloud does not mix with the air in the Mezzanine and then burns at infinite rate producing the constant volume pressure for the mixture. This last assumption is non physical since the constant volume pressure infers a burn with very high turbulence which contradicts the assumption of no mixing of the displaced cloud and the Mezzanine air. The combustion of the displaced, undiluted cloud produces an equal volume of high pressure and temperature gas in the Mezzanine which then expands into the RHIC tunnel. During this expansion the Mezzanine block walls are exposed to the high pressure of the cloud and are free to move.

6.2.2 Pressurization in the Mezzanines

For a mixture of 7% ethane in air, the spherical cloud volume in the IR is 1423 m³, see Section 5.1.4. For a constant pressure burn, for this mixture the ratio of the specific volumes across the flame is 7.82. That is for every 1 m³ of mixture burned 7.82 m³ is produced. Therefore, in order to fill the IR volume of 3350 m³ with

burned gas 428 m³ of the cloud must be burned. This leaves 1000 m³ of the cloud to be displaced into the two Mezzanines. The cross-sectional area of both Mezzanines are 52.4 m². The vent areas on the south and north side are 9.3 and 7.8 m², respectively. Therefore, assuming a slug flow into the Mezzanines where the back of the cloud is confined by the last Muon plate, the cloud length on the south and north sides are 10.4 and 8.7 m, respectively. As calculated using STANJAN, the constant volume gas condition for a 7% ethane in air mixture is: 9.4 atm pressure, 990 m/s speed of sound, and 1.21 for the ratio of specific heats. As in the case of a bursting sphere, a shock wave is formed moving away from the cloud. Expansion waves, traveling at the local speed of sound, propagate into the high pressure region. In this way the pressure in the cloud is progressively lowered starting at the free end (i.e., tunnel side). The expansion waves eventually reach the closed off end of the cloud. At that point they reflect and propagate back to the free end all the time continuing to lower the pressure. Typically the expansion of a region requires a round trip for a wave propagating at the speed of sound. This time for a 10 m long cloud is roughly 0.010 s.

An exact determination of the pressure time-history can be obtained by numerical analysis using the method of characteristics. A sample 1-D expansion problem using this technique for a retracting constant velocity piston (Mach number of 0.5) inside of a pipe is given in Thompson (1972). The retracting piston problem is similar to the problem of the sudden expansion of a 1-D high pressure gas region. The expansion of such a high pressure gas region produces shock wave followed by a contact surface which propagates at a velocity equal to the gas velocity behind the shock wave. This contact surface propagates at a constant velocity until the first reflected expansion wave catches up to it. In effect, the contact surface acts like a piston pushing the shock wave forward and increases the volume of the high pressure gas behind. The velocity of the contact surface, or equivalently the gas velocity behind the shock wave, can be determined by calculating the shock strength produced by the expansion of the high pressure gas region. Using equation 28, the shock wave overpressure is 3.8 atm. Using standard 1-D normal shock jump relations (Thompson, 1972) this corresponds to an absolute gas velocity of 440 m/s, or Mach number of 0.45, directly behind the shock wave. This value is close enough to the Mach 0.5 value used in the sample problem so that we can use the results from this problem directly. Using the results from the sample problem, the pressure time history at three axial points within the cloud were determined. Taking the cloud length to be 10 m (representative of the north and south Mezzanines), the pressure time history at the closed end of the cloud, free end and at the midpoint are given in Figure 21. The pressure at the free end immediately drops from 9.4 atm to 4.5 atmospheres and the pressure at the closed end remains at 9.4 atm until the first expansion wave from the free end arrives at roughly 0.010 s. The pressure time histories are integrated to give the impulse, which is given

in the Figure 20. The maximum impulse occurs at the closed end which corresponds to the portion of the wall bordered by the last Mueon plate. For the analysis we will assume the entire wall is exposed to this pressure loading. As shown in Figure 21, the pressure time history at this point has two parts, in the first 0.010 s the pressure remains constant at the value of 9.4 atm, after 0.010 s the pressure drops exponentially. This second part of the curve is curve fit in Figure 22 to give the following compound pressure-time history for the block wall

$$P = \begin{cases} 9.43 & 0 < L/c < 0.010 \text{ s} \\ 1.582 + 7.714 e^{-2625 t} & 0.010 < L/c < 0.030 \text{ s} \end{cases} \quad (47)$$

where L is the slug length, c is the speed of sound (990 m/s), and P is in units of atm. Note the sample problem solution ends at roughly 0.020 s, but is extended here for longer times. Note the exponential curve fit asymptotes to 1.582, so the pressure never drops to atmospheric. In order to overcome this, the pressure is assumed to drop to 1 atmosphere at 0.030s.

6.2.3 Wall Response

The wall motion is modeled using equation 43 with the pressure time history given in equation 48. No credit is taken for variable venting which occurs once the top of the wall moves

North Mezzanine

The length of the cloud in the North Mezzanine is taken to be 8.7 m long. The wall in this area consists of two separate walls which are placed face to face (modeled as a single unit). The inner wall is constructed from concrete blocks which have a thick steel surface layer. The average density for this wall is taken as 5666 kg/m³ compared to 2408 kg/m³ for the standard blocks which are used on the outer wall and also in the IR. The MathCad worksheet for this calculation is given in Appendix G (PHENIX3b). The predicted wall displacement and velocity is given in Figure 23. At the end of the first 0.009 s, during which the pressure is 9.4 atm, the wall moves 2 mm and attains a velocity of 0.54 m/s. By the end of the pressure loading, at 0.030 s, the wall velocity reaches a maximum of about 0.7 m/s and then starts to slow down due to friction. The wall comes to a stop after traveling a distance of 5.2 cm.

South Mezzanine

The length of the cloud in the South Mezzanine is taken to be 10.4 m long. The wall is constructed from a single row of blocks with an outside steel layer, similar to that found in the North Mezzanine wall. The wall motion is modeled using equation 43 with the pressure time history given in equation 48. The MathCad worksheet for this calculation is also given in Appendix G (PHENIX3a). The predicted wall displacement and velocity is given in Figure 24. At the end of the first 0.011 s, during which the pressure is 9.4 atm, the wall moves 5 mm and attains a velocity of 0.91 m/s. By the end of the pressure loading, at 0.030 s, the wall velocity reaches a maximum of about 1.2 m/s and then starts to slow down due to friction. The wall comes to a stop after traveling a distance of 13.2 cm.

6.2.4 Conclusions

Considering the conservatism of the analysis, wall displacements of 5 and 13 cm can be considered to be acceptable. In the case of the North Mezzanine wall, the structural elements of the adjacent electronics and counting house building would also impede any motion of the wall.

7.0 Summary and Recommendations

The report considers accident scenarios where the PHENIX detector inventory of combustible gas is released into the IR. The release of the full inventory is assumed and an ignition source for the combustible gas mixture is assumed to exist. As a result of these assumptions, it is implied that all of the PHENIX safety systems, which are designed to prevent either from occurring, fail.

The accident scenarios investigated are classified as Design Basis Accident (DBA) and Worst Case Theoretical Accident (WCTA).

For the WCTA, nonphysical assumptions are made to release the maximal energy, thus these results should only be used to provide a perspective for the DBA. For an IR explosion, the block shield wall collapses within the limits of the Assembly Hall excluding any off-site damage. Also, the results indicate that on the time-scale of the explosion the wall remains standing and thereby acts as a blast shield as well as a missile shield for the inhabited parts of Building #1008. For the worst case explosion, in either Mezzanine, the wall displacements are small enough to conclude that the wall would survive any credible explosion in the Mezzanines. The analysis indicates that the blast wave loading is sufficient to topple over the closest Moon Plate. Like a domino effect, this plate would most likely topple over the rest of the plates whereby the last plate would come to rest up against the IR wall.

For the DBA, the analysis assumptions are realistic, and as a result the predictions can be used to make judgements concerning safety system requirements and occupancy limitations. The analysis shows that if the entire combustible gas inventory is released slowly, on a time-scale of hours, such that the IR natural circulation generated by the HVAC system globally mixes the released gas with the existing air to form a uniform mixture, the resulting burn would not topple the block wall over. This is because the natural venting of the IR is sufficient to overcome the low burning rates associated with the low ethane concentration mixture which results. Hypothetically, if a cloud of the correct size and concentration is formed and the ignition time is almost coincident with this release time, the model indicates that the block wall could topple. The requirement for this to occur is that the ethane must be released into the IR, mixed with air and ignited all on a time-scale of tens of seconds. No plausible accident scenarios by which this can occur have been identified.

Based on the analysis described in this report, the results of the DBA analysis indicate that the wall will not topple over, however, the PHENIX group should exercise caution and limit the occupancy of the AH. The justification for this is that there is some degree of inherent uncertainty in the model concerning scaling of the combustion phenomenon. There is also some uncertainty linked to the possibility of producing a higher ethane concentration cloud via some nonidentified accident scenario. The possibility of the North Mezzanine brick wall collapsing due to any credible accident scenario involving the release and ignition of the PHENIX combustibles in the IR is so remote so as not to require any limitations on the occupancy of the electronics and counting house.

8.0 References

- W.E. Baker et al., Explosion Hazard and Evaluation, Fundamental Studies in Engineering, Vol.5, Elsevier Scientific Publishing Company, NY, 1983
- Hoyer et al., "Blast from a Pressurized Sphere", UTIA Report No. 48, Institute of Aerophysics, U. of Toronto, 1958.
- D. Bradley and A. Mitcheson, "The Venting of Gaseous Explosions in Spherical Vessels. II-Theory and Experiment," *Combustion and Flame* 32: 237-255, 1978.
- C. Chan et al., "Influence of Confinement on Flame Acceleration Due to Repeated Obstacles, *Combustion and Flame* 49: 27-39, 1983
- M.W. Chase et al. "JANAF Thermochemical Tables, Third Edition," *Journal of Physical and Chemical Reference Data*, Vol. 14, 1985.
- Factory Mutual, Guidelines for Evaluating the Effects of Vapor Cloud Explosions Using a TNT Equivalency Method, Loss Prevention Data 7-0S, 1994.
- B.J. Hjertager, "Numerical Simulation of Turbulent Flame and Pressure Development in Gas Explosions," *Proceedings of the International Conference on Fuel-Air Explosions*, University of Waterloo Press, 1982.
- J.M. Kuchta, "Investigation of Fire and Explosion Accidents in the Chemical, Mining, and Fuel Industries -A Manual," Bulletin 680, U.S. Bureau of Mines, 1985.
- O. Kunz, "Combustion Characteristics of Hydrogen- and Hydrocarbon-Air Mixtures in Closed Vessels," *Explosion Dynamics Laboratory Report FM98-4*, California Institute of Technology, 1998.
- Liepmann, H.W. and Roshko, A., Elements of Gasdynamics, John Wiley and Sons, Inc., New York, New York, 1967.

Mathsoft Inc., Mathcad7 Professional User's Guide, Cambridge, MA, 1997.

NFPA 68, Guide for Venting of Deflagrations, National Fire Protection Association, Inc., 1994

W.C. Reynolds, "The Element Potential Method for Chemical Equilibrium Calculations: Implementation in the Interactive Program STANJAN Version 3," Dept. Of Mechanical Engineering, Stanford University, Palo Alto, California, 1986.

R.J. Roark and W.C. Young, Formulas for Stress and Strain, 5th ed., McGraw-Hill Book Company, NY, 1975.

R.A. Strelow and R.E. Ricker, "The Blast Wave from a Bursting Sphere," AIChE, 10, pp. 115-121, 1976.

P.A. Thompson, Compressible Fluid Dynamics, McGraw Hill Company, NY, 1972.

R. Weast, CRC Handbook of Chemistry and Physics, 61 Edition, CRC Press, Inc., Boca Raton, Florida, 1980.

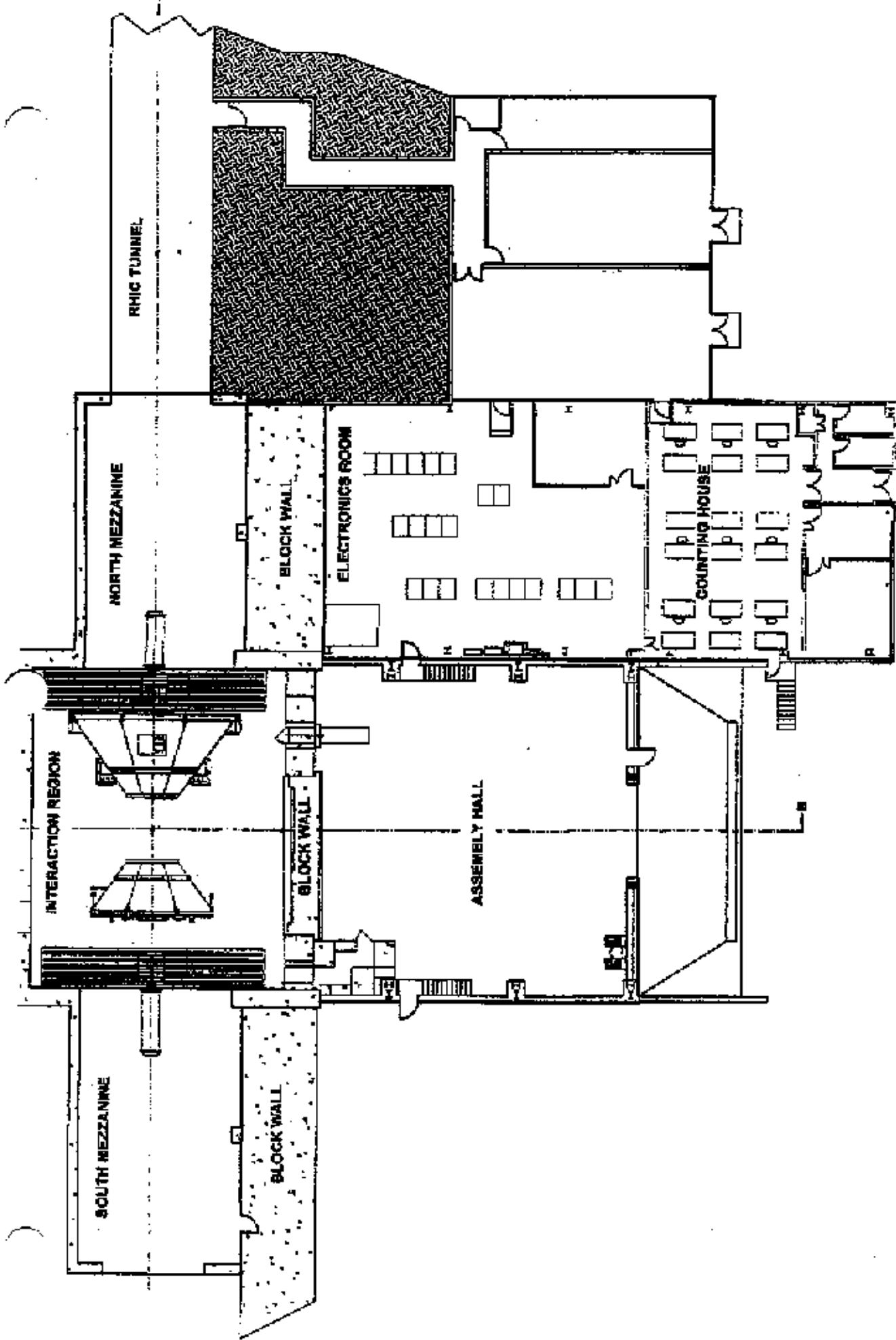


Figure 1: Layout of Building #1006 indicating all the relevant compartments

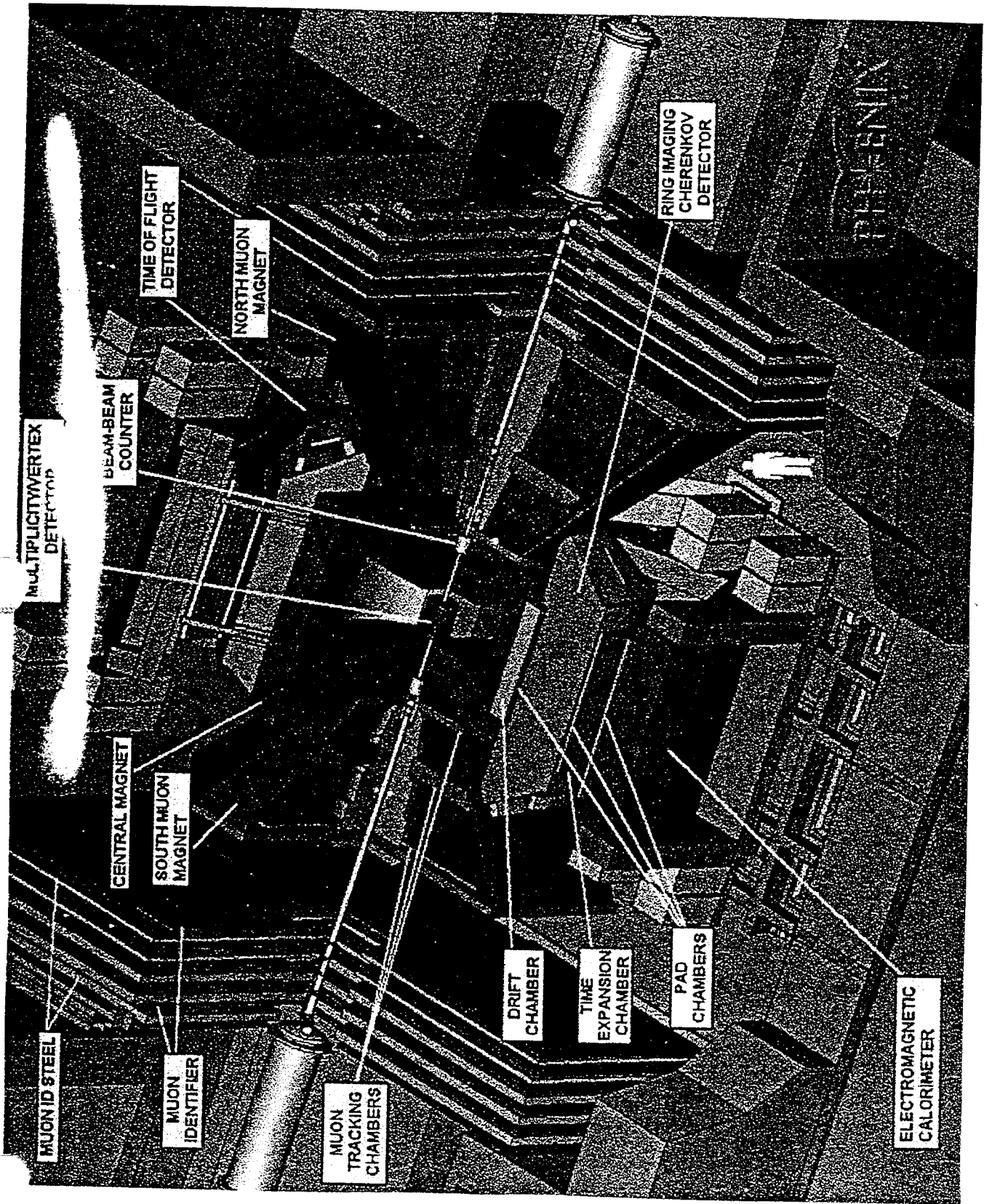


Figure 2: Schematic showing the PHENIX subsystems

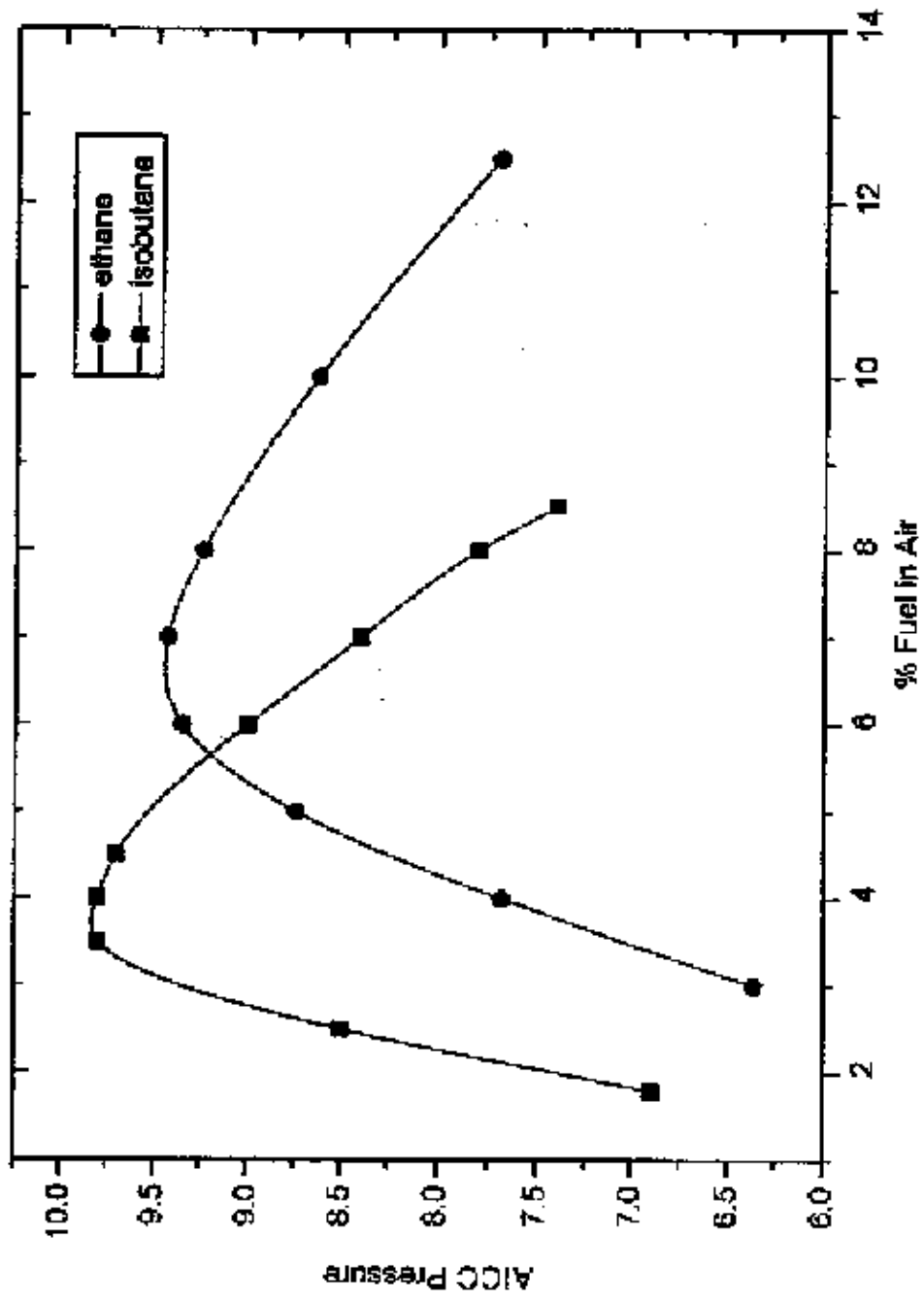


Figure 3: Calculated AICC Pressure vs % Fuel in Air for ethane and isobutane air mixtures

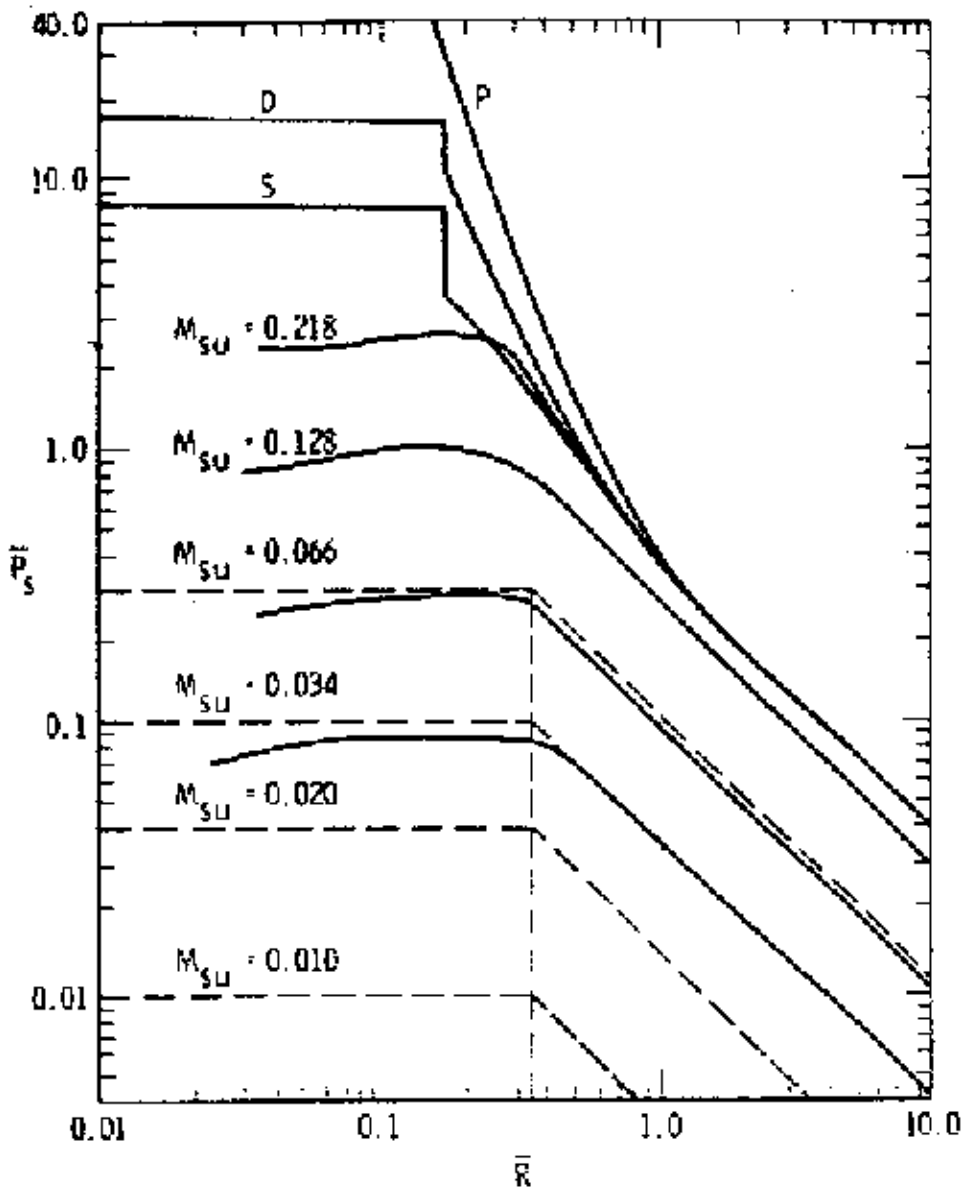


Figure 4: Maximum wave overpressure versus energy scaled distance for deflagrations with various burning rates and for a detonation wave

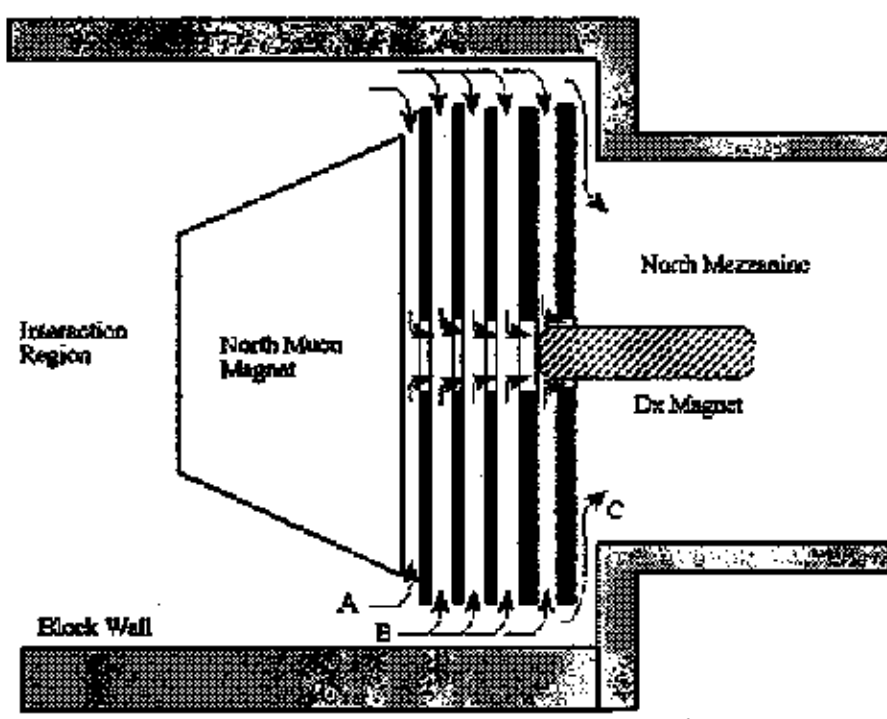


Figure 5: Fixed vent paths through the north Moon plates and IR wall

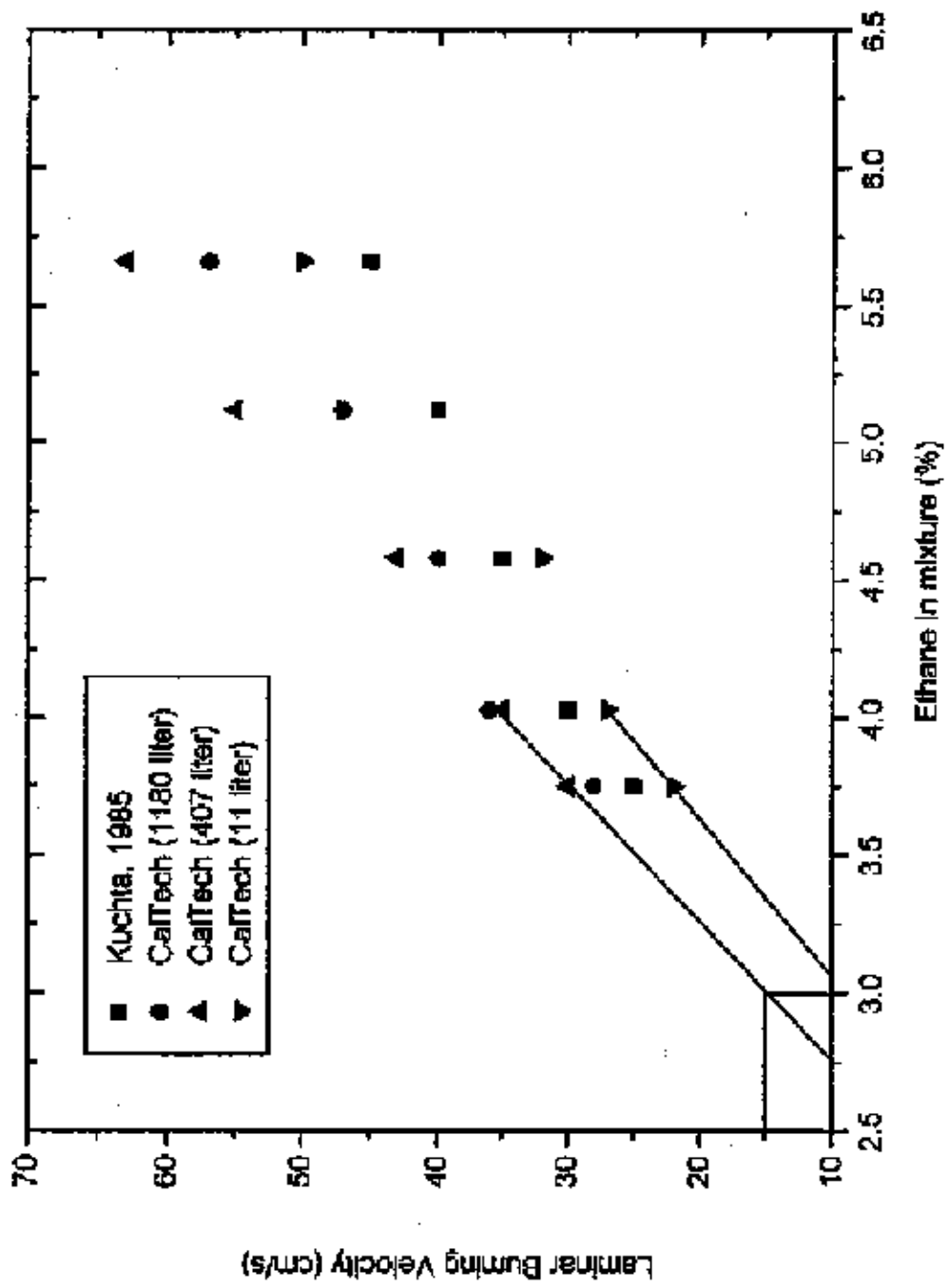


Figure 6: Measured laminar burning velocity in mixtures of ethane-air at 300K and 1 atmosphere

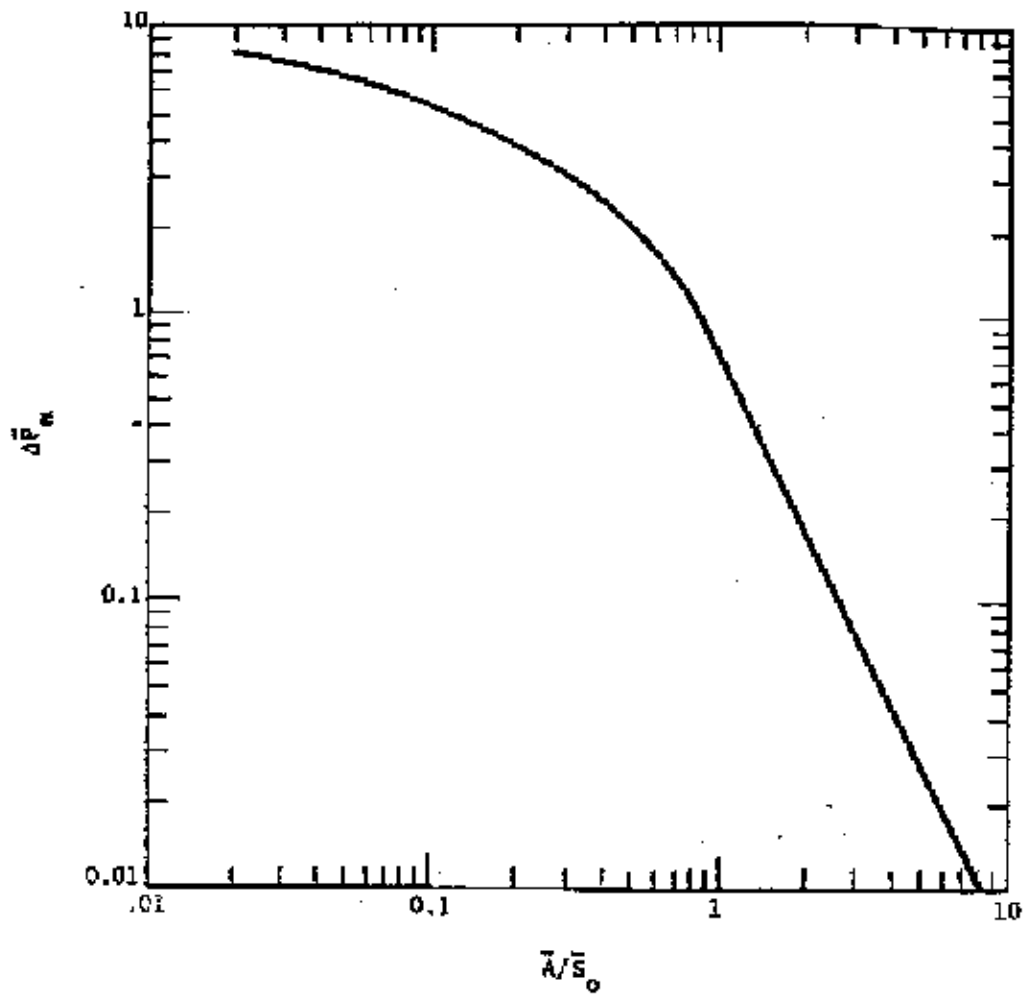


Figure 7: Graph of maximum system pressure versus nondimensional vent parameter
(Bradley and Mitcheson, 1978)

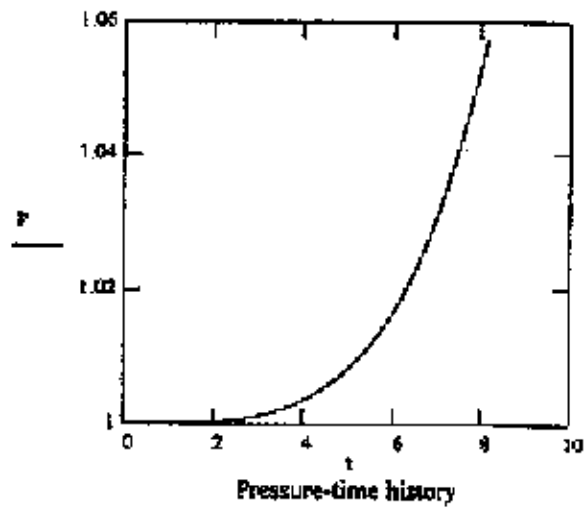
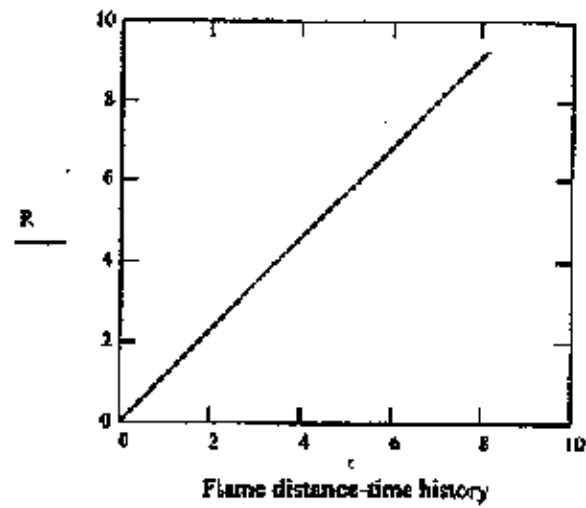


Figure 8: Model predictions for only fixed area venting

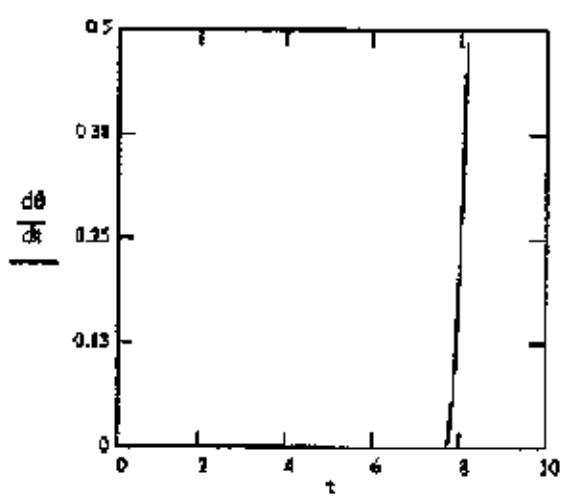
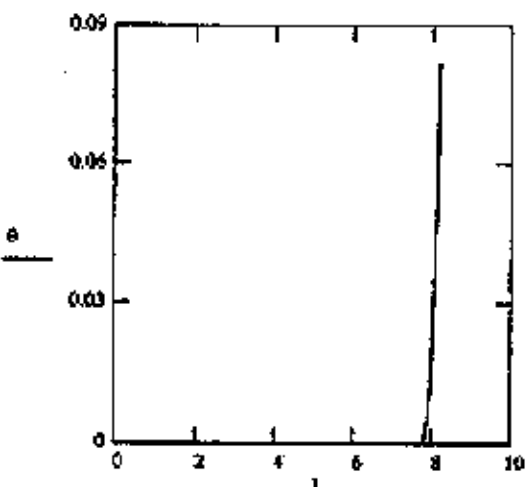
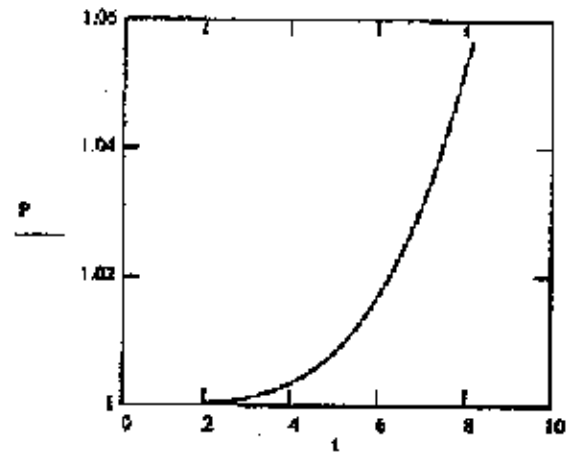
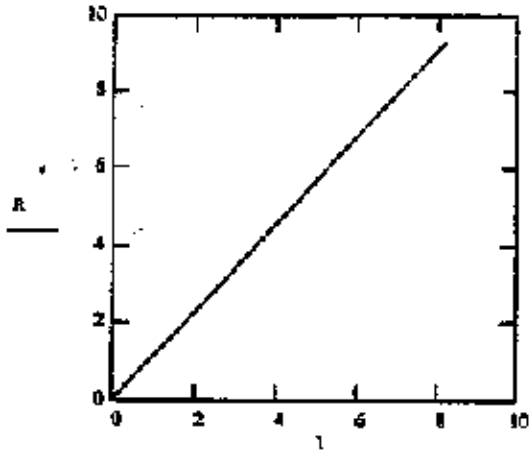


Figure 9: Model predictions for fixed and variable venting, up to time of complete burn

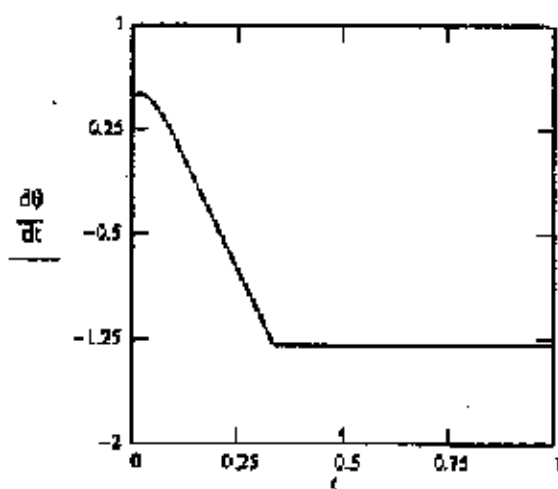
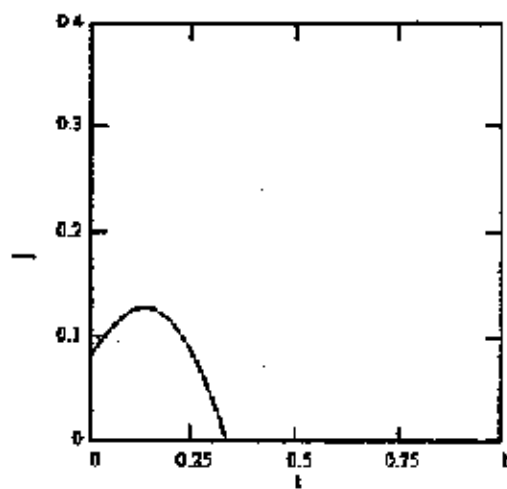
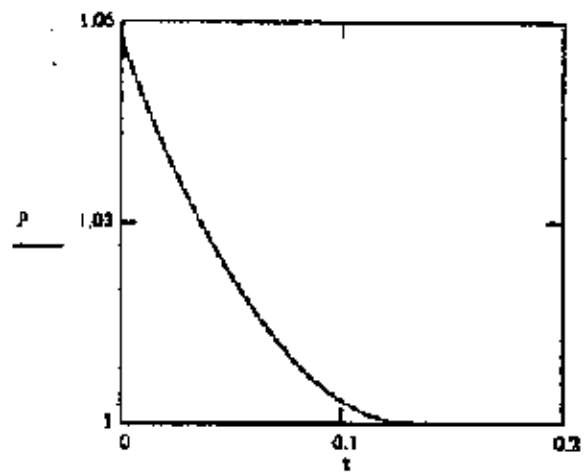
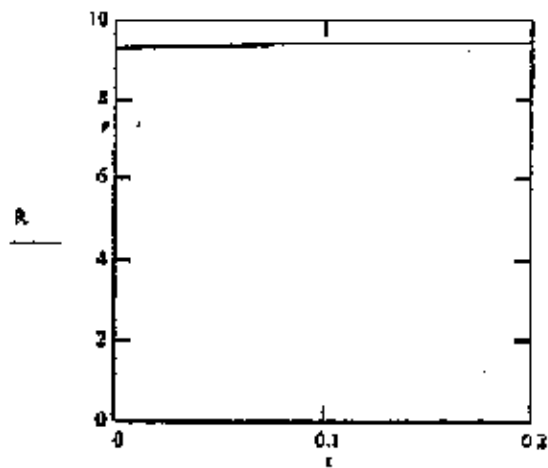


Figure 10: Model prediction with variable and fixed venting, after time for complete burn

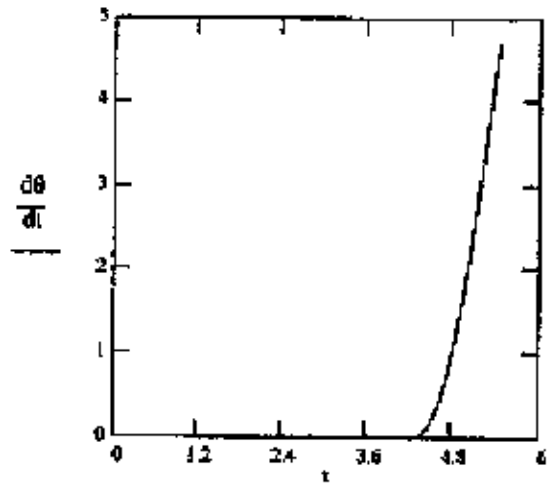
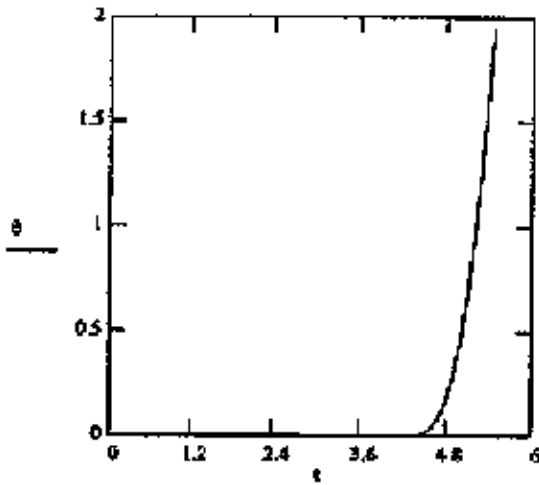
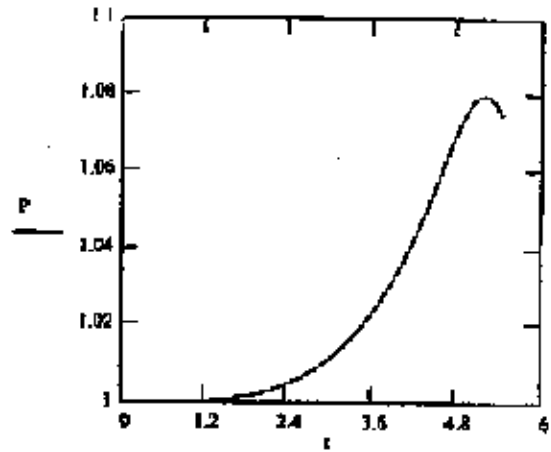
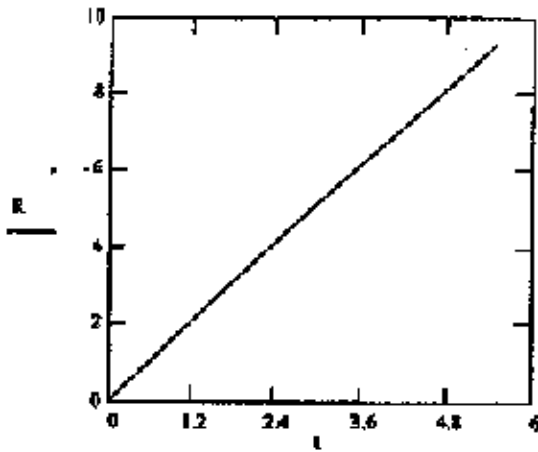


Figure 11: Model predictions enhanced burning, up to time of complete burn

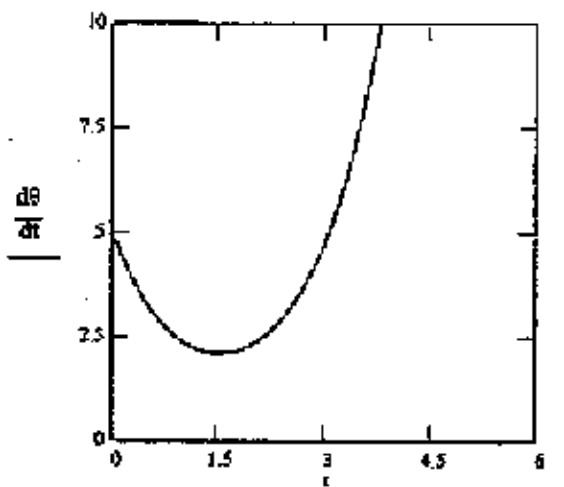
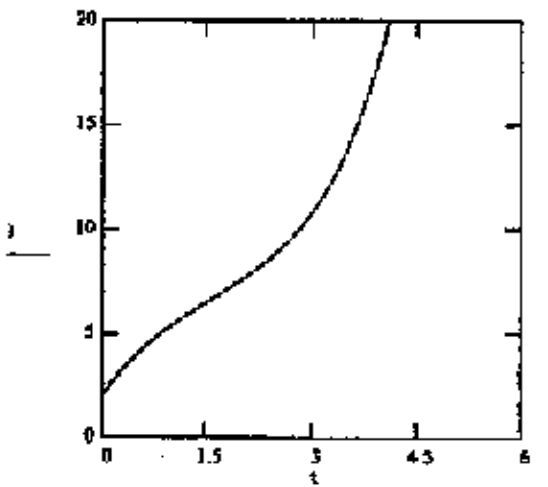
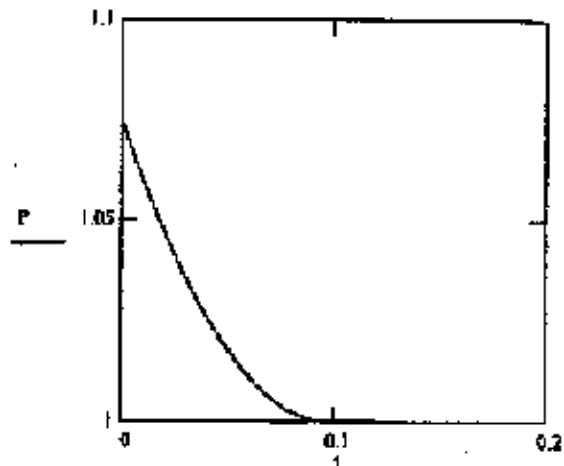
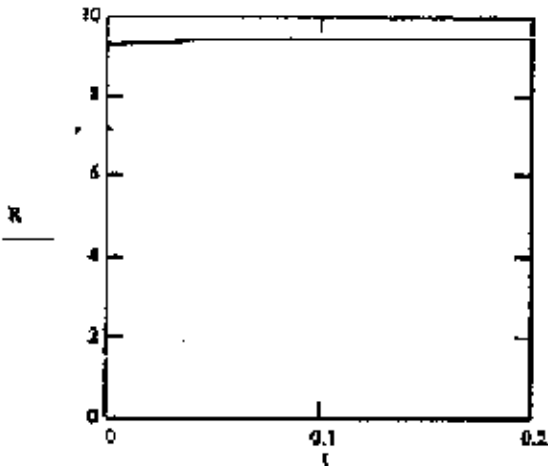
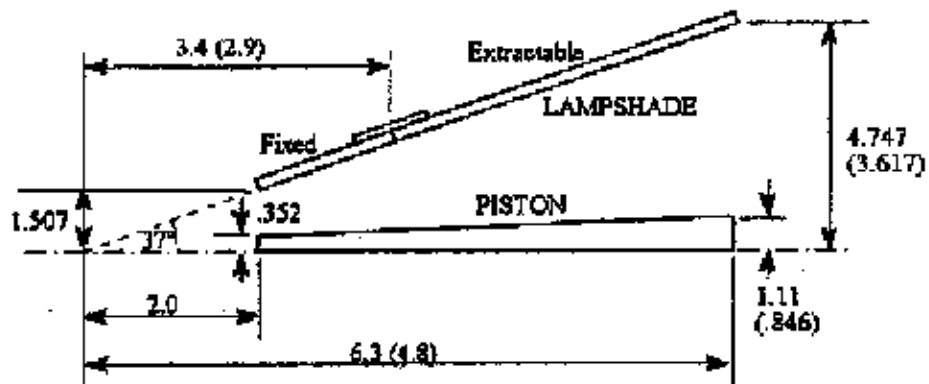
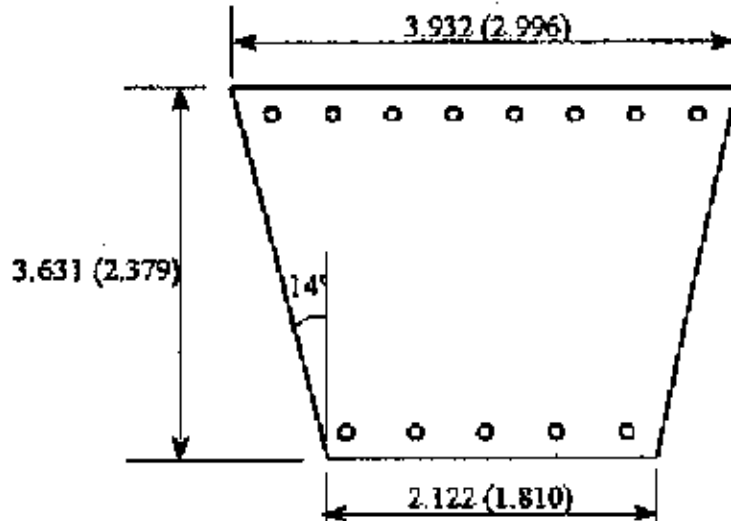


Figure 12: Model prediction with enhanced burning, after time for complete burn.



(a)



(b)

Figure 13: Moon Magnets, (a) X-sectional view, (b) Plan view of retractable lampshade section (small Moon Magnet dimensions in brackets, all dimensions in meters)

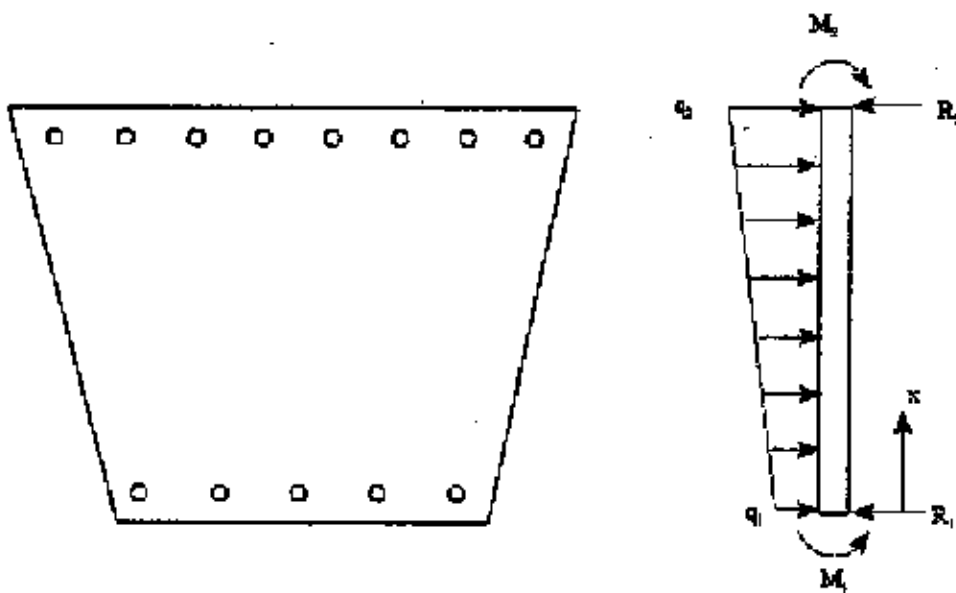


Figure 14. Free body diagram of the simulated lampshade plate

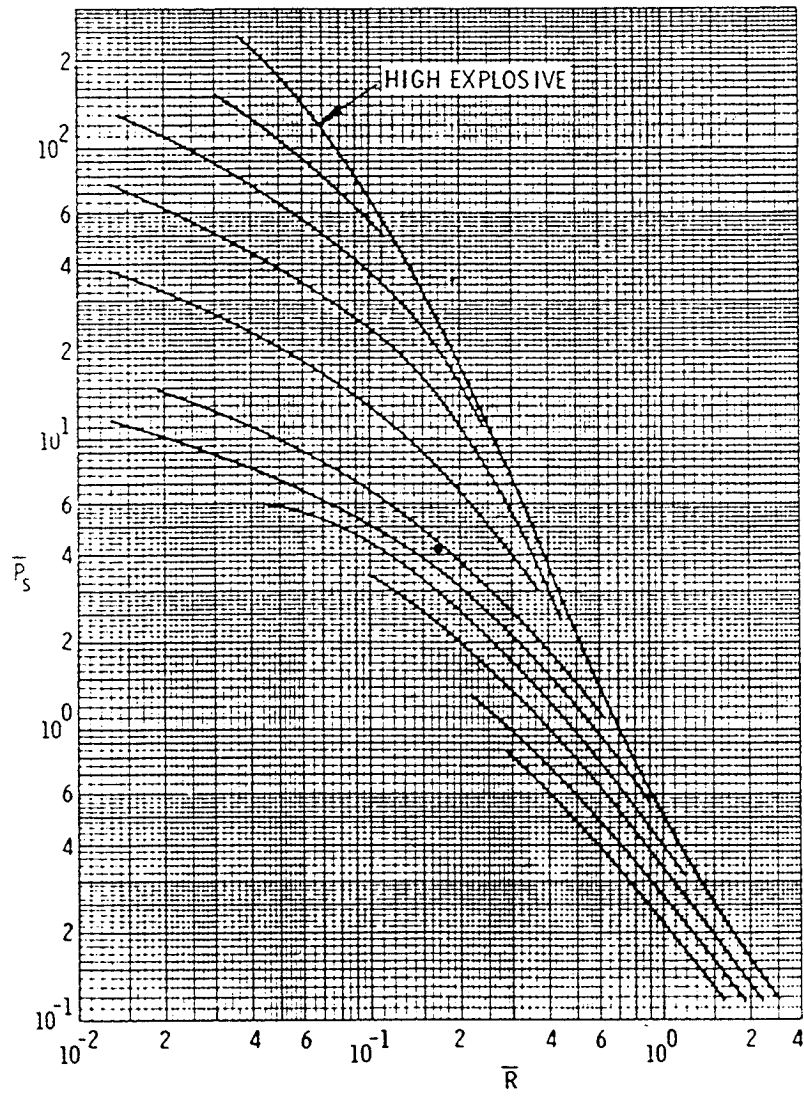


Figure 15: Shock overpressure decay with distance for bursting sphere (Baker et al., 1983)

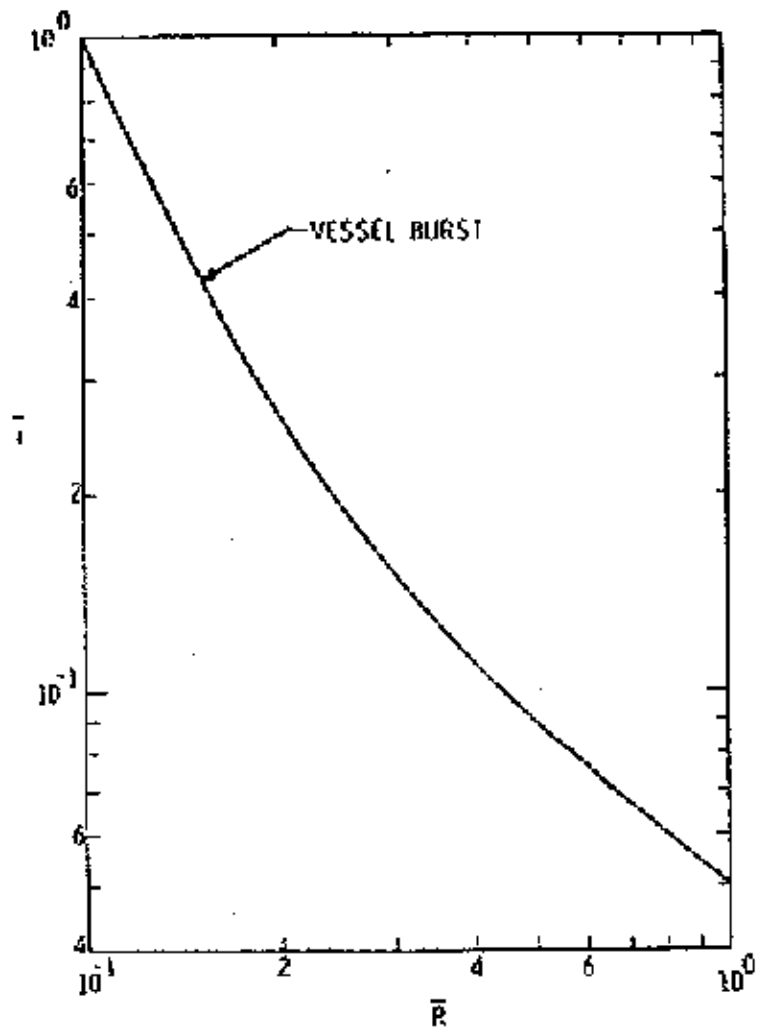


Figure 16: Shock impulse decay with distance for bursting sphere (Baker et al., 1983)

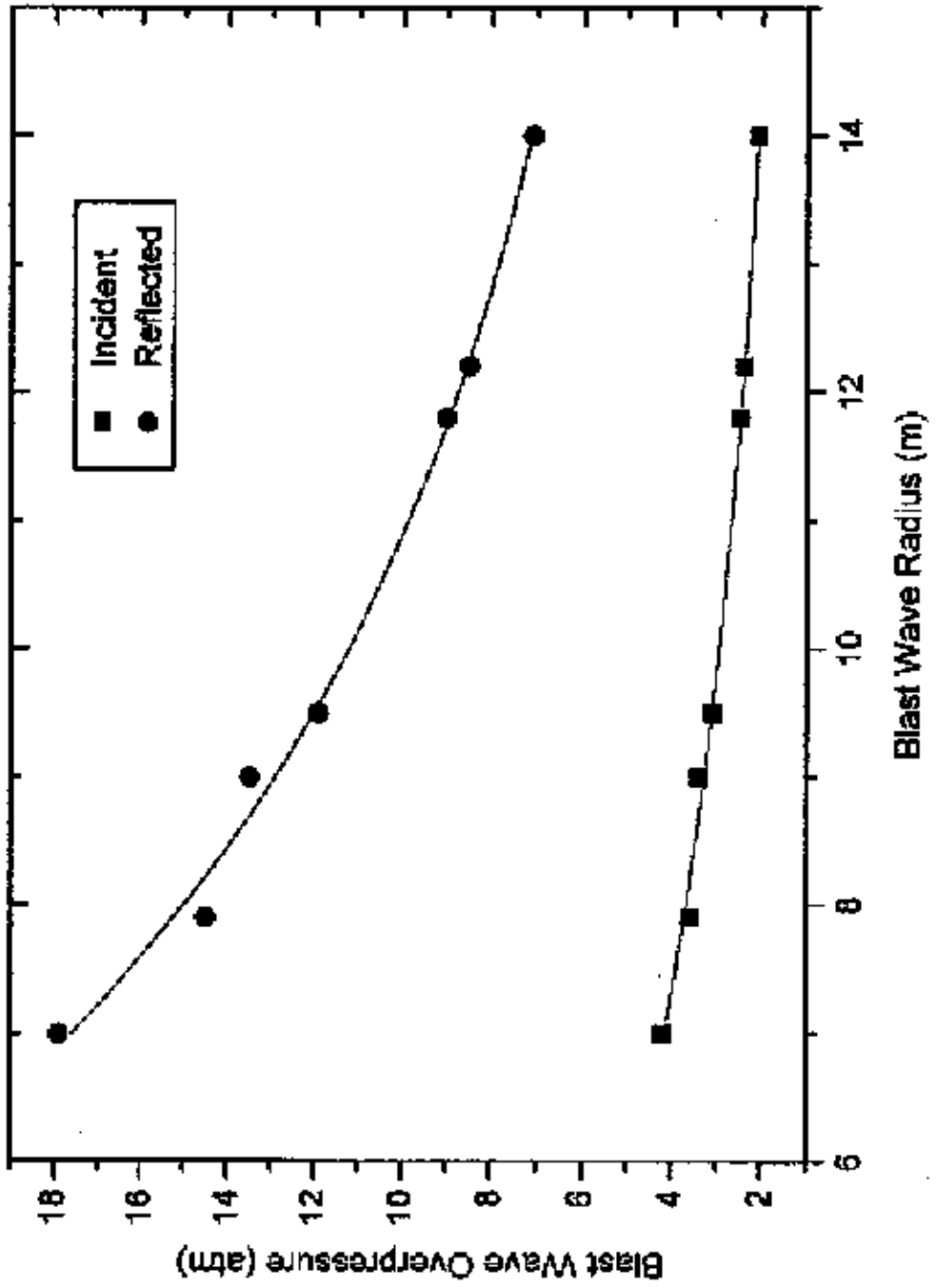


Figure 17: Blast wave decay from bursting sphere

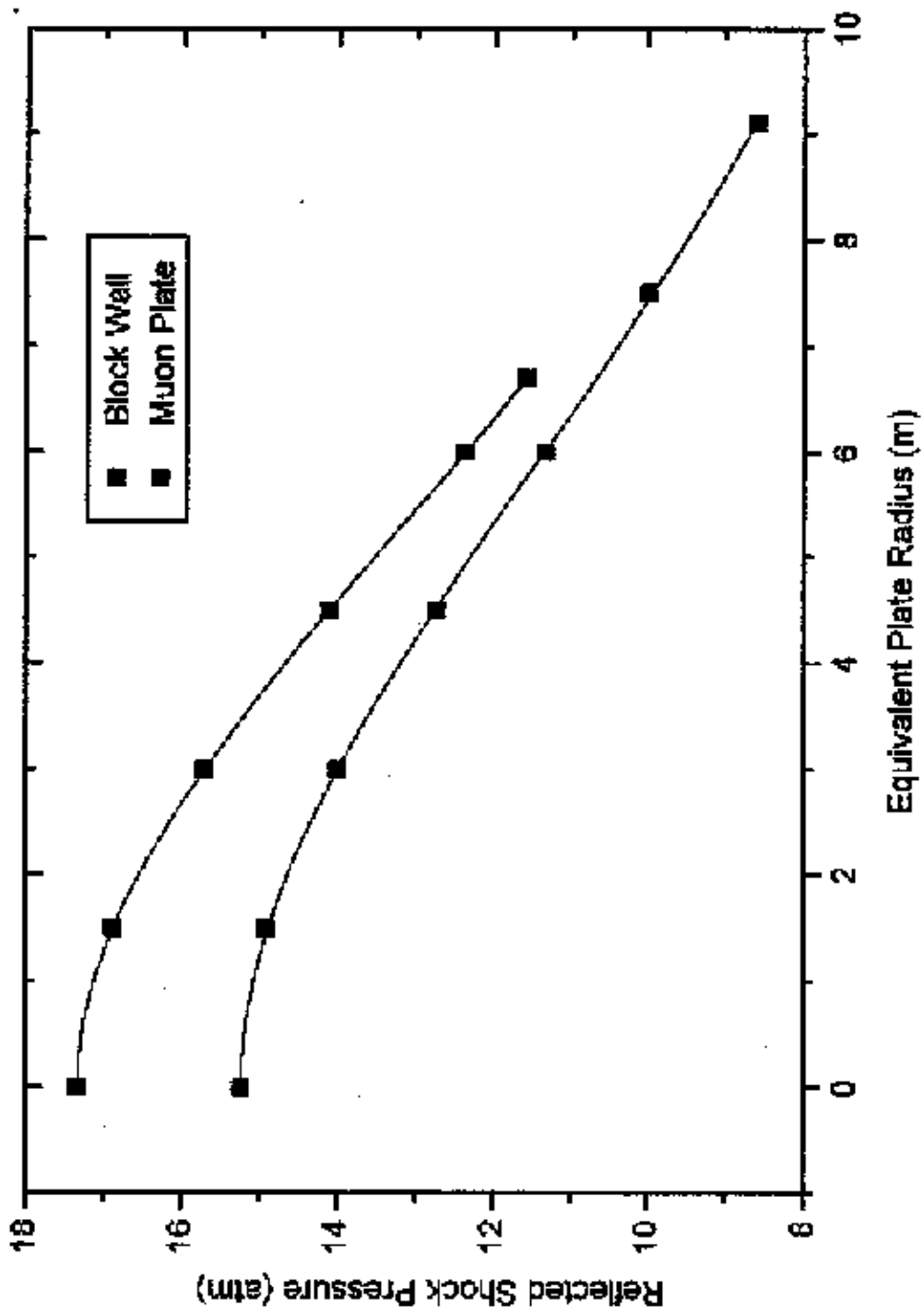


Figure 18: Pressure profile over equivalent circular plates

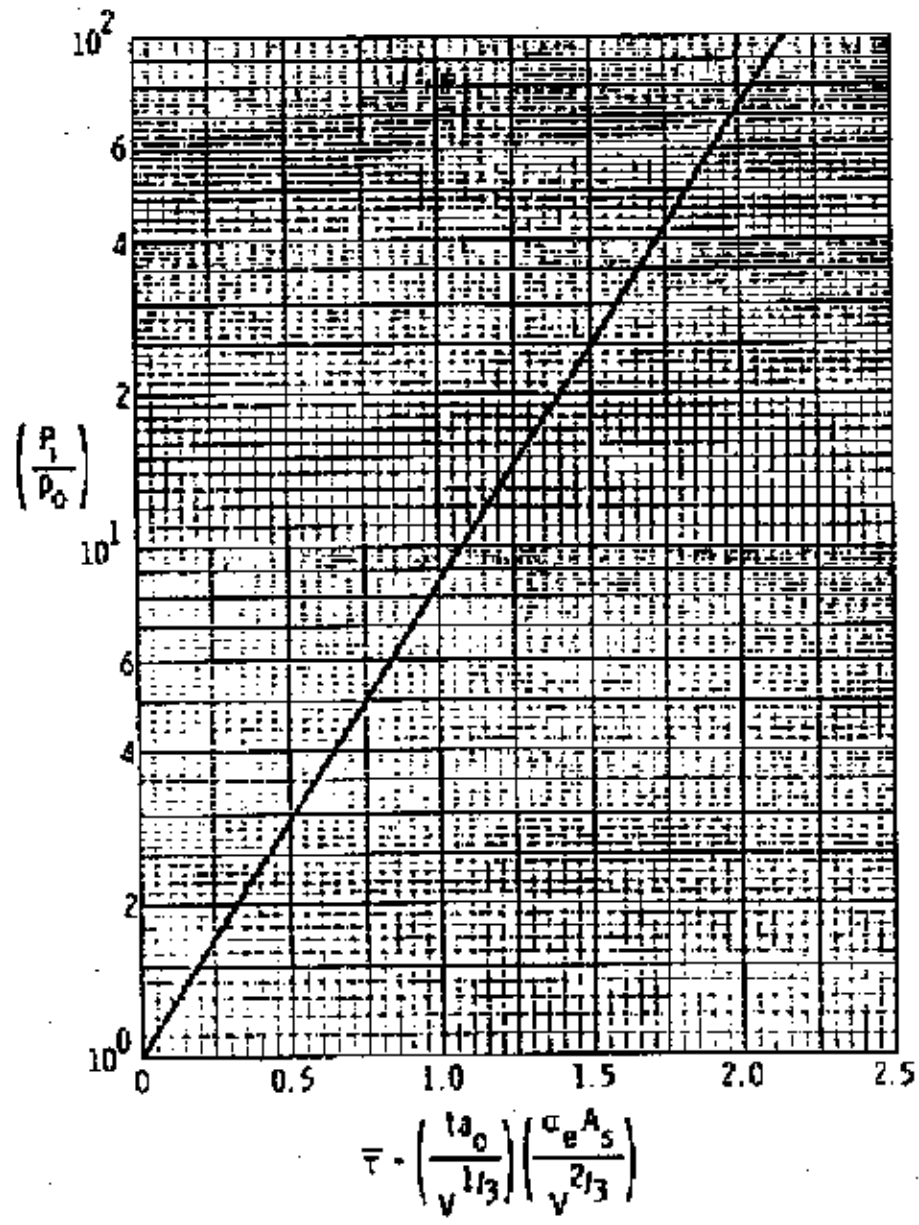


Figure 19: Scaled blowdown duration versus initial pressure ratio (Baker et al, 1972)

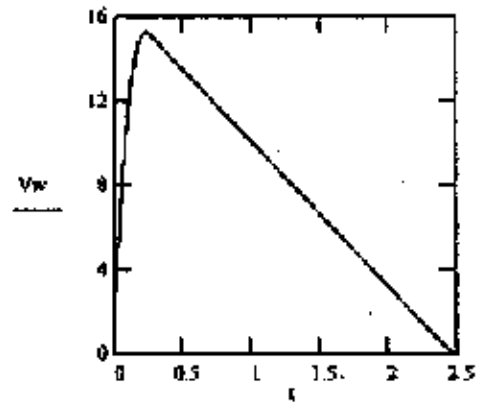
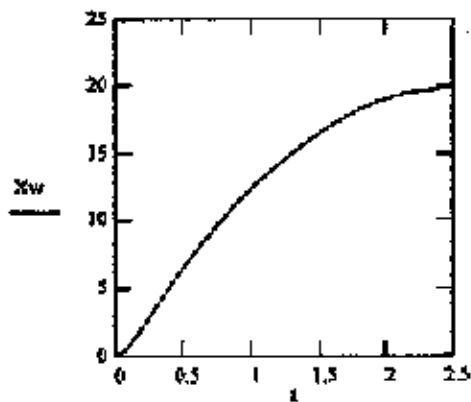
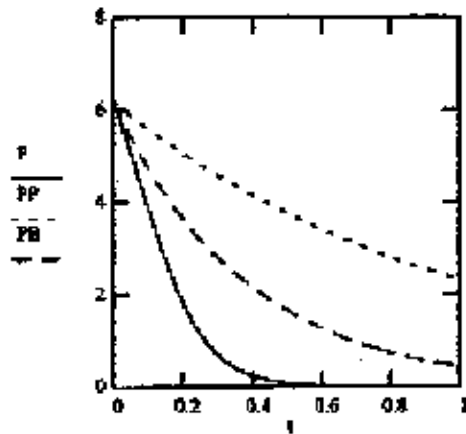


Figure 20: Wall dynamics for variable vent area and IR volume

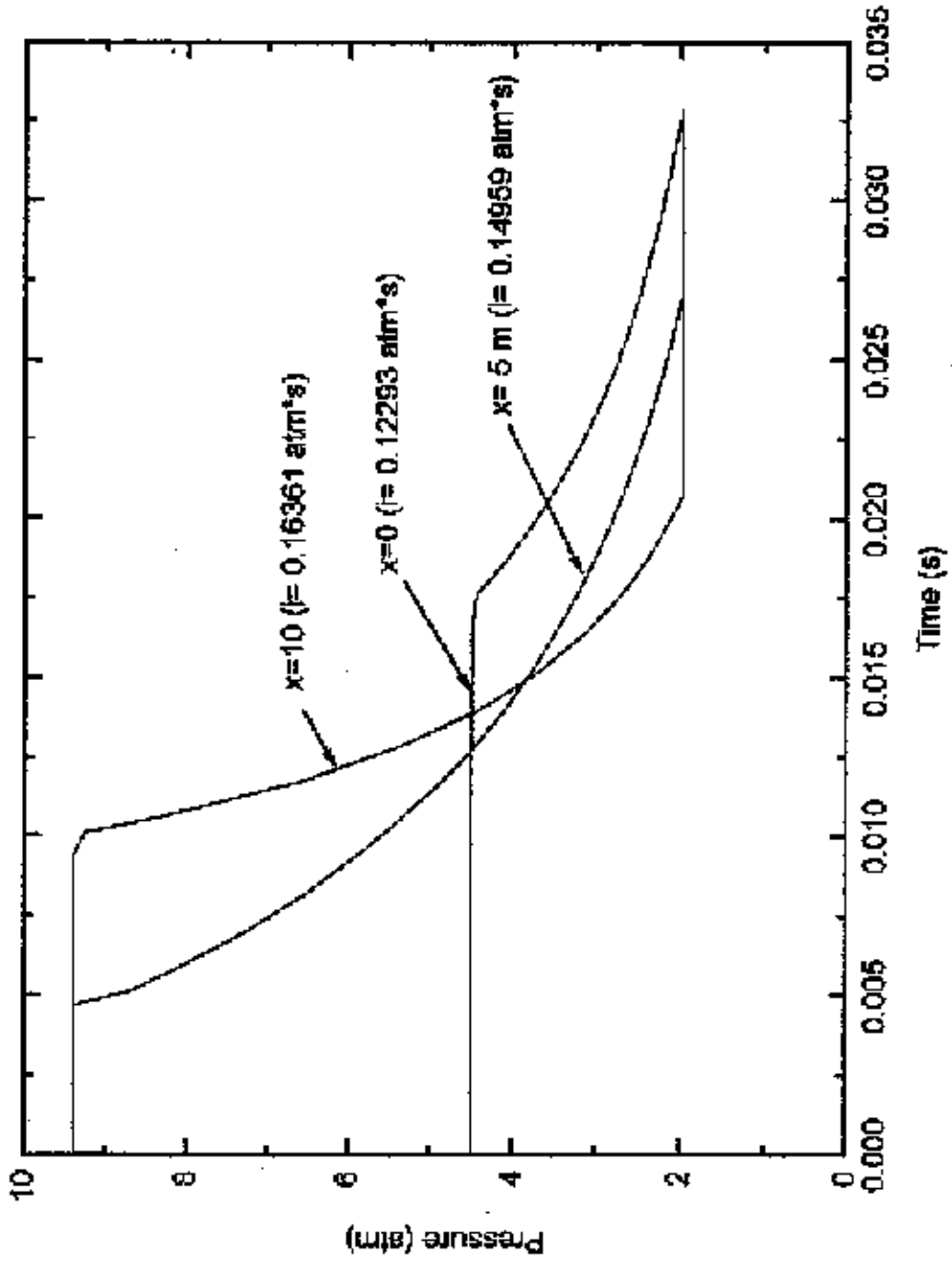


Figure 21: Pressure-time history at three axial positions for 10 m long cloud of 7% ethane

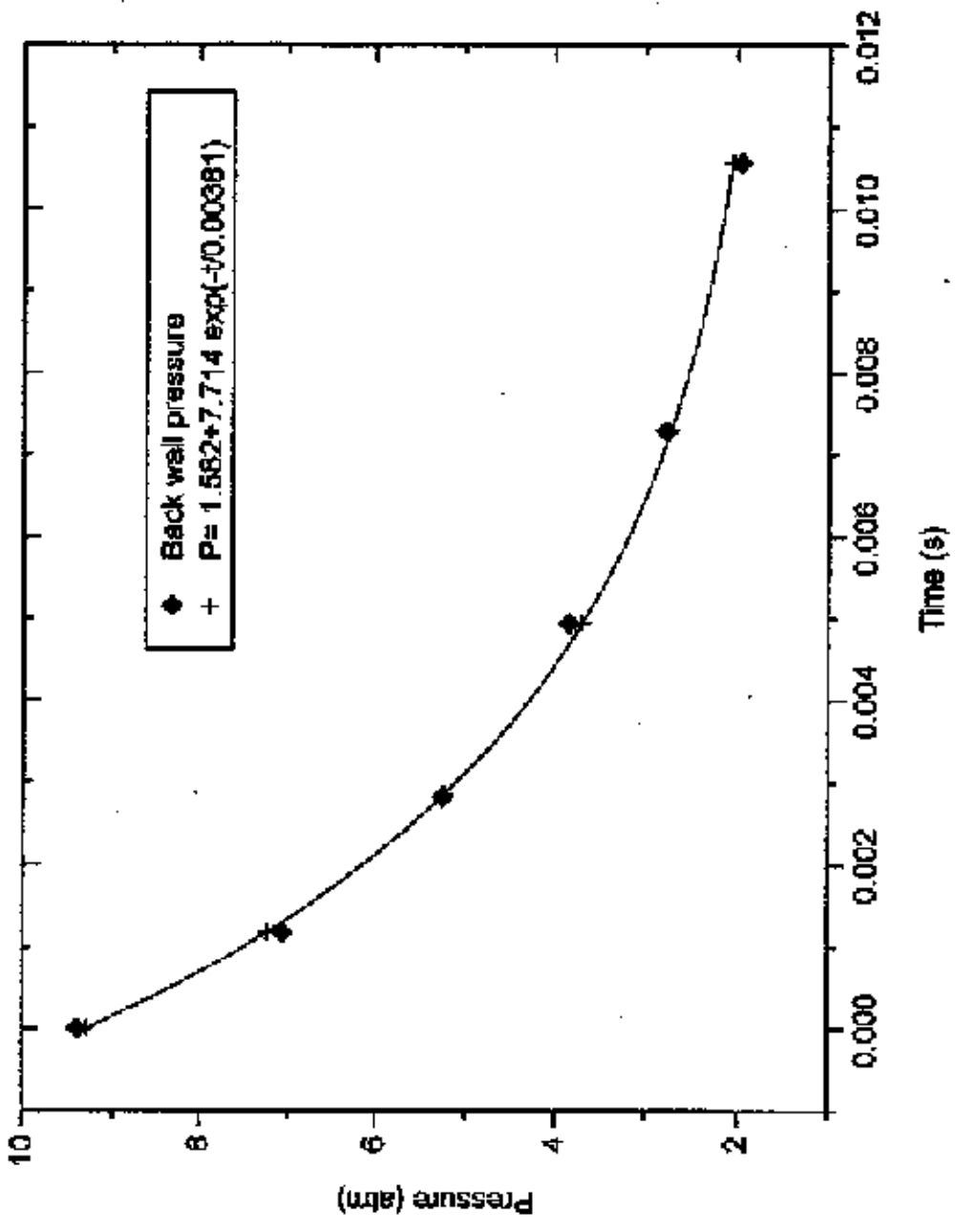


Figure 22: Pressure at closed end of 10 m long cloud of 7% ethane in air

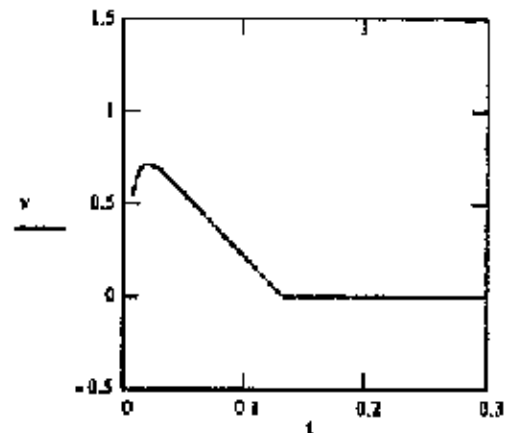
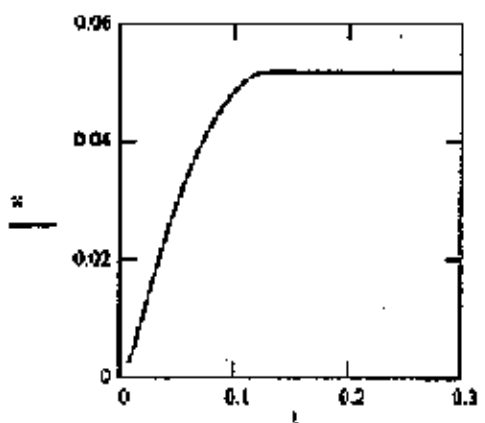
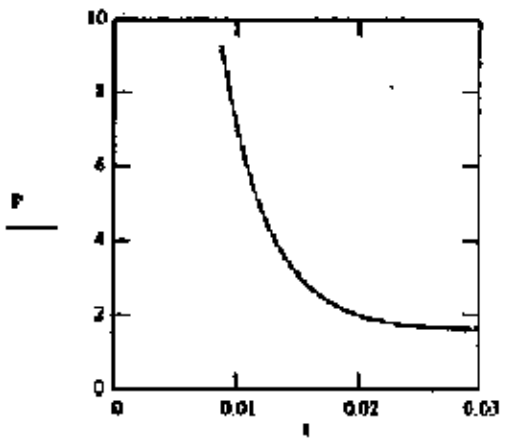


Figure 23: Block wall response to explosion in North Mezzanine

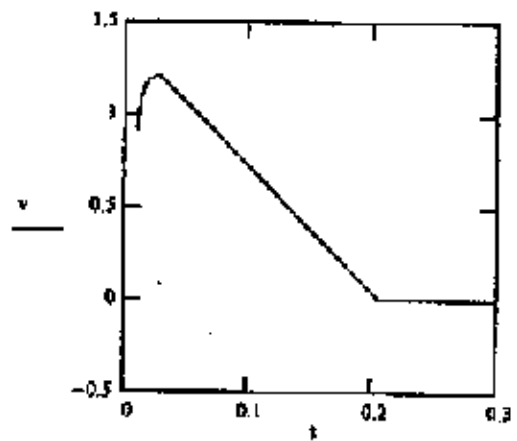
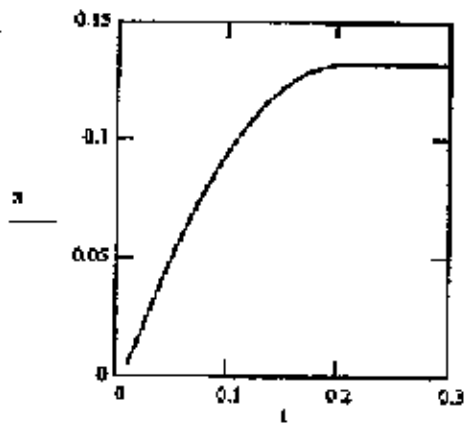
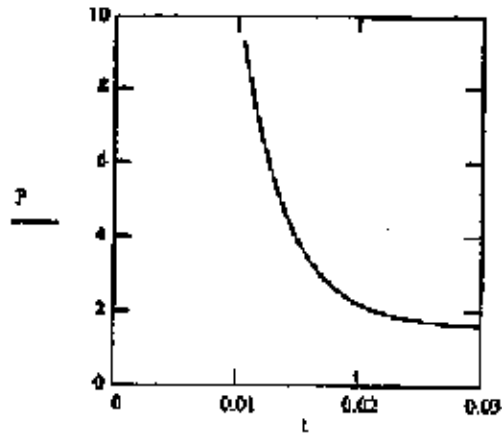


Figure 24: Block wall response to explosion in South Mezzanine

APPENDIX A

Burn and Vent Model

In this section, the model used to describe flame propagation and gas venting in the IR will be outlined. The model is developed based on a control volume analysis where all the gas properties (e.g., pressure and density) are taken to be uniform. A schematic showing the relevant boundary conditions and flame structure is given in Figure A.1. A point ignition source is assumed resulting in a spherically expanding flame. The combustion product gases are confined to a radius R which defines the position of the flame front. All parameters associated with the combustion products have a subscript b and those associated with the fresh unburned gas have a subscript u .

First we analyze the control volume which encompasses the combustion products, i.e., control volume boundary is taken to be the flame surface. From conservation of mass, the rate of increase in the mass of burned gas, m , is equal to the rate at which unburned gas is consumed,

$$\frac{dm_b}{dt} = \frac{d}{dt}(\rho_b V_b) = \rho_u s A_f \quad (1)$$

where V_b is the total volume occupied by the burnt gas, A_f is the flame surface area, and s is the burning velocity. For a given mixture, the burning rate s is a function of the mixture temperature and pressure. For this analysis, the burning rate will be taken as a constant over the full time of the burn since the pressure rise is very small. The gas density, ρ , is assumed to be spatially uniform in both the burned and unburned gas volume.

$$\rho_b \frac{dV_b}{dt} = \rho_u s A_f - V_b \frac{d\rho_b}{dt} \quad (2)$$

This is a good assumption since the burning rates are low. Since the time-scale for compression is short relative to the heat transfer time-scale, the gas compression is assumed to be isentropic, such that

$$\begin{aligned} \frac{d}{dt} \left(\frac{P}{\rho^\gamma} \right) &= 0 \\ \frac{d\rho_b}{dt} &= \left(\frac{\rho_b P}{\gamma} \right) \frac{dP}{dt} \end{aligned} \quad (3)$$

where P is pressure and γ is the ratio of specific heats. Assuming a spherical flame where $V_b = 4/3\pi R^3$ and $A_f = 4\pi R^2$ the flame velocity is given by,

$$\frac{dR}{dt} = \left(\frac{\rho_u}{\rho_b}\right) s - \left(\frac{V_b}{\gamma_b A_f P}\right) \frac{dP}{dt} \quad (4)$$

A similar control volume analysis can be performed for the unburned gas, where the control volume is bounded by the flame and the containment. From the conservation of mass, the rate of change in the mass of unburned gas, is equal to the rate at which unburned gas is consumed by the flame and unburned gas is vented outside the control volume

$$\frac{dm_u}{dt} = \frac{d}{dt}(\rho_u V_u) = \rho_u s A_f + \frac{dm_v}{dt} \quad (5)$$

where dm_v/dt is the rate at which unburned gas is vented. Assuming that the gas density is spatially uniform and the gas is compressed isentropically, using similar arguments as above, one gets the following expression for the flame velocity,

$$\frac{dR}{dt} = s + \left(\frac{V_u}{\gamma_u A_f P}\right) \frac{dP}{dt} + \left(\frac{1}{\rho_u A_f}\right) \frac{dm_v}{dt} \quad (6)$$

The vent mass flow rate, based on the flow through an orifice, depends on whether the flow is choked at the orifice. If the containment pressure, P , is larger than a critical pressure, P_c , the flow is choked. The following are expressions for the vent mass flow rate for both conditions

$$\frac{dm_v}{dt} = \rho c A_v C_D \left[\frac{2}{\gamma-1} \left(\frac{P}{P_o} \right)^{\frac{2}{\gamma}} \left(1 - \left(\frac{P}{P_o} \right)^{\frac{\gamma-1}{\gamma}} \right) \right]^{\frac{1}{2}} \quad P < P_c \quad (7)$$

or

$$\frac{dm_v}{dt} = \rho c A_v C_D \left[\left(\frac{2}{\gamma+1} \right)^{\frac{\gamma+1}{\gamma-1}} \right]^{\frac{1}{2}} \quad P > P_c \quad (8)$$

where P_o is atmospheric pressure, c is the speed of sound in the venting gas, A_v is the vent area, and C_D is the discharge coefficient which is taken to be 0.7. The critical pressure, P_c , is given by

$$P_c = P_o \left(\frac{\gamma+1}{2} \right)^{\frac{\gamma}{\gamma-1}} \quad (9)$$

which for $\gamma = 1.4$ yields a critical pressure of 1.9 times atmospheric pressure.

We now have two equations which can be solved for the two unknowns, i.e., R and P. By rearranging the two equations one can obtain the following two expressions which give the time rate of change of the two unknowns

$$\frac{dP}{dt} = \frac{1}{(V_o - V_b) \frac{1}{\gamma_a} + \frac{V_b}{\gamma_b}} \left[\left(\frac{P_o}{P_b} - 1 \right) s P A_f - P A_f c C_D K \right] \quad (10)$$

$$\frac{dR}{dt} = \frac{1}{\left(\frac{P_o}{P_b} \right) \frac{V_b}{V_o - V_b} + 1} \left[\left(\frac{\gamma_a}{\gamma_b} \right) s + \frac{\left(\frac{\gamma_a}{\gamma_b} \right) \frac{V_b}{V_o - V_b} \left(s + \frac{A_f}{A_f} c C_D K \right) \right] \quad (11)$$

where V_o is the total volume such that $V_a = V_o - V_b$. For the condition $P < P_o$, K is given by

$$K = \left[\frac{2}{\gamma - 1} \left(\frac{P_o}{P} \right)^{\frac{2}{\gamma}} \left(1 - \left(\frac{P_o}{P} \right)^{\frac{\gamma - 1}{\gamma}} \right) \right]^{\frac{1}{2}}$$

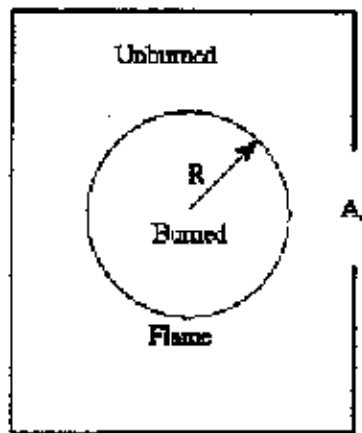


Figure A.1: Schematic showing spherical flame within a vented containment

APPENDIX B

Dynamics of a Tilting Wall

In this section, a model is developed to describe the tilting of a wall under a uniform back pressure. The approach taken is to develop a free body diagram for the wall, as shown in Figure B.1, indicating all the forces acting on the body and then applying Newton's Second Law to determine its dynamic response. It is assumed that the wall pivots about the bottom corner opposite the pressure loading face. This will occur if the pressure load is not sufficient to overcome the frictional force at the bottom of the wall, or if the wall is somehow physically restrained from translating. The wall half-height is H , wall half-width is W , and the wall length is L . The forces include: gravitational force which acts vertically down through the center of mass of the wall, the pressure force which acts normal to the loading surface, and the two reaction forces R_x and R_y applied at the pivot point. As the wall pivots gas is introduced below the wall which produces a second pressure force on the bottom surface of the wall. The minimum amount of pressure, P_{min} , required to pivot the wall can be determined by simply equating the torque generated by the pressure force on the back wall and the torque generated by the gravitational force under static conditions. Taking the torques about the pivot point this yields

$$P_{min} = \frac{M g W}{2H L H} \quad (1)$$

Assuming the pressure on the wall is greater than P_{min} , we can apply Newton's Law for translation in the fixed x and y directions, and taking the sum of torques about the center of mass in the Z direction for rotation, to give

$$-MX'' = -PA_f \cos\theta - PA_b \sin\theta + R_x \quad (2)$$

$$MY'' = -PA_f \sin\theta + PA_b \cos\theta + R_y - Mg \quad (3)$$

$$I\theta'' = F_x (H \cos\theta + W \sin\theta) - R_y (W \cos\theta - H \sin\theta) \quad (4)$$

where X and Y are the displacement of the wall center of mass in the fixed x and y direction and θ is the wall rotation in the z direction. The symbol $''$ is used to denote the second derivative with respect to time, and I is the wall moment of inertia about its center of mass. A_f and A_b denote the front wall load area and the bottom wall load area, respectively. A relationship between the linear acceleration of the wall center of mass and the wall angular acceleration can be obtained by deriving the expressions for the acceleration of the wall center of mass with respect to a rotating auxiliary coordinate system ($x'-y'-z'$) fixed to the rotating wall. This yields

$$X'' = \theta^2 R \cos(\theta + \theta_c) + \theta'' R \sin(\theta + \theta_c) \quad (5)$$

$$Y'' = -\theta^2 R \sin(\theta + \theta_c) + \theta'' R \cos(\theta + \theta_c) \quad (6)$$

where θ' is the wall angular velocity, R is the distance from the pivot point and the center of mass (i.e., $\sqrt{H^2 + W^2}$), and θ_c , shown in Figure B.1, is equal to $\tan^{-1}(H/W)$. Expanding the trigonometric functions

$$X'' = \theta^2 R (\cos\theta \cos\theta_c - \sin\theta \sin\theta_c) + \theta'' R (\sin\theta \cos\theta_c + \cos\theta \sin\theta_c) \quad (7)$$

$$Y'' = -\theta^2 R (\sin\theta \cos\theta_c + \cos\theta \sin\theta_c) + \theta'' R (\cos\theta \cos\theta_c - \sin\theta \sin\theta_c) \quad (8)$$

There is a critical angle θ_c above which the wall becomes unstable and topples over. This corresponds to a condition where the gravitational force vector goes through the pivot point (i.e., wall center of mass directly above the pivot point). For any angle θ below this value gravity restores the wall to its original position, for any angle above the critical gravity acts to topple the wall. The critical angle corresponds to $(\pi/2 - \theta_c)$, or $\tan^{-1}(W/H)$. Inserting actual values for the wall $\theta_c = 6.5^\circ = 0.114$ radians. In this analysis we are only interested in values of $\theta < \theta_c$, since anything greater and the wall topples. Since this angle is very small, we can use small angle approximations, i.e., $\sin\theta = \theta$ and $\cos\theta = 1$. Using this approximation and substituting for θ_c , one gets for equation 6

$$X'' = \theta^2 R \left(1 - \frac{W}{R} - \theta \frac{H}{R} \right) + \theta'' R \left(\theta \frac{W}{R} + 1 + \frac{H}{R} \right) \quad (9)$$

$$X'' = \theta^2 (W - \theta H) + \theta'' (\theta W + H) \quad (10)$$

Performing the same operation to equation 8, one gets

$$Y'' = -\theta^2 (\theta W + H) + \theta'' (W - \theta H) \quad (11)$$

Substituting for R_x and R_y in equations 4, using equations 2 and 3 one gets

$$I\theta'' = (PA_1 \cos\theta + PA_2 \sin\theta - MX'')(H \cos\theta + W \sin\theta) - (PA_1 \sin\theta - PA_2 \cos\theta + MY'' + Mg)(W \cos\theta - H \sin\theta) \quad (12)$$

Using the small angle approximation for θ and substituting for X'' and Y'' in equation 12 from equations 10 and 11,

$$I\theta'' = [PA_1 + PA_2\theta - M(\theta^2(W - \theta H) + \theta''(\theta W + H))](H + W\theta) - [PA_1\theta - PA_2 + M(-\theta^2(\theta W + H) + \theta''(W - \theta H))](W - \theta H) - Mg(W - H\theta) \quad (13)$$

Grouping like terms yields,

$$\theta''[J + M((\theta W + H)^2 + (W - \theta H)^2)] = PA_1 H(1 + \theta^2) + PA_2 W(1 + \theta^2) - Mg(W - H\theta) \quad (14)$$

Substituting for the moment of inertia about the center of mass, the angular acceleration of the wall is given by

$$\theta'' = \frac{PA_1 H(1 + \theta^2) + PA_2 W(1 + \theta^2) - Mg(W - H\theta)}{\frac{M}{12}(4H^2 + 4W^2) + M((\theta W + H)^2 + (W - \theta H)^2)} \quad (15)$$

Neglecting second order terms, i.e., $\theta^2 \ll 1$, yields,

$$\theta'' = \frac{PA_1 H + PA_2 W - Mg(W - H\theta)}{\frac{4}{3}M(H^2 + W^2)} \quad (16)$$

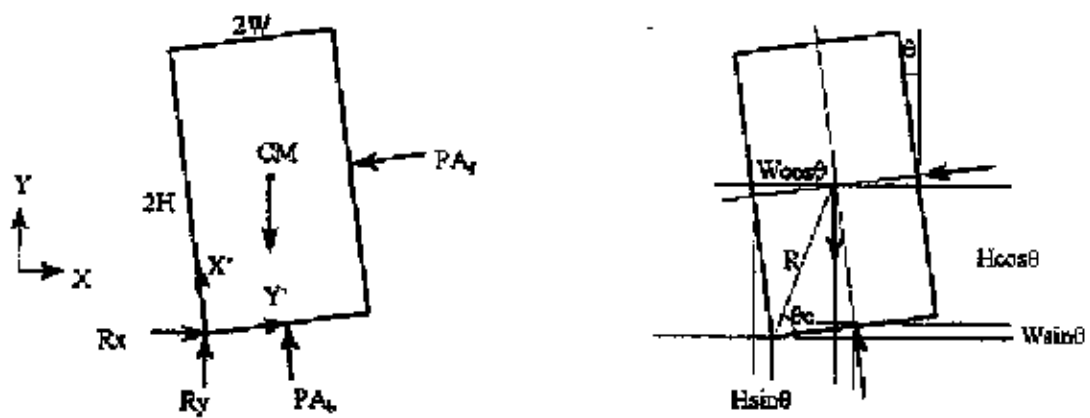


Figure B.1: Free body diagram of a wall tilting due to a uniform face pressure

APPENDIX C

Mathcad Worksheets for Burn/Vent Model

PHENIX1a: Fixed Vent Area

PHENIX1b: Variable Vent Area

PHENIX1c: Post Combustion Blowdown

BURNVENT MODEL WITH FIXED VENT AREA (PHENIX1a)

Wall characteristics:	Mixture properties:	IR characteristics:	Constants
H := 24.12-0.0254 L := 61.12-0.0254	$\rho_u := 1.181$ $\rho_b := 1.4$	$V_{ir} := 3350$	$P_0 := 101300$
W := 2.75-12-0.0254 $A_{wf} := 2 \cdot H \cdot L$	$\rho_b := 0.2262$ $\gamma_b := 1.28$	$A_v := 17.1$	$C_d := 0.6$
M := 1098000 $A_{wb} := 2 \cdot W \cdot L$	c := 336.4 s := .220		g := 9.81

$$\gamma := \frac{\rho_u}{\rho_b}$$

$$\gamma = 1.094$$

$$\gamma_1 := \frac{2}{\gamma_u - 1}$$

$$l = 5$$

$$\gamma_2 := \frac{2}{\gamma_u}$$

$$\gamma_2 = 1.429$$

$$\gamma_3 := \frac{(\gamma_u - 1)}{\gamma_u}$$

$$\gamma_3 = 0.286$$

$$P_{cr} := \frac{M \cdot g \cdot W}{A_{wf} \cdot H}$$

$$P_{cr} = 4.537 \cdot 10^3$$

$$s := \frac{\rho_u}{\rho_b}$$

$$R_0 := \left[\frac{(3 \cdot V_{ir})}{4 \cdot \pi} \right]^{(1/3)}$$

$$R_0 = 9.282$$

$$s = 5.221$$

Initial conditions:

$$x := \begin{bmatrix} .01 \\ P_0 \end{bmatrix} \quad \begin{array}{l} x_0 \text{ is radius} \\ x_1 \text{ is pressure} \end{array}$$

$$t(x) := \frac{\left[\frac{1}{1 + \gamma \cdot \frac{(x_0)^3}{(R_0)^3 - (x_0)^3}} \right] \left[s \cdot s + \gamma \cdot \frac{(x_0)^3}{(R_0)^3 - (x_0)^3} \right] \left[s + \frac{A_v \cdot c \cdot C_d}{4 \cdot \pi \cdot (x_0)^2} \left[\gamma_1 \cdot \left(\frac{P_0}{x_1} \right)^{\gamma_2} \left[1 - \left(\frac{P_0}{x_1} \right)^{\gamma_3} \right] \cdot (x_1 > P_0) \right]^{\gamma_1} \right]}{\frac{1}{\left[(R_0)^3 - (x_0)^3 \right] \frac{1}{\rho_u} + \frac{1}{\rho_b} \cdot (x_0)^3} \left[(s-1) \cdot s \cdot x_1 \cdot \left[4 \cdot \pi \cdot (x_0)^2 \right] - x_1 \cdot A_v \cdot c \cdot C_d \left[\gamma_1 \cdot \left(\frac{P_0}{x_1} \right)^{\gamma_2} \left[1 - \left(\frac{P_0}{x_1} \right)^{\gamma_3} \right] \cdot (x_1 > P_0) \right]^{\gamma_1} \right]} \cdot \frac{1}{4 \cdot \pi}}$$

$$Z := \text{rkfixed}(x, 0, 3.167, 1000, D)$$

$$t := Z^{(0)}$$

$$R := Z^{(1)}$$

$$P := \frac{Z^{(2)}}{P_0}$$

$$R_{max} := \max(R)$$

$$R_{max} = 9.282$$

$$P_{max} := \max(P)$$

$$P_{max} = 1.058$$

**BURN/VENT MODEL WITH FIXED AND VARIABLE VENT AREA
(PHENIX1b)**

Wall characteristics:

H := 24 · 12 · 0.0254 L := 61 · 12 · 0.0254
 W := 2.75 · 12 · 0.0254 Awf := 2 · H · L
 M := 1096000 Awb := 2 · W · L

Mixture properties:

pu := 1.181 yu := 1.4
 pb := 0.2262 yb := 1.28
 c := 336.4 s := .220

IR characteristics:

Vir := 3350
 Av := 17.1

Constants

Po := 101300
 Cd := 0.6
 g := 9.81

$\gamma := \frac{\gamma_u}{\gamma_b}$
 $\gamma = 1.094$
 $\gamma_f := \frac{2}{\gamma_u - 1}$
 $\gamma_f = 5$

$\gamma_2 := \frac{2}{\gamma_u}$
 $\gamma_2 = 1.429$
 $\gamma_3 := \frac{(\gamma_u - 1)}{\gamma_u}$
 $\gamma_3 = 0.286$

$Per := \frac{M \cdot g \cdot W}{Awf \cdot H}$
 $Per = 4.537 \cdot 10^3$
 $\epsilon := \frac{p_u}{p_b}$

$Ro := \left[\frac{(3 \cdot Vir)}{4 \cdot \pi} \right]^{(1/3)}$
 $Ro = 9.282$
 $\epsilon = 5.221$

Initial conditions:

$x := \begin{bmatrix} 0.01 \\ Po \\ 0.0 \\ 0.0 \end{bmatrix}$ x0 is flame rad
 x1 is pressure
 x2 wall angle
 x3 wall ang vel

$$D(x, x) := \begin{bmatrix} \frac{1}{1 + \gamma \cdot \left[\frac{(x_0)^3}{(Ro)^3 - (x_0)^3} \right]} \left[\epsilon \cdot s + \gamma \cdot \left[\frac{(x_0)^3}{(Ro)^3 - (x_0)^3} \right] \right] \left[s + \frac{(Av + 2 \cdot L \cdot H \cdot x_2) \cdot c \cdot Cd}{4 \cdot \pi \cdot (x_0)^2} \left[\gamma \cdot \left(\frac{Po}{x_1} \right)^2 \left[1 - \left(\frac{Po}{x_1} \right)^{\gamma_3} \right] \cdot (x_1 > Po) \right]^{\gamma_2} \right] \right] \\ \frac{1}{\left[Ro^3 - (x_0)^3 \right] \cdot \frac{1}{\gamma_u} + \frac{1}{\gamma_b} \cdot (x_0)^3} \left[(\epsilon - 1) \cdot s \cdot x_1 \cdot \left[4 \cdot \pi \cdot (x_0)^2 \right] - x_1 \cdot (Av + 2 \cdot L \cdot H \cdot x_2) \cdot c \cdot Cd \cdot \left[\gamma \cdot \left(\frac{Po}{x_1} \right)^2 \left[1 - \left(\frac{Po}{x_1} \right)^{\gamma_3} \right] \cdot (x_1 > Po) \right]^{\gamma_2} \right] \\ \frac{3}{4 \cdot \pi} \\ x_3 \\ \frac{[(x_1 - Po) \cdot (Awf \cdot H + Awb \cdot W) - M \cdot g \cdot (W - H \cdot x_2)] \cdot [(x_1 - Po) > Per]}{\left(\frac{4}{3} \right) \cdot M \cdot (H^2 + W^2)} \end{bmatrix}$$

Z := rkfixed(x, 0, 3.165, 1000, D)

t := Z<0> R := Z<1> P := $\frac{Z<2>}{Po}$ $\theta := \frac{360}{2 \cdot \pi} \cdot Z<3>$ $d\theta/dt := \frac{360}{2 \cdot \pi} \cdot Z<4>$

Rmax := max(R) Rmax = 9.282
 Pmax := max(P) Pmax = 1.057
 $\theta_{max} := \max(\theta)$ $\theta_{max} = 0.082$ critical angle is 5.54 deg
 $d\theta/dt_{max} := \max(d\theta/dt)$ $d\theta/dt_{max} = 0.487$

BURN/VENT MODEL POST COMBUSTION MODEL (PHENIX1c)

Wall characteristics:	Mixture properties:	IR characteristics:	Constants
H := 24-12-0.0254 L := 61-12-0.0254	$\rho u := 1.181$ $\rho v := 1.4$	Vir := 3350	Po := 101300
W := 2.75-12-0.0254 Awf := 2-H-L	$\rho b := 0.2262$ $\gamma b := 1.24$	Av := 17.1	Cd := 0.6
M := 1094000 Awb := 2 W-L	c := 756.9 s := 0		g := 9.81

$$\gamma := \frac{\rho v}{\rho}$$

$$\gamma = 1$$

$$\gamma_1 := \frac{\rho_1}{\rho}$$

$$\gamma_1 = 5$$

$$\gamma_2 := \frac{2}{\rho v}$$

$$\gamma_2 = 1.429$$

$$\gamma_3 := \frac{(\gamma v - 1)}{\rho v}$$

$$\gamma_3 = 0.286$$

$$Per := \frac{M \cdot g \cdot W}{Awf \cdot H}$$

$$Per = 4.537 \cdot 10^3$$

$$\epsilon := \frac{\rho u}{\rho b}$$

$$\epsilon = 5.22$$

$$Ro := \left[\frac{(3 \cdot Vir)}{4 \cdot x} \right]^{(1)}$$

$$Ro = 9.282$$

$$\epsilon := 5.22$$

Initial conditions:

$$x := \begin{bmatrix} 9.282 \\ 107100 \\ 0.001434 \\ 0.0085 \end{bmatrix}$$

x0 is flame rad
x1 is pressure
x2 wall angle
x3 wall ang vel

$$D(t, x) := \left[\frac{1}{\epsilon + \gamma \frac{(x_0)^3}{(Ro)^3 - (x_0)^3}} \right] \left[\epsilon s + \gamma \frac{(x_0)^3}{(Ro)^3 - (x_0)^3} \right] \left[s + \frac{(Av + 2 \cdot L \cdot H \cdot x_2) \cdot c \cdot Cd}{4 \cdot \pi \cdot (x_0)^2} \left[\gamma_1 \cdot \left(\frac{Po}{x_1} \right)^{\gamma_2} \left[1 - \left(\frac{Po}{x_1} \right)^{\gamma_3} \right] \cdot (x_1 > Po) \right]^3 \right]$$

$$(-1 - \gamma b) \cdot x_1 \cdot c \cdot Cd \cdot \frac{(Av + 2 \cdot L \cdot H \cdot x_2)}{Vir} \left[\gamma_1 \cdot \left(\frac{Po}{x_1} \right)^{\gamma_2} \left[1 - \left(\frac{Po}{x_1} \right)^{\gamma_3} \right] \cdot (x_1 > Po) \right]^3$$

$$\frac{[(x_1 - Po) \cdot (Awf \cdot H + Awb \cdot W) - (x_1 \geq Po) - M \cdot g \cdot (W - H \cdot x_2) \cdot (x_2 > 0)]}{\left(\frac{4}{3} \right) \cdot M \cdot (H^2 + W^2)}$$

$$Z := \text{rkfixed}(x, 0, 7, 1000, D)$$

$$t := Z^{<0>} \quad R := Z^{<1>} \quad P := \frac{Z^{<2>}}{Po} \quad \theta := \frac{360}{2 \cdot \pi} \cdot Z^{<3>} \quad \frac{d\theta}{dt} := \frac{360}{2 \cdot \pi} \cdot Z^{<4>}$$

$$R_{max} := \max(R) \quad R_{max} = 9.417$$

$$P_{max} := \max(P) \quad P_{max} = 1.057$$

$$\theta_{max} := \max(\theta) \quad \theta_{max} = 6.127$$

critical angle is 6.54 deg

APPENDIX D

IR Blowdown With Fixed Vent Area and Volume

In this section a model is developed to predict the pressure time-history of an initially pressurized containment with a fixed volume and vent area. The model is developed based on a control volume analysis where all the gas properties (e.g., pressure and density) within the containment are taken to be uniform. Applying the conservation of mass to the control volume which encompasses the gas within the containment yields

$$\frac{dM}{dt} = \left[\frac{dm}{dt} \right]_{out} = -\sum(\rho u A_v) \quad (1)$$

where ρ_u , u_u , and A_u is the gas density, flow velocity, and cross sectional area evaluated at each vent opening. Equation 1 simply states that the rate of change of the mass in the volume, M , is equal to the mass flow rate out of the control volume, dm/dt . Equation 1 is general and applies to multiple vent openings. For our analysis we will consider only one opening. If we assume that the flow is choked, the mass flow rate through the vent is

$$\frac{dm}{dt} = \rho u A_v = \rho \left(\frac{2}{\gamma+1} \right)^{\frac{1}{\gamma-1}} c \left(\frac{2}{\gamma+1} \right)^{\frac{1}{2}} A_v \quad (2)$$

where ρ and c are the gas density and speed of sound of the bulk gas within the containment. Using the ideal gas definition for the speed of sound and reorganizing yields

$$\frac{dm}{dt} = \rho A_v \left(\frac{\gamma P}{\rho} \right)^{\frac{1}{2}} \left(\frac{2}{\gamma+1} \right)^{\frac{\gamma+1}{2(\gamma-1)}} \quad (3)$$

where P is the bulk gas pressure. Substitution equation 3 into equation 1 and applying the restriction of constant containment volume, V , yields

$$\frac{dp}{dt} = -\frac{\rho A_v}{V} \left(\frac{\gamma P}{\rho} \right)^{\frac{1}{2}} \left(\frac{2}{\gamma+1} \right)^{\frac{\gamma+1}{2(\gamma-1)}} \quad (4)$$

For an isentropic expansion process (see equation 3 in Appendix A)

$$\frac{dp}{dt} = \frac{\rho}{\gamma P} \frac{dP}{dt} \quad (5)$$

substituting into equation 4 yields

$$\frac{dP}{dt} = -\frac{\gamma P A_v}{V} \left(\frac{\gamma P}{\rho} \right)^{\frac{1}{2}} \left(\frac{2}{\gamma+1} \right)^{\frac{\gamma+1}{2(\gamma-1)}} \quad (6)$$

For an isentropic process, $P\rho^{-\gamma} = P_i \rho_i^{-\gamma}$, where the subscript i refers to initial volume conditions, gives

$$\frac{dP}{dt} = -\frac{\gamma P^{\frac{3\gamma-1}{2\gamma}} A_v}{V} \left(\frac{\gamma P_i^{-\gamma}}{\rho_i} \right)^{\frac{1}{2}} \left(\frac{2}{\gamma+1} \right)^{\frac{\gamma+1}{2(\gamma-1)}} \quad (7)$$

Applying the ideal gas definition for the speed of sound yields

$$\frac{dP}{dt} = -\frac{\gamma A_v c_s}{V} P^{\frac{3\gamma-1}{2\gamma}} P_i^{\frac{1-\gamma}{2\gamma}} \left(\frac{2}{\gamma+1} \right)^{\frac{\gamma+1}{2(\gamma-1)}} \quad (8)$$

integrating both sides where time goes from 0 to t and the pressure goes from P_i to P yields

$$\left(\frac{P}{P_i} \right)^{\frac{1-\gamma}{2\gamma}} - 1 = -\frac{A_v c_s t}{V} \left(\frac{1-\gamma}{2} \right) \left(\frac{2}{\gamma+1} \right)^{\frac{\gamma+1}{2(\gamma-1)}} \quad (9)$$

which yields

$$\left(\frac{P}{P_i} \right) = \left[1 + \frac{A_v c_s t}{V} \left(\frac{\gamma-1}{2} \right) \left(\frac{2}{\gamma+1} \right)^{\frac{\gamma+1}{2(\gamma-1)}} \right]^{\frac{2\gamma}{1-\gamma}} \quad (10)$$

APPENDIX E

IR Blowdown With Variable Vent Area and Volume

In this section, the model developed in Appendix D is extended for variable volume and vent area. From Appendix D we have

$$\frac{dM}{dt} = -\frac{dm}{dt} = -\rho A_v \left(\frac{\gamma P}{\rho} \right)^{\frac{1}{2}} \left(\frac{2}{\gamma+1} \right)^{\frac{\gamma+1}{2(\gamma-1)}} \quad (1)$$

where P is the bulk gas pressure. Expanding the left hand side and re-organizing yields

$$\frac{d\rho}{dt} = -\frac{\rho A_v}{V} \left(\frac{\gamma P}{\rho} \right)^{\frac{1}{2}} \left(\frac{2}{\gamma+1} \right)^{\frac{\gamma+1}{2(\gamma-1)}} - \frac{\rho}{V} \frac{dV}{dt} \quad (2)$$

The last term on the right hand side takes into account the change in volume. For an isentropic expansion process (see equation 3 in Appendix A)

$$\frac{d\rho}{dt} = \frac{\rho}{\gamma P} \frac{dP}{dt} \quad (3)$$

substituting into equation 2 yields

$$\frac{dP}{dt} = -\frac{\gamma P A_v}{V} \left(\frac{\gamma P}{\rho} \right)^{\frac{1}{2}} \left(\frac{2}{\gamma+1} \right)^{\frac{\gamma+1}{2(\gamma-1)}} - \frac{\gamma P}{V} \frac{dV}{dt} \quad (4)$$

For an isentropic process, $P\rho^{-\gamma} = P_i \rho_i^{-\gamma}$, where the subscript i refers to initial volume conditions, gives

$$\frac{dP}{dt} = -\frac{\gamma P^{\frac{3\gamma-1}{2\gamma}} A_v}{V} \left(\frac{\gamma P_i^{-\gamma}}{\rho_i} \right)^{\frac{1}{2}} \left(\frac{2}{\gamma+1} \right)^{\frac{\gamma+1}{2(\gamma-1)}} - \frac{\gamma P}{V} \frac{dV}{dt} \quad (5)$$

Applying the ideal gas definition for the speed of sound yields

$$\frac{dP}{dt} = -\frac{\gamma A_v \rho_i}{V} P^{\frac{2\gamma-1}{2\gamma}} P_i^{\frac{1-\gamma}{2\gamma}} \left(\frac{2}{\gamma+1} \right)^{\frac{\gamma+1}{2(\gamma-1)}} - \frac{\gamma P}{V} \frac{dV}{dt} \quad (6)$$

For the box enclosure shown in Figure E-1, where there is a fixed vent area and a variable vent area above the wall, the equation 6 becomes

$$\frac{dP}{dt} = -\frac{\gamma(A_v + bx)c_i}{A_v(W+x)} P^{\frac{2\gamma-1}{2\gamma}} P_i^{\frac{1-\gamma}{2\gamma}} \left(\frac{2}{\gamma+1} \right)^{\frac{\gamma+1}{2(\gamma-1)}} - \frac{\gamma P}{(W+x)} \frac{dx}{dt} \quad (7)$$

Another approach is to define a fixed control volume whose boundaries coincide with the fixed box sides and the initial wall position, applying the energy equation to this control volume yields

$$\frac{dU}{dt} = \frac{dm_{ex}h}{dt} + \frac{dm_{in}h}{dt} \quad (8)$$

where U is the internal energy stored in the control volume, the first term on the right hand side is the enthalpy which goes out the fixed vent area and the second term is the enthalpy which passes the control volume boundary located at the initial wall position. Again assuming choked flow through the vent areas, equation 8 becomes

$$c_v \frac{d}{dt}(\rho VT) = -\frac{\rho A_v}{V} \left(\frac{\gamma P}{\rho} \right)^{\frac{1}{2}} \left(\frac{2}{\gamma+1} \right)^{\frac{\gamma+1}{2(\gamma-1)}} c_p T - \rho A_w \frac{dx}{dt} c_p T \quad (9)$$

where the heat capacities are taken to be constant. Applying the ideal gas equation of state and substituting c_p/c_v with γ , yields

$$\frac{d}{dt}(PV) = -\gamma \rho R T A_v \left(\frac{\gamma P}{\rho} \right)^{\frac{1}{2}} \left(\frac{2}{\gamma+1} \right)^{\frac{\gamma+1}{2(\gamma-1)}} - \gamma \rho R T A_w \frac{dx}{dt} \quad (10)$$

Noting that the control volume is constant and again applying the ideal gas equation of state gives

$$\frac{dP}{dt} = -\frac{\gamma P A_v}{V} \left(\frac{\gamma P}{\rho} \right)^{\frac{1}{2}} \left(\frac{2}{\gamma+1} \right)^{\frac{\gamma+1}{2(\gamma-1)}} - \frac{\gamma P}{V} \frac{dV}{dt} \quad (11)$$

which is the same as equation 4.

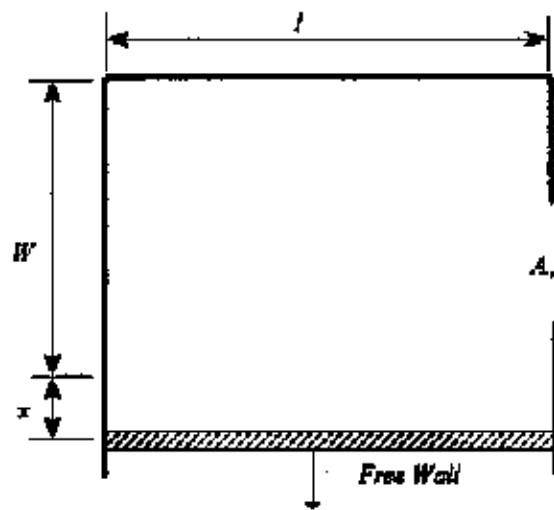


Figure E.1: Schematic showing the box enclosure with one wall free to move

APPENDIX F

Mathcad Worksheets for IR Depressurization Model (PHENIX2)

VARIABLE VENT AREA & IR VOLUME BLOWDOWN MODEL
(PHENIX2)

$\gamma := 1.26$ $l := 18.6$ $g := 9.81$
 $Av := 17.1$ $w := 12.6$ $Po := 101300$
 $Mw := 1098000$ $h := 14.3$ $Pi := 628060$
 $\mu := 0.7$ $Aw := l \cdot h$ $ci := 821.4$

$$\gamma_c := \left(\frac{2}{\gamma + 1} \right)^{\frac{\gamma + 1}{2 \cdot (\gamma - 1)}}$$

$$x := \begin{bmatrix} Pi \\ 0.017 \\ 1.86 \end{bmatrix} \quad D(t, x) := \begin{bmatrix} -\frac{(Av + 1 \cdot x_1)}{Aw \cdot (w + x_1)} \cdot \gamma \cdot ci \cdot \gamma_c \cdot (x_0) \left[\frac{(3\gamma - 1)}{2\gamma} \right] \cdot Pi \frac{(1 - \gamma)}{2\gamma} - \frac{\gamma \cdot (x_0 \cdot x_2)}{(w + x_1)} \\ x_2 \\ \frac{Aw}{Mw} \cdot (x_0 - Po) \cdot [(x_0 - Po) > 0] - \mu \cdot g \cdot (x_2 > 0) \end{bmatrix}$$

x_0 is P
 x_1 is Xw
 x_2 is Vw

$Z := \text{rkfixed}(x, 0, 3, 1000, D)$

$t := Z^{<0>}$

$P := \frac{Z^{<1>}}{101300}$

$m := 0..1000$

$PP_m := 6.2 \cdot \left(1 + 0.32 \cdot \frac{m}{1000} \right)^{-9.69}$

$Vw := Z^{<3>}$

$Xw := Z^{<2>}$

$PB_m := 6.2 \cdot \exp\left(-7.96 \cdot \frac{m}{1000}\right)$

APPENDIX G

Mathcad Worksheets for Burn/Vent Model

PHENIX3a: North Mezzanine

PHENIX3b: South Mezzanine

Depressurization of the North Mezzanine
PHENIX3a

$$Ap := 49.5 \cdot 22.5 \cdot 0.0929$$

$$Pa := 101300$$

$$b := 1.582 \cdot Pa$$

$$L := 8.7$$

$$Vw := 49.5 \cdot 25.5 \cdot 5 \cdot 0.0283$$

$$\mu := 0.7$$

$$c := 7.714 \cdot Pa$$

$$co := 990$$

$$M := Vw \cdot (2408 + 5666)$$

$$g := 9.81$$

$$\tau := 0.00381$$

$$\Delta Po := 8.4 \cdot Pa$$

$$to := \frac{L}{co}$$

$$\frac{Ap}{M} = 7.175 \cdot 10^{-5}$$

$$vo := \frac{Ap}{M} \cdot \Delta Po \cdot to$$

$$xo := \frac{Ap}{2 \cdot M} \cdot \Delta Po \cdot to^2$$

$$vo = 0.537$$

$$xo = 2.357 \cdot 10^{-3}$$

$$x := \begin{bmatrix} xo \\ vo \end{bmatrix} \quad D(t, x) := \begin{bmatrix} x_1 \\ \left(b + c \cdot \exp\left(\frac{-t}{\tau}\right) - Pa \right) \cdot \frac{Ap}{M} \cdot ((t + to) < 0.03) - \mu \cdot g \cdot (x_1 > 0) \end{bmatrix}$$

$$Z := \text{rkfixed}(x, 0, 0.5, 1000, D)$$

$$m := 0..100$$

$$t := Z^{<0>} + to$$

$$x := Z^{<1>}$$

$$v := Z^{<2>}$$

$$P_m := \frac{b}{Pa} + \frac{c}{Pa} \cdot \exp\left(\frac{-m}{\tau}\right)$$

$$\text{maximum displacement } \max(x) = 0.052$$

Depressurization of the South Mezzanine
PHENIX3b

$$\begin{array}{llll}
 A_p := 49.5 \cdot 22.5 \cdot 0.0929 & P_a := 101300 & b := 1.582 \cdot P_a & L := 10.4 \\
 V_w := 49.5 \cdot 25.5 \cdot 5 \cdot 0.0283 & \mu := 0.7 & c := 7.714 \cdot P_a & c_0 := 990 \\
 M := V_w \cdot (5666) & g := 9.81 & \tau := 0.00381 & \Delta P_0 := 8.4 \cdot P_a \\
 & & & t_0 := \frac{L}{c_0}
 \end{array}$$

$$\frac{A_p}{M} = 1.022 \cdot 10^{-4}$$

$$v_0 := \frac{A_p}{M} \cdot \Delta P_0 \cdot t_0 \quad x_0 := \frac{A_p}{2 \cdot M} \cdot \Delta P_0 \cdot t_0^2 \quad v_0 = 0.914 \quad x_0 = 4.8 \cdot 10^{-3}$$

$$x := \begin{bmatrix} x_0 \\ v_0 \end{bmatrix} \quad D(t, x) := \begin{bmatrix} x_1 \\ \left(b + c \cdot \exp\left(\frac{-t}{\tau}\right) - P_a \right) \frac{A_p}{M} \cdot ((t + t_0) < 0.03) - \mu \cdot g \cdot (x_1 > 0) \end{bmatrix}$$

$$Z := \text{rkfixed}(x, 0, 0.5, 1000, D) \quad m := 0..100$$

$$t := Z^{<0>} + t_0 \quad x := Z^{<1>} \quad v := Z^{<2>} \quad P_m := \frac{b}{P_a} + \frac{c}{P_a} \cdot \exp\left(\frac{-m}{\tau}\right)$$

maximum displacement $\max(x) = 0.132$